The Effects of Extracorporeal Shockwave Therapy on Osteoporotic Changes in a Pre-Clinical Model

by

Ashley Wright

Supervisor: Dr. Paolo Sanzo

Committee Members: Dr. Simon Lees and Dr. Carlos Zerpa

A thesis

presented to Lakehead University

in partial fulfillment of the

thesis requirements for the degree of

Master of Science in Kinesiology

SCHOOL OF KINESIOLOGY

LAKEHEAD UNIVERSITY

THUNDER BAY, ONTARIO, CANADA

September 16th 2026

Abstract

Introduction

Osteoporosis (OP) is a musculoskeletal disease that is defined by reduction in bone porosity, leading to increased risk and prevalence of falls and fractures. Extracorporeal shockwave therapy (ECSWT) has been reported to assist in tissue regeneration and osteogenesis by mechanotransduction. Evidence from prior studies demonstrated that ECSWT facilitated healing in non-unionized and stress fractures, supporting its potential utility as a treatment modality for OP. Bone-specific alkaline phosphatase (BAP) and osteocalcin (OCN) are blood biomarkers that are secreted by bone formation cells. These biomarkers may be effective as a screening tool to measure osteoporotic changes, as dual x-ray absorptiometry is unavailable in remote and rural regions in Canada, or during space travel. Therefore, the purpose of the study was to examine the effects of ECSWT on osteoporotic changes evident on bone microarchitecture computed tomography imaging and blood biomarkers using a pre-clinical model.

Methodology

The 32 rats in the study were divided into two conditions (ovariectomy and sham surgery) and two treatments (ECSWT and placebo treatment). The treatment groups received five shockwave treatments, once weekly to the right femur (1,000 shockwaves, energy flux density 0.33 mJ/mm^2, at 3 Hz). 1 week after the final treatment, blood was extracted, the rats were exsanguinated, and right femur dissected for analysis. The blood biomarkers were analyzed using an enzyme linked immunosorbent assay and femora were examined by computed tomography imaging. A two-way, independent measures analysis of variance was used to analyze changes in blood biomarkers and bone microarchitecture.

Results

There was a nonsignificant main effect on condition (OVX and sham) and treatment (ECSWT and placebo) on central 10% of bone mineral density (BMD), with a small effect size. There was a statistically significant simple main effect in BMD for 80% of the right femoral diaphysis between treatment groups (ECSWT and placebo; $F(1, 28)=7.84$, $p=.009$, $\eta^2=.219$) with a large effect size. There was a statistically significant main effect in medial cortical bone thickness between condition (OVX and sham surgery; $F(1,28)=6.17$, $p=.019$, $\eta^2=.180$) with a large effect size. There was a statistically significant main effect in lateral cortical bone thickness between condition (OVX and sham surgery; $F(1,28)=6.17$, $p=.019$, $\eta^2=.180$) with a large effect size. There was a nonsignificant main effect on condition (OVX and sham) and treatment (ECSWT and placebo) on anterior cortical bone thickness, with a small effect size. There was a nonsignificant main effect on condition (OVX and sham surgery) and treatment (ECSWT and placebo) on posterior cortical bone thickness, with a small effect size. There was a statistically significant main effect between OVX and sham surgery condition in mediolateral trabecular bone thickness, $F(1,28)=12.978$, $p=.001$, $\eta^2=.317$) with a large effect size. There was a nonsignificant interaction or main effect between OVX and sham surgery condition in anteroposterior trabecular bone thickness, with a small effect size. There was a nonsignificant

interaction or main effect between OVX and sham surgery condition in BAP concentration, with a small effect size. There was a statistically significant main effect between OVX and sham surgery condition in OCN concentration ($F(1,28)=11.278$, $p=.002$, $\eta^2=.287$) with a large effect size.

Conclusion

ECSWT treatment resulted in nonsignificant changes in cortical bone thickness, trabecular bone thickness, BMD, or biomarker concentrations of OCN and BAP under these experimental conditions. BMD did not decrease as expected from the OVX surgery, and ECSWT did not cause any alteration in bone microarchitecture. However, the measurements used in the present study may not show a comprehensive analysis of trabecular and cortical microarchitecture as the study only assessed trabecular and cortical bone thickness. ECSWT treatment created nonsignificant changes in blood biomarkers. OCN concentration increased in the OVX group when compared to the sham surgery group, suggesting altered bone remodeling following estrogen deficiency. BAP concentration was not significantly altered by OVX. OCN or BAP alone do not reflect OP changes but may be used as an adjunct assessment of altered osteoblast activity. Future studies should consider assessing additional microarchitecture parameters such as bone volume fraction, trabecular number, trabecular separation, and structural model index, using a repeated measures study design comprehensive and comparative analysis of bone microarchitecture.

Acknowledgements

I cannot begin to express my thankfulness for this experience, and a project I am lucky to be a part of. It is an incredible feeling to see this project come to fruition after spending ample hours working on it. This project could not have come together without my support system.

First and foremost, I wish to acknowledge my supervisor Dr. Sanzo - thank you for this incredible opportunity to be a part of this project. Your leadership, encouragement, and kind words have made all the difference whilst completing this thesis. I cannot express how much your guidance has taught me that I will use and carry through into my professional career. You were so patient and thorough during the stages of this project and it made this experience one I won't forget. Thank you again for believing in me.

I also wish to recognize my committee members Dr. Lees and Dr. Zerpa - thank you for your knowledge and expertise. Your feedback has been valuable and has shaped the project into what it has become. Thank you for your attention to details in my project and presentations. Your feedback encouraged me to think deeply and your support strengthened this project.

To Dr. Tinius - thank you for teaching me how to extract and analyze my data. The project would not have been the same if it weren't for your efforts to teach me the technology and coding.

To Eija - thank you for everything you taught me in the lab. Your expertise and knowledge guided me through the lab process - something that was new to me at the start of this project. I will miss our times in the wet lab!

To my family and friends - thank you for trying to discuss my thesis with me, even though you had no idea what I was talking about. Thank you, mum and dad especially, for supporting me through my academic journey at Lakehead over the last 6 years. Thanks to Leo for his companionship. To Derek- thank you for always showing up to support me. Thank you to my friends for their support and attentiveness – Amy, Avery, Bryanne.

Table of Contents

List of Figures

List of Tables

List of Abbreviations

ANOVA: Analysis of variance

BAP: Bone-specific alkaline phosphatase

BMD: Bone mineral density

BMI: Body mass index

BV/TV: Bone volume/total volume

CT: Computed tomography

DXA: Dual energy x-ray absorptiometry

ECSWT: Extracorporeal shockwave therapy

EDTA: Ethylenediaminetetraacetic acid

FSH: Follicular stimulating hormone

Hz: Hertz

Horseradish Peroxidase: HRP

J: Joules

LH: Luteinizing hormone

LUACF: Lakehead University Animal Care Facility

mJ/mm^2: Millijoules per square millimetre

MRI: Magnetic resonance imaging

OP: Osteoporosis

OCN: Osteocalcin

OVX: Ovariectomy

PA: Physical Activity

QoL: Quality of life

RPWT: Radial pressure wave therapy

SMI: Structural model index

SOP: Standard operating procedure

TGF-β: Transforming growth factor-β

3D: Three-Dimensional

2D: Two-dimensional

μm: Micrometers

Chapter 1: Introduction

Overview

Osteoporosis (OP) is the most common systemic skeletal disease worldwide (Morin et al., 2023). In Canada, more than 2 million people have OP (Osteoporosis Canada, 2024). Micro-architectural deterioration in the skeletal tissue causes OP, resulting in fragility subsequently leading to an increased risk of a fracture (Mohammadi et al., 2024). OP has no clinical manifestations until a fracture occurs. Fractures of the spine and pelvis may lead to increased morbidity, mortality, and a decrease in the individual's quality of life (QoL; Morin et al., 2023). Primary OP is caused by aging and menopause. Secondary OP is caused by the presence of external factors, co-morbidities, and medications (e.g., hypothyroidism, diabetes mellitus), microgravity, and relative energy deficiency in sport (also known as RED-S). OP is more prominent in females due to menopausal changes; and since the incidence of OP is positively correlated with age, the increasing female lifespan results in even higher frequencies of OP (Atalay et al., 2012). During menopause, reproductive hormone levels decrease significantly. Within a female's lifespan, 75% of total bone loss is seen during the postmenopausal period due to estrogen deficiency and aging (Atalay et al., 2012). The mechanism behind menopausal OP is an imbalance in new bone formation and increased bone resorption which parallels the decreased estrogen level (Atalay et al., 2012). The treatment for primary OP focuses on fracture prevention by manipulating medications, diet, exercise, and vitamin therapy (Osteoporosis Canada, 2024). Bone demineralization also occurs in microgravity situations, immobilization, or with prolonged bedrest (Rowe et al., 2023). The skeletal system is non-weight-bearing for extended periods of time during this, due to the length of the mode of travel and distance or health-related issues, so skeletal tissue demineralization is commonly observed in astronauts and patients due to prolonged periods of microgravity, immobilization, and bedrest (Man et al., 2021). Conservative

treatments including physical therapy is the primary treatment for microgravity-induced OP after return to Earth and after prolonged bedrest (Burkhart et al., 2020).

The first step in treatment for OP involves the assessment of bone mineral density (BMD) using diagnostic imaging. The gold standard diagnostic imaging used to diagnose OP after prolonged bedrest/immobilization and spaceflight are dual-energy x-ray absorptiometry (DXA) and computed tomography (CT; Alawi et al., 2021). This imaging equipment is often unavailable in some rural communities in Northern Ontario and during spaceflight, so a screening tool to assess bone demineralization and an accessible treatment would allow for a readily available monitoring tool for astronauts during spaceflight and increased treatment outcomes for individuals living in remote communities with OP (Singh, 2015).

Extracorporeal shockwave therapy (ECSWT) is an acoustical medical therapy that uses shockwaves to produce mechanical energy that is transferred to the tissue to create biological responses in the tissue (*mechanotransduction*). It is currently used in clinical practice to treat musculoskeletal pathologies including unresolving tendinopathies, non-uniting fractures, and stress fractures (Wang et al., 2014). In previous research using pre-clinical models, ECSWT demonstrated promising results in the treatment of osteoporotic changes (Lama et al., 2017; Mackert et al., 2017; Wang et al., 2014). Positive findings have also been reported on bone turnover and fracture healing studies with the use of ECSWT; however, the method and equipment has varied significantly between studies (Wen et al., 2026). Using a modality such as ECSWT to enhance skeletal microarchitecture, especially at high-risk fracture sites (femur and lumbar vertebrae) would alleviate the burden of osteoporotic fractures, enhance treatment outcomes, and QoL. ECSWT may be used as an adjunct to, or in combination with, other treatment methods to enhance bone microarchitecture during spaceflight and after prolonged bedrest (Man et al., 2021).

Osteocalcin (OCN) is non-collagenous protein and bone-specific alkaline phosphatase (BAP) is a glycoprotein (Chen et al., 2018; Xu et al., 2022). Analyzing blood biomarkers, such as BAP and OCN related to bone formation could be effective in monitoring skeletal changes in individuals at risk of OP. Both blood biomarkers are associated with osteoblast activity which are bone formation markers. OCN and BAP can also reflect the rate of new skeletal tissue formation and provide insight on skeletal remodeling. The presence of BAP or OCN would indicate elevation in bone formation markers, indicating skeletal demineralization, a skeletal fracture, or concentration may be elevated in a pediatric population due to normal growth and development and the closing of epiphyseal growth plates (Atalay et al., 2012). A blood biomarker would be useful to assess the severity of bone demineralization as a monitoring tool during spaceflight and for those with limited access to appropriate imaging and medical services in remote communities presenting with bone injuries or after prolonged bedrest due to complex medical conditions. Therefore, the purpose of the proposed pre-clinical study was to examine the effects of ECSWT on osteoporotic changes examined on imaging and blood biomarkers.

Prior research has yet to establish standardized treatment guidelines for OP using ECSWT, although existing studies indicate that ECSWT can enhance bone remodeling and mineralization. Treatment parameters such as energy flux density, frequency, and application have yet to be optimized for clinical practice (Wen et al., 2026). ECSWT may have therapeutic value in conditions of reduced mechanical loading, such as microgravity exposure or prolonged bedrest, where maintaining bone density is difficult, and in combination with other OP treatments to enhance skeletal microarchitecture. Systemic blood biomarkers such as OCN and BAP may offer a practical means of monitoring skeletal status, given the established inverse relationship with bone demineralization. These biomarkers would be advantageous for

individuals in rural or remote communities, patients with immobility, or prolonged bedrest, and astronauts during spaceflight, where access to gold-standard imaging (DXA, CT) is restricted.

Chapter 2: Review of the Literature

Extracorporeal Shockwave Therapy

Shockwave Therapy Overview

ECSWT is an acoustical medical therapy that uses shockwaves to produce mechanical energy that is transferred to the tissue to create biological changes. This process is often referred to as *mechanotransduction* (Tenforde et al., 2022). There are three different methods of generation and transmission of shockwave therapy which include electromagnetic, piezoelectric, and electrohydraulic mechanisms (Crevenna et al., 2021). The shockwave energy per unit area is called the energy flux density which is measured in millijoules per square millimetre **(**mJ/mm^2). It reflects the flow of energy perpendicularly to the direction of dissemination (Crevenna et al., 2021). The energy flux density is an essential parameter of dosage for focused ECSWT. There are low energy flux density (< 0.1 mJ/mm^2) and high energy flux density (> 0.12 mJ/mm^2). Higher energy flux densities increase mechanical stress and cellular stimulation delivered to the tissue, compared to a low energy flux density (Crevenna et al., 2021). The literature has not yet identified which energy flux density (high or low energy), and application is ideal for the treatment of OP.

An electromagnetic shockwave device has an electromagnetic coil and metal membrane on the opposing side (see Figure 1). The electromagnetic forces pull the metal membrane, and it accelerates away from the coil creating a low-pressure acoustic pulse. Electromagnetic shockwave generators can be categorized into two types based on their wave generation and focusing mechanisms (Tenforde et al., 2022). The first type operates using a cylinder-shaped electromagnetic source, which produces a cylindrically expanding pressure wave. High energy is generated near the applicator surface and dissipates with increasing tissue depth (Tenforde et al., 2022). Ultimately, this results in a radial pressure wave because there is not a fixed focal point

within the tissue and the energy dissipates at the surface of the tissue. The second type of electromagnetic shockwave generator is a fixed plane acoustic wave, which is focused by an acoustic lens to a defined focal point within the tissue (Tenforde et al., 2022). This configuration produces a focused shockwave, meaning there is low energy at the skin surface and high energy deep into the tissue.

Piezoelectric shockwave generators employ an arrangement of piezoelectric crystals that convert electrical energy into acoustical pressure waves (Crevenna et al., 2021). When an electrical pulse is applied, the crystals deform simultaneously and produce pressure waves that converge at a focal point within the tissue (see Figure 2). This configuration produces a focused shockwave with relatively low energy at the skin surface and concentrated energy at the depth of the focal point (Crevenna et al., 2021). A piezoelectric shockwave generator is used for focused ECSWT, that targets deep tissue injuries, such as tendinopathy or stress fractures (Beling et al., 2023; Crevenna et al., 2021)

An electrohydraulic shockwave generator produces high-energy pressure waves in a liquid by a high-voltage electrical current between two submerged electrodes. This technique creates a plasma spark that rapidly expands and generates a shockwave. The shockwave is focused using an acoustic lens to deliver concentrated energy to a target (see Figure 3). Electrohydraulic shockwave generators produce high peak pressures, for generating focused ECSWT treatments (Crevenna et al., 2021).

Figure 1

Electromagnetic Shockwave Generator

Note. Figure 1 demonstrates an electromagnetic shockwave diagram from International Society of Medical Shockwave Therapy (2025). The top of the photo represents a focal point, where the plane ECSWT is focused, and the rings underneath represent the cylindrical waves that create radial pressure wave therapy (RPWT; Crevenna et al., 2021).

Figure 2

Piezoelectric Shockwave Generator

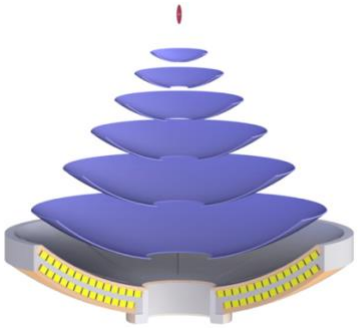

Note. Figure 2 demonstrates an electrohydraulic shockwave diagram. The yellow on the bottom represents the piezoelectric crystals that expand to generate ECSWT. The cylinders represent the trajectory of the shockwave, it is noted that the piezoelectric technology has a unique geometric shape which means it does not require a focusing lenses or reflector to transfer the energy (Tenforde et al., 2022).

Figure 3

Electrohydraulic Shockwave Generator

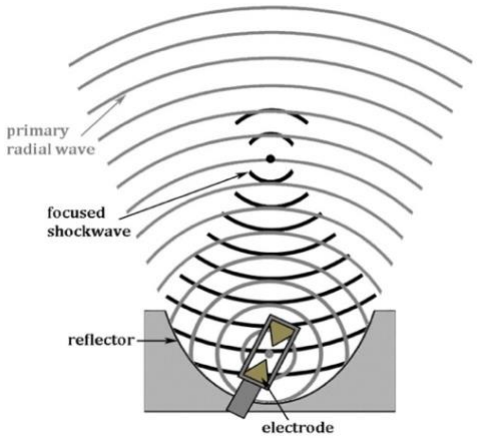

Note. Figure 3 demonstrates an electrohydraulic shockwave generator. First, the electrode is placed in the bottom focal point which then an electric spark is generated, and a spherical shockwave is created by rapid evaporation of the water particles. The shockwave first spreads radially, followed by a focused wave around the focal point (Tenforde et al., 2022).

Radial pressure wave therapy (RPWT) and focused ECSWT differ in the physical properties, depth of penetration, and biological effects, which influences clinical usage (Crevenna et al., 2021). RPWT produces a pressure wave that disperses energy over a broad area and decreases in intensity with tissue depth (Tenforde et al., 2022). An RPWT generator consists of a ballistic mechanism, where a projectile is stimulated by compressed air, and the projectile strikes the applicator tip to initiate the pressure wave (Tenforde et al., 2022, see Figure 4). This mechanism generates an expanding pressure wave at a low peak pressure. The energy density is highest at the applicator tip and dissipates radially, resulting in shallow tissue penetration, creating pressure pulses. The results produce surface-level stress and vibration which may result in analgesic effects. RPWT only penetrates tissues superficially, making it suited for treating superficial musculoskeletal injuries, where the primary effects are increased circulation and short-term pain reduction rather than tissue remodeling and biological changes seen when focused ECSWT is used (Crevenna et al., 2021).

Focused ECSWT delivers high-energy acoustic waves precisely to targeted tissues. The device generates shockwaves using electromagnetic, piezoelectric, or electrohydraulic generators and mechanisms, which all converge at a focal point beneath the skin to stimulate cellular and tissue responses (Tenforde et al., 2022). Focused shockwaves have a high peak pressure and concentrate at a predetermined depth, to allow selective targeting of deep pathologies such as stress fractures and non-uniting fractures (Crevenna et al., 2021). These waves are then focused by an acoustic lens, converging at a small focal point beneath the skin (see Figure 5). This allows high energy to reach deep tissues while minimizing exposure to the surrounding structures. A coupling gel or water cushion is applied between the applicator and the patient to eliminate air gaps and allow efficient transmission of the acoustic energy into the body (Crevenna et al., 2021). By adjusting the energy level, pulse frequency, and focal depth of the target tissue, there is controlled delivery of mechanical energy to deep and specific tissues. Knowledge of the physical properties involved in shockwave generation is crucial to understand how ECSWT is applied to soft tissue injuries, as the energy flux density, application, and frequency influence treatment outcomes.

Figure 4

Radial Pressure Wave Therapy

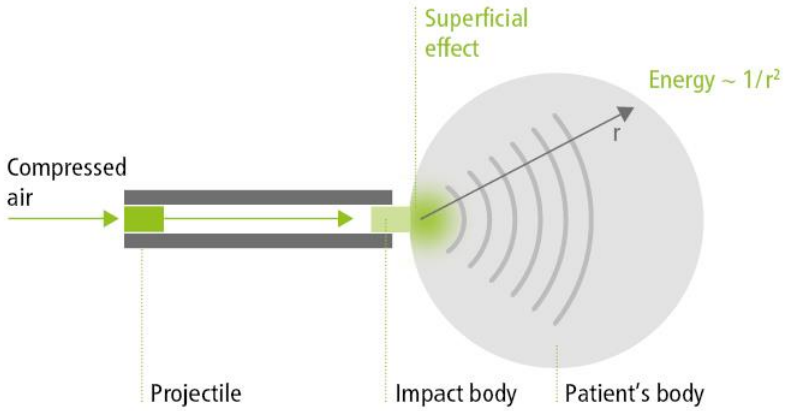

Fig. 14: Formation of pneumatically generated ballistic pressure waves and their superficial effects

Note. Figure 4 shows a ballistically generated radial pressure wave entering a patient's body. A projectile travels through compressed air, impacting the head of the device, which creates a rapid pressure wave 2-4 cm below the patient's skin (Crevenna et al., 2021).

Figure 5

Focused Extracorporeal Shockwave Therapy

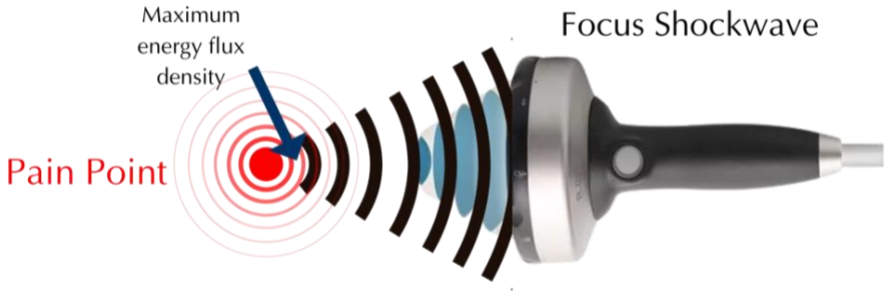

Note. Figure 5 demonstrates the mechanism of a focused shockwave. The energy diverts around a focal point to produce high energy, deep tissue penetration at a targeted structure (Crevenna et al., 2021).

Extracorporeal Shockwave Therapy Treatment

Effects of ECSWT

ECSWT is a modality used to treat musculoskeletal injuries. It has been reported that ECSWT initially causes microtrauma in the tissues to induce physiological events at the site of impact. Previous research revealed that focused ECSWT aids to lower inflammation by reducing pro-inflammatory cytokines (i.e., interleukin-6, interleukin-1, and tumor necrosis factor-alpha), subsequently, accelerating the tissue regeneration process (Wang et al., 2014). Pro-inflammatory cytokines initiate and sustain inflammatory responses by recruiting immune cells and enhancing pain sensitivity (Crevenna et al., 2021). Downregulation of pro-inflammatory cytokines limits excessive inflammation and creates a biological environment receptive to tissue regeneration (Crevenna et al., 2021). Focused ECSWT may also result in vasodilatation and angiogenesis when low-to-moderate treatment intensities are administered (Li et al., 2021a). Focused ECSWT also initiates vascular endothelial growth factor to stimulate capillary growth, creating angiogenesis, which minimizes scarring, improves muscle and tendon healing, and ultimately improves the tendon attachment strength in a tendinopathy injury. An example of a signaling pathway activated by focused ECSWT is transforming growth factor-β (TGF-β) pathway stimulating fibroblastic proliferation, and increasing type I collagen production to restore tendon, ligament, and bone structure. It is reported that TGF-β helps tissues strengthen, organize, and function during healing (Crevenna et al., 2021).

Shockwave Therapy and Muscular Injuries

Karimiahmadabadi et al. (2025) examined the effects of focused ECSWT versus deep friction massage in supraspinatus tendinopathy. The primary measurements were pain and pressure pain threshold. Pressure pain threshold was defined as the minimal amount of pressure that produced pain and was measured using a pressure algometer. Pressure pain

threshold was measured by finding a fixed point on the most sensitive area of the supraspinatus muscle then pressure was applied to the area using an algometer. Pressure was gradually increased until the participants indicated they felt pain. Pain was measured using the numeric pain rating scale, with participants rating the severity of their pain on a scale of 0–10, with 0 indicating no pain and 10 representing severe pain. The secondary objectives were the measurement of shoulder abduction and external rotation range of motion, supraspinatus strength, and QoL. QoL was measured using the SF-36 survey, which encompasses eight subscale items. These subscales cover various aspects of health and well-being. Range of motion and strength were measured at baseline, the end of the treatment period, and 1 week later. The QoL assessment was done at baseline and at the end of the study. One randomly generated group of participants received the ECSWT treatment, and the other randomly generated group had deep friction massage once per week, totaling four sessions, for 10 minutes per session. Deep friction massage is a physical therapy technique using deep, firm pressure with short strokes applied perpendicular to muscles to improve mobility (Karimiahmadabadi et al., 2025). The ECSWT treatment group received 4 ECSWT sessions, once weekly, for a total of 4 weeks. The ECSWT intensity ranged from .01 to 0.55 mJ/mm^2 and operated at a frequency of 4–8 Hertz (Hz), with 500 shockwaves administered.

Both the deep friction massage treatment group and the ECSWT treatment group revealed improvements in pain pressure threshold with a statistically significant reduction in pain intensity of the supraspinatus and deltoid muscles compared to baseline measurements. When comparing the ECSWT treatment group to the deep friction massage group, the ECSWT group exhibited a statistically significant reduction in pain intensity and an increase in the pressure pain threshold, meaning the minimal amount of pressure to the supraspinatus that produced pain. There was a significant increase in shoulder abduction range of motion in the ECSWT treatment

group. There were nonsignificant differences between the two treatment groups for shoulder external rotation range of motion, supraspinatus strength, and QoL but reported an overall increase when compared to baseline measures (Karimiahmadabadi et al., 2025).

Similar to Karimiahmadabadi et al. (2025), Li et al. (2021b) compared ECSWT to RPWT to treat rotator cuff tendinopathy (non-calcified). The aim of the study was to assess the effectiveness of RPWT compared to focused ECSWT to determine which is superior to treat rotator cuff tendinopathy. There were 46 participants ages 21-75 that had a baseline numerical pain rating scale with a score of 5 or higher, a decline in supraspinatus range of motion, pain with overhead shoulder motion, symptoms for 3 months or more, and a positive magnetic resonance image (MRI). Half of the participants received focused ECSWT treatment group, and the others received RPWT, both receiving four treatments total. The main objective was to assess the effect of the treatments on pain in the rotator cuff before and after the two interventions (Li et al., 2021b).

The focused ECSWT treatment group received 4 treatment sessions, once per week, for 4 weeks total. The rotator cuff was assessed using MRI and the affected areas were marked prior to administration of the ECSWT. The researchers used pain-adapted dosing, by increasing the energy levels each session. The mean energy flux density between all participants for the 3,000 focused applications per session were .09±.018 mJ/mm^2, and the frequency was 5.11±0.46 Hz. The RPWT treatment group underwent the same screening measurements as the focused ECSWT treatment group. The RPWT intensity was increased progressively, with a mean pressure of 4.0±0.35 bar and frequency of 3.2±.01 Hz over 200 applications. The participants received follow up assessments at weeks 4, 12, 24, and 48 weeks after the final treatment. The results revealed that focused ECSWT with a frequency of 5 Hz resulted in the same effects as RPWT delivered with a frequency of 3 Hz in the short-term on pain. There were no statistically

significant differences between RPWT and ECSWT until 24 weeks after the intervention. The researchers reported that medium energy, focused ECSWT was superior to RPWT on long-term follow up, due to the pressure wave form and mechanism of delivery. The researchers reported that both RPWT and ECSWT resulted in analgesic effects, however, focused ECSWT was superior at creating longer-term pain reduction (Li et al., 2021b).

Sanzo and Oakley (2014) conducted a randomized clinical trial on the effects of RPWT, joint mobilizations, and exercise on plantar heel pain in patients with plantar fasciitis. The purpose of the study was to assess the effects of RPWT on plantar heel pain, using RPWT in isolation and RPWT combined with joint mobilization or exercise on individuals with plantar fasciitis. Plantar fasciitis is described as inflammation of the plantar fascia and is the most common cause of heel pain (Boonchum et al., 2026). The researchers used a visual analog pain scale to assess the intensity of heel pain at rest, after activity, and overall improvement in heel pain between treatments. A secondary objective of the study was the measurement of functional ability, using the Lower Extremity Functional Scale. Both pain and functional ability were measured pre-intervention and 3 months post-intervention. There were three different treatment groups, including a RPWT, RPWT with joint mobilization, and a RPWT with stretching treatment group. Three RPWT treatment sessions were administered, once weekly, for 3 weeks. All three groups received 2,000 radial pressure waves at an intensity of 2.5 bars, 10-15 Hz and 11.5 Mp using a D Actor 100 Radial Shockwave Unit by Storz Medical© on the plantar fascia and where the pain was localized (Sanzo & Oakley, 2014). The joint mobilization group had the same RPWT treatment as described above, and also had three mobilization treatments including posterior glides at the talocrural joint, lateral calcaneus glides of the subtalar joint, and dorsal glides of the first metatarsophalangeal joints. The RPWT and stretching group had the same RPWT treatment as explained above and also completed a stretching and strengthening exercise

program for the gastrocnemius and soleus muscles, and the plantar fascia, and completed ankle strengthening exercises for the peroneal and intrinsic foot muscles using a TheraBand and towel, three times per day.

The researchers reported clinically significant improvements in all three treatment groups, however, the combination of RPWT and joint mobilizations was clinically and statistically significant and had a large effect size, when compared to RPWT and RPWT with exercise. RPWT and joint mobilization revealed a significant decrease in pain and increase in functional abilities, demonstrating a large effect size which was clinically meaningful. A limitation of the study, however, was that there was no control group, so to truly analyze the effects of RPWT on plantar fasciitis a control or placebo was needed to compare the differences. Long-term improvements were reported but there was variability in treatment parameters for RPWT (Sanzo & Oakley, 2014). This pattern of treatment variability was also noted in prior studies when analyzing RPWT and focused ECSWT for muscular and bone injuries (Haffner et al., 2016; Makert et al., 2017; Wang et al., 2014).

Shockwave Therapy and Osteoporosis

Many studies have investigated the relationship between ECSWT and OP but there are no standardized parameters set for application, energy flux density, frequency, or the length of the proposed treatment to see BMD improvements (Haffner et al., 2016; Makert et al., 2017; Wang et al., 2014). Currently, ECSWT has been used in clinical settings for non-uniting fractures and stress fractures (Haffner et al., 2016). A non-uniting fracture is a fracture in which normal bone healing has ceased, and union will not occur without further intervention (Haffner et al., 2016). A stress fracture is a partial or complete bone fracture caused by repetitive submaximal loading, rather than a single acute event (Beling & Tenforde, 2023). ECSWT has been reported to be effective in treating fractures because mechanotransduction creates biological changes such as

osteogenesis and activates cellular signaling pathways, such as mitogen-activated protein kinase. (Lama et al., 2017; Tam et al., 2009; Wang et al., 2014). The mitogen-activated protein kinase signaling pathway communicates to cells on differentiation, in the context of bone, signaling influences osteoblast and osteoclast activity so it is relevant to remodeling and mechanotransduction processes (Wang et al., 2014). ECSWT also activates Wnt/β-catenin signaling pathway, which controls stem cells to differentiate into osteoblasts and increases the bone matrix production (Haffner et al., 2016). ECSWT also activates the bone morphogenic protein synthesis pathways that stimulate mesenchymal stem cells to differentiate into osteoblasts and subsequently, osteocytes (Wang et al., 2014).

Lama et al. (2017) explored ECSWT alone and combined with raloxifene on how ECSWT supported bone formation and suppressed resorption in ovariectomized rats. Half of the rats underwent an ovariectomy (OVX) and the others received a sham surgery. An OVX model reproduced the molecular and biochemical alterations of OP. After the OVX, the rats were housed for 16 weeks which was the necessary time needed to reproduce osteoporotic changes. The rats were then divided into three different treatment groups with some groups receiving raloxifene, ECSWT, or sham. Raloxifene is a selective estrogen receptor modulator drug used to treat OP in post-menopausal women. It acts as an estrogen agonist for bone tissue. Raloxifene binds to estrogen receptors activating pathways that reduce bone resorption. To perform the ECSWT, the researchers placed the applicator on the lumbar spine and the antero-lateral aspect of the right thigh. The ECSWT treatment was high energy, at 1,000 electro-magnetically generated shockwaves at 3 Hz with an energy flux density of 0.33 mJ/mm^2. A total of five ECSWT treatments were completed over 5 weeks and bone changes were measured with histological analysis using diagnostic ultrasound imaging.

The researchers reported that using ECSWT on the lumbar vertebrae and its combination with raloxifene created an improvement in trabecular thickness and organization compared with OVX in the sham surgery treatment group. Trabecular thickness is the average thickness of an individual's trabecular structures within cancellous bone which serves as a microarchitectural parameter indicative of bone quality and strength (Rowe et al., 2023). The trabecular thickness and organization were improved with ECSWT treatment or raloxifene alone and in combination of treatments which ultimately restored the trabecular structure. Lama et al. (2017) concluded that ECSWT was an anti-osteoporotic therapy, alone or in combination with medications such as raloxifene. This approach also further demonstrates that combined therapies are a common and effective approach and consideration in the treatment of chronic and systemic diseases, such as OP.

Makert et al. (2017) also investigated the effects of low-energy ECSWT on metaphyseal fracture healing in an osteoporotic rat model. The purpose of the study was to examine the effect of ECSWT on the healing properties of metaphyseal fractures in an OP rat model while investigating the optimal ECSWT energy flux density and the ideal application volume throughout the healing period. The researchers also explored the most beneficial healing parameters to promote osteoporotic fracture healing. The rats in the study had an OVX to induce the same hormonal effects as OP in humans. The OVX as well as the sham-OVX rats then underwent a bilateral metaphyseal transverse osteotomy of the proximal tibia under anesthetic producing a fracture. A bilateral metaphyseal transverse osteotomy is a straight, horizontal cut made through the metaphyseal region of the long bone, and the researchers did this bilaterally to replicate a metaphyseal fracture. 35 days for healing were allotted because callus formation during this time was reported to be stable and resorption of the callus has not yet begun. The study design included three treatments, each with increased energy flux intensities (0.15

mJ/mm^2; 0.35 mJ/mm^2; and 0.55 mJ/mm^2) each at 2,000 impulses and at a frequency of 1 Hz. The differences were examined using micro-CT scanning, and trabecular bone and nodes were assessed. A trabecular node is a junction point within trabecular bone where three or more trabeculae intersect which is important information to assess the mechanical strength and overall porosity of the bone tissue (Mackert et al., 2017). The investigation of the trabecular bone found in the micro-CT analysis revealed that there were no differences between rats in the OVX group. Since no significant differences were found between OVX groups with and without treatment, the researchers concluded that further investigation be done as to whether or not the ECSWT solely had an influence on the callus and not on the trabecular network. This finding poses the question of whether ECSWT could be effective in treating osteoporotic fractures but indicated it may not have any beneficial effects when used for treating osteoporotic bone or OP in general.

Makert et al., (2017) reported that low energy (0.15 mJ/mm^2), focused ECSWT produced the greatest bone callusing in the endosteal and dorsal areas of the bone. The researchers reported that the optimal treatment range for osteoporotic fracture healing seems to lie in the combination of lower energy flux intensities, such as 0.15 mJ/mm^2 and lower numbers of one to three treatments during the fracture healing period.

Haffner et al. (2016) researched the effects of ECSWT on non-uniting tibial fractures that were unresponsive to conventional therapy. The study included 56 individuals suffering from a non-uniting tibial fracture. The fractures were assessed using radiography and CT imaging, to confirm the non-union sites. Visualization of non-union was done under fluoroscopic projection in the anterior, posterior, and lateral views. The non-union gap was marked on the skin with a marker to ensure ECSWT was applied in the correct location(s). Participants received ECSWT treatment consistently over a six-month time period. Treatment consisted of 3,000–4,000 impulses of electrohydraulic shockwaves at an energy flux density of 0.4 mJ/mm^2. The

researchers reported that 88.5% of the participants in the study were fully weight-bearing and painfree after 6 months of ECSWT treatment. The participants initially failed to respond to previous surgical and non-surgical interventions. Successful healing in the study was defined clinically as painfree weight bearing. The researchers reported that ECSWT achieved a significantly comparable healing rate to surgical treatment but with a more favorable risk-to-benefit ratio and fewer short-term complications due to ECSWT being minimally invasive. The researchers concluded that ECSWT was an effective, low-risk treatment alternative or complimentary treatment consideration for non-uniting fractures, comparable to surgical revision. They also suggested that ECSWT should be applied early in the callusing process, as earlier treatment was associated with improved healing rates (Haffner et al., 2016). A limitation of the study was that in the current literature there are deviations between typical suggested treatment parameters such as the energy flux density, device, generators, application, and frequency used to treat non-uniting fractures. Ultimately, this makes it complicated to compare success rates of ECSWT for different injuries.

Wang et al. (2014) examined the effect of ECSWT on osteoporotic and osteoarthritic conditions in the tibiofemoral joints of osteoporotic rats. There were 56 rats split into condition and treatment groups including sham; OA, OP, OA and OP; OA and ESWT; OP and ESWT; and OA, OP, and ESWT groups. The OP groups received a bilateral OVX to induce hormonal differences that would replicate OP in a human. The osteoarthritis groups received anterior cruciate ligament transection and medial meniscectomy on the left tibiofemoral joint. Anterior cruciate ligament transection is when the ligament is severed or cut and medial meniscectomy is removal of the medial meniscus, to induce osteoarthritis like symptoms and pathology. The ECSWT was performed on 28 rats total, eight rats per group, a week after the ligament transection surgery. 800 pulses of ECSWT at an energy-flux density of 0.22 mJ/mm^2 was given

to the medial tibial condyle 0.5 cm below the tibiofemoral joint line in one session. Bone strength testing was done by testing peak compression strength and the breaking moment of inertia, after the rats were exsanguinated and the femur, fibula, and tibia were analyzed. These were measured by using the slow-load compression technique until a fracture occurred. The slow-load compression technique means that the bone was subjected to gradually increasing compressive force at a controlled, slow rate until mechanical failure, allowing measurement of mechanical properties and loading.

The researchers reported differences in BMD between groups and treatments. The BMD values in the rats treated with ECSWT revealed significant improvement as compared to animals without ECSWT. The osteoarthritis and OP group had the lowest BMD, but ECSWT treatment improved both osteoarthritis and OP in the study. After ECSWT treatment, improvements in cartilage were shown, as well as improvements in bone architecture. As for bone strength, the peak load and the breaking moment of the femur and tibia significantly decreased in ECSWT treatment groups, for osteoarthritis, OP, and osteoarthritis and OP compared to the sham treatment groups. The final conclusion of the study was that ECSWT was effective in the repair and recovery of osteoporotic osteoarthritis of the tibiofemoral joint in rats (Wang et al., 2014). A limitation in the study was that the ECSWT energy flux density and dosages were based on a pilot study performed in small animals, therefore, there needs to be further validation of shockwave dosage and application.

Tam et al. (2009) examined the osteogenic effects of ECSWT on osteoporotic bone in an OVX goat model, designed to mimic post-menopausal bone loss. The researchers also examined differences in weight bearing versus non-weight bearing bones. The researchers performed ECSWT on the left calcaneus (non-weight bearing in goats), distal radius (weight-bearing), and femoral condyle (weight-bearing), and the right calcaneus, distal radius, and femoral condyle

were used as the control side. Each ECSWT treatment applied 6,000 pulses at an energy flux density of 0.5 mJ/mm^2 and a frequency of 4 Hz. The penetration depth was set to 10 mm to target the trabecular, inner region of the bone. This was performed once monthly, for 9 months total. The researchers assessed the goat's bone microarchitecture using micro-CT imaging pre- and post-ECSWT treatment. The researchers reported a change in skeletal microarchitecture, specifically trabecular bone, when compared pre- and post-intervention. The researchers also reported an overall higher deposit of trabecular bone in the bones that received treatment. There were no differences identified in the distal radius and femoral condyle out of the bones that were treated. The explanation behind this finding was that the calcaneus may have been sensitive to extra mechanical stimulation because it is a non-weight bearing bone, unlike the distal radius and femoral condyle bones that are constantly bearing load. Monthly treatment may allow the mechanical adaptions from ECSWT to occur. The ECSWT treatment was clinically effective and localized at the treatment regions, increasing BMD from 2% to 5%. The researchers reported that this osteogenic effect may be clinically applicable for preventing OP at non-weight-bearing sites in humans, such as the radius, humerus, or ulna. Ultimately, the researchers concluded that ECSWT may enhance BMD by inducing bone formation, particularly in non-weight bearing areas.

A general finding in the prior literature was the substantial methodological variability within ECSWT treatments and dosages used. The energy flux density, applications, and frequency all differed between methodologies, making it challenging to directly compare previous literature (Haffner et al., 2016; Lama et al., 2017; Mackert et al., 2017; Wang et al., 2014). The previous studies revealed clinical and statistical significance, highlighting the need for standardized ECSWT treatment procedures and the possible benefit of treatment but with more research required. Blood biomarkers are a minimally invasive and potential diagnostic tool

complementing additional gold-standard imaging techniques to assess bone demineralization and remodeling in individuals at risk of OP.

Blood Biomarkers

Bone Formation Markers and Remodeling

BAP is an enzyme released by osteoblasts, the cells for bone formation, and it plays a crucial role in bone mineralization (Chen et al., 2018). Osteoblasts are derived from mesenchymal stem cells and are responsible for deposition, mineralization, and synthesis of the bone matrix. Since BAP is produced by osteoblasts, it is hypothesized that BAP is reflective of bone formation and bone turnover rates (see Figure 6). Osteoblasts aid in bone mineralization by creating the chemical environment for calcium and phosphate to create hydroxyapatite crystals, which give skeletal tissue strength and rigidity (Schindeler et al., 2008). Hydroxyapatite is a mineral form of calcium phosphate that make up human skeletal tissue, in a form of microscopic crystals that are deposited within collagen fibers in the bone matrix. Hydroxyapatite promotes skeletal rigidity and the ability for the skeleton to withstand mechanical loads (Chen et al., 2018). Hydroxyapatite crystals are continuously degraded and rebuilt during skeletal remodeling, allowing the skeleton to adapt to stress and regulate calcium and phosphate levels (Schindeler et al., 2008). On the other hand, osteoid is the unmineralized portion of the bone matrix produced by osteoblasts. It is composed mainly of collagen fibers and ground substance, providing flexibility and structure before hydroxyapatite crystals are added (Chen et al., 2018). The combination of osteoid and hydroxyapatite creates a hardened and, subsequently, mineralized skeletal tissue. OCN binds calcium in the region of osteoblasts and BAP is also released during binding. This process forms osteoblasts and causes an accumulation of phosphate ions. This yields a high concentration of both BAP and OCN in the blood and creates hydroxyapatite. Prior

research demonstrates a relationship between BAP and bone turnover rates but has yet to define the clinical relevance between BAP and OP (Chen et al. 2018).

Figure 6

Bone Remodeling Cycle

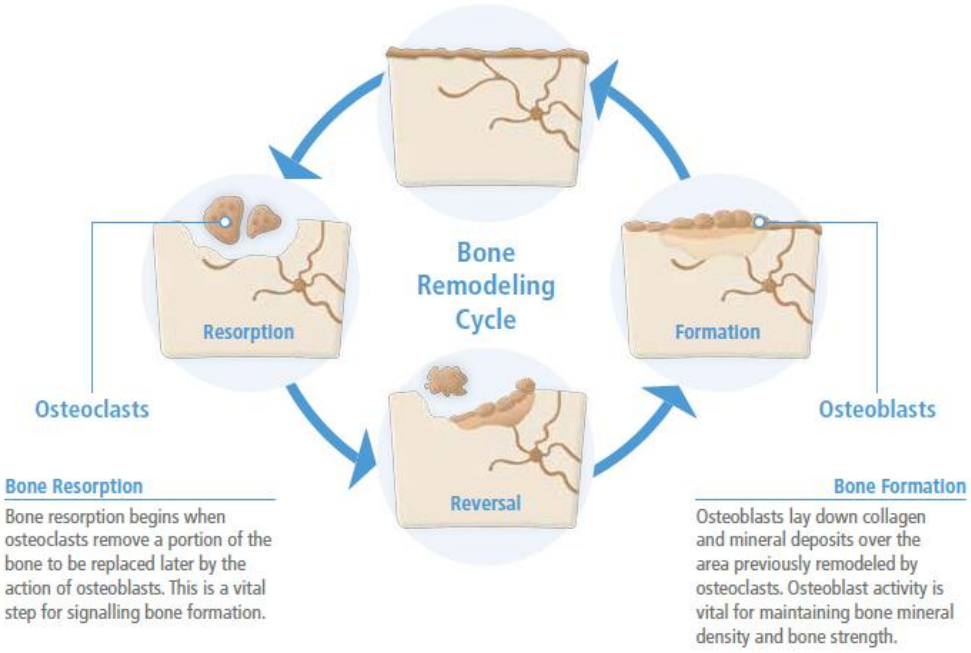

Note. Figure 6 demonstrates the main stages of bone remodeling which are resorption, reversal, and formation. Resorption is when osteoclasts remove bone to signal formation. Reversal is when mononuclear cells clean up the site and signal for osteoblasts to create new bone tissue. Formation is the building stage, where osteoblasts create osteoid, which is an immature form of bone (Schindler et al., 2008).

Wu et al. (2026) explored bone turnover markers (β-C-terminal telopeptide of type I collagen, procollagen type I N-terminal propeptide, and BAP) in patients with OP and evaluated the predictive value for secondary fracture risk. 180 participants were included in the study, with the OP group divided into fracture and non-fracture sub-groups. Correlations between the three biomarkers (β-C-terminal telopeptide of type I collagen, procollagen type I N-terminal propeptide, and BAP) were analyzed at the femoral neck and the lumbar spine, and evaluated using a Pearson correlation co-efficient, to see if the blood biomarkers were related to BMD values. A binary logistic regression was used to assess which factors increased the chance that an

individual with OP had a secondary fracture, and to identify independent risk factors and demographic variables. A receiver operating characteristic curve was used to identify how well the demographics and biomarkers predicted fracture risk.

Individuals with OP had significantly higher bone turnover markers ((β-C-terminal telopeptide of type I collagen, procollagen type I N-terminal propeptide, and BAP) and lower BMD in the lumbar spine and pelvis than the healthy matched controls. These markers were strongly and negatively correlated with BMD. As the biomarker concentrations increased, BMD decreased. Individuals with a fracture also had even higher biomarker concentration than those without a fracture present. Blood turnover markers in combination with BMD assessment provided strong predictive accuracy for fracture risk, outperforming any single measure on the ROC curve. The researchers concluded that elevated biomarker concentration negatively correlated with BMD and could independently predict secondary fracture risk in individuals with OP.

Lumachi et al. (2009) explored bone formation marker changes related to post-menopausal OP. The researchers used a sample of 48 participants, who underwent BMD assessment using DXA, on the lumbar spine and hip. 48 women with a median age of 62 years old, with OP and T-score on DXA images of less than –2.5 standard deviations (see Table 1) were enrolled in the study. Participants were grouped by age (group A: aged 49-59 years; group B: aged over 59 years). Serum biochemical screening was performed in all patients, with serum calcium and creatinine measured spectrophotometrically, meaning that the amount of light absorbed was proportional to the concentration of the substance. This allowed compounds to be quantified such as enzymes or blood biomarkers. BAP was analyzed using an immunoassay kit.

The researchers reported that OCN and BAP concentrations increased with age in individuals aged 59 years or older (Group B), and there was no relationship present with BMD.

Women in the older group had significantly higher concentrations of both OCN and BAP compared to the younger group, and age was significantly correlated with increases in both markers, suggesting that bone turnover increased with age. No significant differences were observed in parathyroid hormone, calcium, or creatinine concentration between groups, and there was no association between these biomarkers and BMD. The researchers concluded that the elevated bone formation markers in the older aged participants may have reflected increased bone turnover that contributed to the pathology of OP in this population.

Clinical diagnostic testing parameters are not yet fully established or presented in prior literature for the diagnostic utility of BAP and defining OP severity, however, clinical and statistically significant improvements have been reported in prior studies such that BAP reflects the bone remodeling processes (Lumachi et al., 2009; Wu et al., 2026).

Osteocalcin

OCN is a non-collagenous protein and a key biomarker of bone formation, making it an important indicator of skeletal health and remodeling (Xu et al., 2022). OCN is produced by osteoblasts and secreted during bone formation and plays a critical role in regulating bone mineralization (Atalay et al., 2012). OCN is also known as bone γ-carboxyglutamic acid protein. Following protein synthesis, the mature peptide first undergoes several splicing events and then gets γ-carboxylated at three residues, resulting in a peptide with high affinity toward bone and the extracellular matrix. Due to the low pH inside the osteoclast resorption compartments, OCN is decarboxylated again, which reduces its affinity for bone and triggers the release of uncarboxylated OCN into the bloodstream. Elevated OCN concentration may reflect high bone turnover or bone metabolic activity; for example, an elevation of OCN in an elderly individual may mean that they have significant bone loss and developing OP (Moser & van der Eerden., 2019). OCN concentrations are sensitive to changes in bone turnover and are closely associated

with overall rates of skeletal remodeling (Atalay et al., 2012). Since skeletal remodeling is a continuous process that maintains bone integrity, OCN serves as insight of the bone's metabolic status of normal physiological processes (fracture healing) or pathological processes (OP or other metabolic bone diseases). Individuals may have increased OCN concentration if increased bone modeling is prevalent (bone fracture, closing growth plates). It is also elevated in individuals with bone diseases, such as Paget's Disease (excessive and disorganized bone remodeling) or chronic kidney disease (kidney functioning affects bone turnover). Since OCN is secreted during skeletal bone remodeling by osteoblasts, it is elevated under these circumstances where skeletal bone remodeling and formation were prominent (Xu et al., 2022)

Atalay et al. (2012) explored the diagnostic utility of undercarboxylated OCN, OCN, and alkaline phosphatase in peri- and post-menopausal females. Undercarboxylated OCN is incomplete γ-carboxylated form of OCN that exhibits reduced binding affinity to bone and serves as a biomarker of bone turnover (Xu et al., 2022). The participants were divided into four groups by age (group one was between 25-34 years, group two was between 35-40 years, group three was in the first five years of menopause, and group four was 5 years or more after the onset of menopause). The blood samples were taken and analyzed by an electrochemiluminescence immunoassay, which detected specific biomarkers, in this case OCN, undercarboxylated OCN, and alkaline phosphatase. It detected biomarkers by measuring light emitted from the chemical reaction and is triggered by electricity on an electrode surface (Atalay et al., 2012). The researchers measured BMD using the femoral neck of the left leg, lumbar spine vertebrae 1-4, and lumbar spine vertebrae 2-4 using DXA imaging and OP diagnosis was determined by calculating standardized T-scores.

The researchers performed multiple logistic regression analyses (N=84) to determine which single parameter was most discriminative for OP (i.e., age, BMI, OCN, undercarboxylated

OCN, total acid phosphatase, alkaline phosphatase, calcium, and phosphorus). The findings revealed that OCN had the highest predictive value for assessing OP when compared and analyzed with the participant demographics. The average OCN, undercarboxylated OCN, and BAP concentration were significantly higher in post-menopausal women than in peri-menopausal women in the study. The highest serum OCN, undercarboxylated OCN, and alkaline phosphatase concentrations were observed in patients within 1-5 years after the onset of menopause. This finding may be due to decreased estrogen during menopause, causing bone turnover to increase. The researchers stated that BMD is the most valuable diagnostic tool to diagnose OP, however, only long-term damage can be measured by BMD, therefore, OCN can be an effective pre-screening or risk assessment tool that gives biochemical insight into the risk of developing OP. Biochemical bone markers are non-invasive and less expensive diagnostic tools that may be beneficial for the diagnosis and treatment follow-up of metabolic bone diseases. The researchers concluded that measuring OCN concentrations may be helpful to monitor follow-up changes that currently cannot be assessed with BMD measurements from DXA imaging, and the elevation of OCN concentrations could be an efficient method to assess individuals with a rapid post-menopausal bone turnover rate (Atalay et al., 2012).

Xu et al. (2022) explored undercarboxylated OCN concentration changes due to age or gender, and the prevalence of OP in this cross-sectional design in a sample of 900 participants (431 men and 469 women). The researchers collected clinical and demographic information and BMD of the lumbar spine (L1–4), left femoral neck, and left hip. Biochemical markers including hepatic and renal function, serum calcium, serum phosphorus, procollagen type 1 N-propeptide, β-CrossLaps of type I collagen-containing cross-linked C-telopeptide, intact parathyroid hormone, 25-hydroxyvitamin D, and undercarboxylated OC were measured. The researchers

collected the blood samples with electrochemiluminescence immunoassay, which was a diagnostic technique to assess blood biomarkers.

The researchers reported that higher undercarboxylated OCN concentration were associated with lower BMD in the pelvis and lumbar spine regions. Undercarboxylated OCN was also reflective of vitamin K status in bone, and vitamin K deficiencies also noted to increase with age. This finding may explain the correlation between undercarboxylated OCN and age (Atalay et al., 2012; Xu et al., 2022). The researchers also identified that the relationship between undercarboxylated OCN and OP was unclear but predicted that an abnormally high level of undercarboxylated OCN may reflect accelerated bone turnover and indicate decreased BMD, subsequently, leading to the risk of skeletal fractures (Xu et al., 2022).

Singh (2015) explored serum OCN as a diagnostic biomarker for primary OP in 82 post-menopausal females aged 40-70 years. Each participant was subjected to measurements of BMD assessment and serum OCN testing. Based on the results of DXA scan they were divided into either the control group or case group. The case group was further subdivided as osteopenia or OP depending on their individual T-score value from the DXA assessments. The results of serum calcium, BAP, and OCN concentrations were compared with BMD and the relationship was assessed by correlational analysis.

The researchers reported that OCN concentrations were significantly higher in post-menopausal osteopenic and osteoporotic women, and BMD at the femoral neck and lumbar spine regions were significantly lower in the case group than the control group. These results revealed an inverse relationship, which has already been identified in prior literature (Atalay et al., 2012; Xu et al., 2022). A limitation of the study was that there were no standardized values in the study to measure OCN or OP severity range using the biomarkers, so having a standardized, practical

methodology would need to be tested before implementing OCN as a biomarker as a screening tool.

Preventative medicine and pre-screening are emerging trends, therefore, using OCN as a pre-screening assessment may be an effective measurement to assess bone remodeling and identify the risk for individuals who may be susceptible to OP. Since microgravity has similar consequences on the skeletal system as menopause, OCN as an assessment and screening biomarker could be effective to monitor bone demineralization severity during long-duration spaceflight. Another practical use is for individuals in northern, remote communities with limited access to DXA imaging, or individuals who are bedridden due to severe health conditions and at risk of bone demineralization and OP development. Each of these individuals as well as the general population would benefit from a pre-screening tool to assess bone formation changes, and this would also reduce wait times, travel, and costs to receive DXA imaging and prevent complications associated with reduced bone mineralization and OP.

These considerations highlight the importance of understanding bone metabolism and turnover, not only in monitoring bone demineralization but also in interpreting bone tissue's repair processes. By examining how bone tissue heals and remodels following injury, differences in biomarkers like OCN are better understood as well as the potential use in assessing bone formation and overall skeletal status (Xu et al., 2022). ECSWT and its impact on bone tissue healing are also better understood by reviewing the bone tissue healing processes (Li et al., 2021a).

Bone Tissue Healing

A skeletal fracture is the result of damage to the compact and cancellous bone structures at the site of injury. A fracture also impedes the integrity of the soft tissue structures, nerves, and blood vessels at the site of injury (Schindeler et al., 2008). A skeletal fracture initiates a sequence

of inflammation, healing, and remodeling to repair injured bone to its original state. The healing process may be divided into the initial inflammatory response, soft callus formation, hard callus formation, and bone remodeling phases. Bone fracture repair entails both anabolic, which is new formation of cells, and catabolic processes, which is the breakdown of cells. Anabolic processes occur during tissue formation, while catabolic processes prevail during the remodeling phase (Schindeler et al., 2008).

Stage One

The initial inflammatory stage of bone fracture healing is the first stage, which lasts up to 4 days. Since blood vessels and soft tissue are damaged at the site of the injury, inflammatory cells migrate to the injured region. Damaged blood vessels cause blood pooling, which forms a hematoma, acting like a mechanical plug (Palanisamy et al., 2022). Platelets, macrophages, and other inflammatory cells infiltrate the hematoma and fracture site. These cellular events facilitate the recruitment of additional inflammatory cells in a positive feedback loop. This loop is a phenomenon where histamine, prostaglandins, and bradykinins in the signaling pathway amplifies the initial signal from the injury by activating an upstream component, leading to a rapid cellular response. Cytokines and growth factors are also present at the site, which develops the hematoma into a fibrinous thrombus (Schindeler et al., 2008). Eventually, capillaries develop in the clot, creating new vascular tissue in a granular form. Macrophages and additional phagocytic cells clear degenerated cells and other debris at the injury site (Schindeler et al., 2008). Casting or fixation may also occur at this stage (Su et al., 2018).

Stage Two

The soft callus stage of bone healing is where the bone tissue immaturely bridges the fracture site and fractures at this stage are often mechanically unstable. Most fractures heal by the process of endochondral ossification. Endochondral ossification occurs when a temporary

cartilage model is preceded by bone tissue (Schindeler et al., 2008). The most prominent cells in this stage are chondrocytes and fibroblasts that produce the soft callus. The soft callus provides mechanical support to the fracture and is a template for the bony callus that will later replace it. At the cellular level, the chondrocytes create a cartilaginous matrix until all the granulation tissue from stage one is replaced with cartilage. Fibroblasts replace any fibrous tissue at the hematoma site from stage one and this creates the cartilaginous mechanical plug at the injury site. The final event in this stage is the chondrocytes' hypertrophy, which mineralizes the matrix with calcium. The chondrocytes are then subjected to apoptosis, allowing for the formation of a hard callus (Schindeler et al., 2008; Su et al., 2018).

Stage Three

Stage three in the bone healing process is called the hard callous formation phase (primary bone formation). Firstly, the soft callus phase in stage two is gradually abolished from the site of injury. Osteogenesis and increased concentration of osteoblasts are prominent in this stage, as primary bone building is the objective. Although the hard callus is still under modelled at this stage, clinicians can assess radiological union at this stage (Schindeler et al., 2008). Radiological union is defined when the fracture line is no longer visible on radiographs and the bone appears to be mechanically stable (Beling et al., 2023). Radiological union takes 8-10 weeks in adults and 6-8 weeks in children (Dagklis et al., 2023). Radiological union is a crucial milestone that determines when an individual can return to weight-bearing activities of daily living (Su et al., 2018).

Stage Four

The fourth stage of the bone healing cycle is the bone remodeling phase. It is characterized by the resorption process induced by osteoclasts, which consists of bone strengthening and reshaping of the bone into the original compact and cancellous bony structures

and is also known as secondary bone formation (Palanisamy et al., 2022). Osteoclasts and osteoblasts are crucial in this stage for weaving and remodeling the bone callus from stage three into compact and structurally sound tissue (Schindeler et al., 2008). This stage can last from 1-2 years before total bone healing has occurred (Beling et al., 2023). Strength and range of motion exercises are crucial to ensure the bone remodels itself to withstand mechanical tension (Su et al., 2018) during this stage. Bone tissue healing is important to understand when discussing the hormonal changes of menopause and OP. Fractures are prevalent in menopausal females since estrogen plummets during menopause, which imbalances the bone modeling cycle. As a result, menopausal women are at a higher risk of falls, bone fragility, and fractures.

Primary Osteoporosis

Primary OP is an age and hormone related metabolic bone disorder defined by reduced BMD and deterioration of bone microarchitecture, resulting from an imbalance between osteoclastic resorption and osteoblastic formation, in the absence of secondary causes (Atalay et al., 2012). It predominantly affects postmenopausal women and elderly individuals and may result in significant increases in fall risk, fragility, and fractures (Yong & Logan, 2021).

Menopause

By the year 2030, it is estimated that there will be approximately 1.2 billion menopausal females and 47 million people transitioning to post-menopause each year until 2030 (Gatenby et al., 2024). Menopause is the stage in a female's life when ovarian reproductive function halts, resulting in the cessation of the menstrual cycle (Gatenby et al., 2024). Females spend approximately one-third of life either peri- or post-menopausal, since the average menopausal age is 51 years, and the average female lifespan in Canada is 83 years (Gatenby et al., 2024). The main symptoms of menopause are insomnia, hot flashes, heart palpitations, polyuria, and

amenorrhea. These symptoms range in severity and affect daily QoL. Clinically, menopause is diagnosed after 12 months of consistent amenorrhea (Gatenby et al., 2024).

When reproductive functioning halts, physiological events occur within the female body (Talaulikar, 2022). There may be significant changes in reproductive hormone levels, particularly with estrogen, luteinizing hormone (LH), follicle-stimulating hormone (FSH), and progesterone (see Figure 7; Talaulikar, 2022). As estrogen and progesterone levels fall during menopause, negative feedback on the hypothalamus and pituitary is lost, leading to elevated FSH and LH levels (Talaulikar, 2022). FSH is responsible for stimulation of ovarian follicles to produce estradiol. Estradiol is a hormone that also provides negative feedback to the pituitary gland and hypothalamus to stabilize the secretion of FSH, to balance hormone levels (Talaulikar, 2022). LH is secreted by the anterior pituitary gland and triggers ovulation by stimulating the ovarian follicle to release an egg and promotes the formation of the corpus luteum during ovulation. A corpus luteum is a temporary endocrine structure in the ovary that helps to form a mature ovarian follicle after ovulation, and this structure also secretes progesterone and estrogen to prepare the endometrium for fertilization (Yong & Logan, 2021). If the egg is not fertilized, the corpus luteum diminishes after 10 days, leading to a drop in progesterone and the onset of menstruation. The rise of LH and FSH indicate ovarian cessation and are considered a diagnostic biomarker for menopausal changes. Hormonal changes during menopause also lead to changes in bodily systems, especially in the skeletal system (Gatenby et al., 2024). Skeletal resorption outpaces skeletal remodeling, leading to a loss of BMD (Atalay et al., 2012). A females' peak bone mass is reached near the age of 30 years and females lose approximately 10% of their BMD in the first three years of menopause due to a sharp decline in circulating estrogen levels (Yong & Logan, 2021). Trabecular bone, which has a higher surface area and faster remodeling rate than cortical bone, is vulnerable to estrogen deficiency and experiences rapid microarchitectural

changes during menopause. Cortical bone is also affected during menopause, and deteriorates more gradually due to its dense structure, making it resistant to short-term hormonal changes. The loss of trabecular bone contributes to increased fracture risk, particularly in high weight-bearing anatomical regions. Estrogen plays a critical role in mediating formation versus resorption in the bone modeling cycle (Atalay et al., 2012).

Figure 7

Hormone Levels During the Female Lifespan

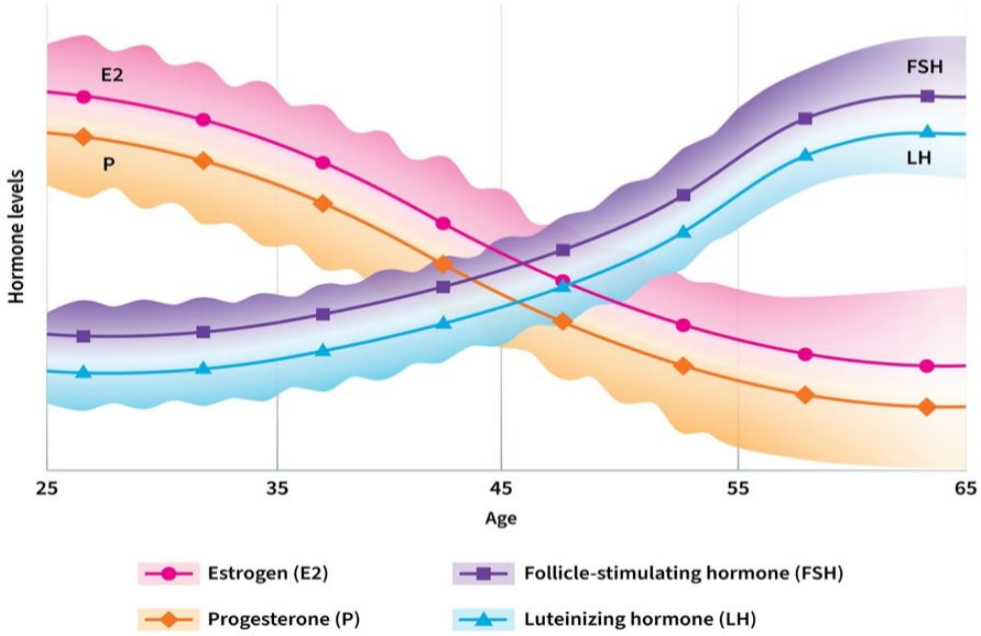

Note. Estrogen and progesterone levels peak and start to decline around age 30, as FSH and LH increase. FSH and LH increase to try and stimulate ovarian function, which halts at menopause. FSH is used clinically as a biomarker for menopause (Talaulikar, 2022).

Secondary Osteoporosis

Secondary OP is a form of OP that arises as a result of an underlying medical condition, medication, or environmental factor**,** rather than being due to aging or menopause (Baran et al., 2022). OP resulting from microgravity exposure, immobilization, or prolonged bedrest is

classified as secondary OP, as it arises from mechanical unloading rather than intrinsic age- or hormone-related factors (Baran et al., 2022).

Microgravity

It is critical to understand the impacts of long-term space travel on human health, since the North American Space Agency has extensive plans for space exploration (Baran et al., 2022). Astronauts are also spending longer durations on the International Space Station, to expand astronomical research and space exploration (Man et al., 2021). Since the human body is intrinsically adapted to Earth's gravity, exposure to microgravity compromises almost every bodily system (Man et al., 2021). Microgravity decreases the effort needed for movement; therefore, the peripheral muscles atrophy in microgravity. Bodily fluid is also redistributed within the body, causing compromises in the cardiovascular, neurological, and immunological systems. The skeletal system is also highly compromised, and bones are subject to demineralization at rapid rates (Man et al., 2021). Baran et al. (2022) reported that microgravity-induced reduction in BMD occurs at a rate of 0.5–1.5% loss per month spent in space. The risk of fracture in a microgravity environment is believed to be low but the potential risk for fracture increases upon return to a gravity environment (Swaffield et al., 2018). Gravity provides external and constant load on the skeletal tissues, subsequently balancing skeletal formation and resorption (Dagklis et al., 2023). Microgravity causes the same outcome but due to different signaling pathways. Rather than reduced estrogen, this signaling is altered by osteocytes (sclerostin). In menopause, bone resorption is mediated by increased osteoclast activity in the absence of mechanical load, however, during spaceflight the loss of BMD is due to extrinsic factors, unlike menopause which is due to hormonal factors (Swaffield et al., 2018). Previous studies indicated that major skeletal bone mass is lost in anatomical regions that have the highest weight-bearing function on Earth, such as the femur and lumbar spine bones (Baran et al., 2022;

Burkhart et al., 2020; Man et al., 2021). The BMD loss from microgravity conditions exceeded levels common in menopausal OP, as the amount of damage in a few months of spaceflight is comparable to years of post-menopausal OP (Burkhart et al., 2020; Gabel et al., 2022; Man et al., 2021). Both cortical and trabecular bone are affected by gravitational changes in space, however, trabecular damage occurs much more rapidly than cortical damage (Burkhart et al., 2020). Trabecular bone has a higher remodeling rate, greater surface area for resorption, and is dependent on mechanical loading for remodeling. This makes it highly subjected to the effects of microgravity in anatomical weight bearing regions.

Burkhart et al. (2020) conducted a study on vertebral integrity pre- and post-spaceflight. CT imaging, finite element analysis, and fracture risk were assessed. Finite element analysis is a computer modeling method used to estimate how a structure behaves under physical forces such as loading, bending, or compression (Burkhart et al., 2020). A structure is divided into small pieces called finite elements, where forces or loads can be simulated, then calculating how each element mechanically fails, in this case it tested bone strength and detected the fracture risks (Burkhart et al., 2020). The researchers compared post-flight changes in the lumbar spine DXA BMD and vertebral strength to determine the effects of spaceflight and recovery on spinal loading. The study used previously collected CT images of the lumbar spine from nine long-duration astronauts and eight long-duration cosmonauts, with mission lengths of 4-7 months. CT images were taken pre- and post-flight to assess for changes (Burkhart et al., 2020).

By using pre-flight, post-flight, and long-term follow-up CT imaging and finite element analysis, the researchers reported that 6 months of exposure to microgravity resulted in a median 6.1% reduction in vertebral strength compared with pre-flight measures, and these deficits persisted for up to four years after return to Earth. Although the BMD measured by DXA imaging also declined, the findings suggested that DXA may have underestimated the skeletal

changes after spaceflight (Burkhart et al, 2020). Daily activities posed a low risk of vertebral fracture, however, some individuals faced moderate fracture risk during highly strenuous efforts, such as full trunk rotation and flexion, indicating the long-lasting impact of microgravity on vertebral integrity and the need for anti-OP treatment or prevention measures to protect astronaut skeletal health. Those who fly multiple missions in their lifetime, may be at a higher risk for developing OP earlier in life compared to healthy Earth-bound individuals, as well as other health complications. In addition, although the deficits in vertebral strength were modest and the risk of vertebral fracture remained low following 6 months of spaceflight, it is not known whether bone loss and declines in vertebral strength continued at the same rate or plateaued during longer duration missions, for 2-3 years. Interventions to preserve bone strength and density are warranted to allow for longer spaceflight and deep space exploration (Burkhart et al., 2020). Understanding gold-standard imaging methods to monitor OP is important, to acknowledge the limitations in medical equipment during spaceflight and to apprehend how important medical equipment is to monitor bone demineralization.

Imaging for Assessment of Osteoporosis

Dual X-Ray Absorptiometry

DXA is an imaging method that measures the density (g/cm^2) of bone mineral mass. DXA imaging is the most common and accessible method for assessing BMD. A DXA scanner utilizes two low dose x-ray beams to measure BMD and body composition (Sangondimath & Sen, 2023). These beams eliminate the soft tissues from the image (Schultz & Wolf, 2019). The x-ray beams pass through the body and are absorbed by the soft tissue and bone to create a bone density or body composition image. BMD is interpreted from the femoral neck and lumbar spine regions because these locations are the body's highest weight-bearing points and most dense bones (Dagklis et al., 2023). The femoral neck and lumbar spine trabecular bone measurements

are analyzed by T-scores (see table 1). A T-score expresses BMD in standard deviations. Using a comparator group, the T-score calculates BMD from what the peak measurements would be at aged 30 years for the matched sex and ethnicity of the patient (Alawi et al., 2021).

Table 1

T-scores to Assess Osteoporosis Using Dual X-Ray Absorptiometry

T-Score	Normal	Osteopenia	Osteoporosis	Severe Osteoporosis
Score	> -1.0	< -1.0 to >-2.5	< -2.5	< -2.5 or higher

Note. Osteoporosis z-scores are measured in g/cm^2. Values are from Sangondimath & Sen (2023). A normal T-score is anything above -1.0, and any score below -2.5 is considered osteoporotic. The score between normal and osteoporotic is considered osteopenic, meaning lower than normal BMD.

A limitation of DXA imaging is that it is a two-dimensional (2D) image, providing the interpreter less structural detail than three-dimensional (3D) modalities such as CT imaging (Sangondimath & Sen, 2023). As a result, DXA cannot directly assess volumetric BMD or differentiate trabecular from cortical bone compartments, limiting its ability to characterize bone microarchitecture and mechanical information. DXA images create areal BMD, a measurement of the amount of bone tissue projected over a 2D area, which is influenced by bone size. Smaller individuals tend to have lower areal BMD values despite potentially normal volumetric density, leading to an overestimation of fracture risk when compared with average-sized individuals (Alawi et al., 2021). This size dependency can introduce error and reduce the accuracy of clinical interpretation. Pelvic and vertebral DXA measurements are also sensitive to degenerative changes, including osteophyte formation which are developments of bony outgrowths along joint margins or vertebral bodies, from mechanical stress or degenerative changes and joint disease. Vascular calcifications may also cause artifact in imaging, because of abnormal calcium phosphate deposition within the blood vessels. These calcifications may increase x-ray attenuation and falsely elevate the measured BMD in lumbar spine DXA images. All of these

conditions artificially increase BMD values, which may produce a falsely low estimated fracture risk (Alawi et al., 2021). Furthermore, the presence of spinal pathologies or external artifact such as surgical hardware, contrast agents, or calcified soft tissues may interfere with x-ray attenuation and change BMD measurements, further compromising diagnostic accuracy.

DXA imaging is the most commonly used quantitative radiological assessment for bone mass due to its many benefits, low costs, and convenience (Alawi et al., 2021). DXA exposes individuals to minimal radiation compared with other radiographic modalities, such as x-ray or CT imaging, which reduces the associated health risks to radiation exposure. Low radiation doses allow DXA to be suitable for multiple assessments longitudinally, and to monitor changes in BMD for the management of OP. Additionally, DXA provides precise and reproducible measurements, allowing for the timely diagnosis of OP.

Computed Tomography Imaging

CT imaging is a method of diagnostic radiography that creates detailed, cross-sectional, 3D images of internal bodily structures (Kim et al., 2021). A benefit of CT scanning is the different angles at which a structure is captured. DXA imaging assesses volumetric BMD which is independent of an individual's body side (g/cm^3), as opposed to true BMD from DXA (g/cm^2); this makes CT imaging superior to DXA imaging because of the 3D capabilities. CT imaging creates accurate, detailed evaluations of both cortical and trabecular components and precise values of bone mass. CT imaging may be used for musculoskeletal assessments in elderly individuals who have advanced lumbar spine degeneration or morphological abnormalities, as opposed to DXA imaging to decrease irregularities in scanning or artifact that creates false negatives (Sangondimath & Sen 2023). CT imaging is informative for individuals with irregular complexities since high quality and specific images can provide increased treatment outcomes (Alawi et al., 2021). There are several measures taken during a CT scan, including identifying

landmarks such as a region of interest. From the region of interest, the cortical and trabecular measurements can be taken (Kim et al., 2021).

Region of interest refers to a defined subset of the total volume in an imaging dataset or 3D model where detailed analysis or measurements are focused. A region of interest can be applied to the femur where a standardized segment of the femur is extracted from the image and bone microarchitecture is analyzed and ensures consistency across samples. Generally, the most common region of interest when analyzing trabecular thickness is anywhere from 2-4 mm from the distal growth plate because it is structurally consistent and sensitive to bone microarchitectural changes (Kim et al., 2021). Using a fixed distance from the growth plate provides consistent and standardized measurement locations across animals to reduce the variability by anatomical differences.

Cortical bone is a key determinant of bone shape, strength, and fracture risk (Kim et al., 2021). Cortical bone is the outer layer of bone and sometimes referred to as compact bone. This area of bone provides most of the bone's mechanical strength, particularly in weight-bearing regions. Cortical bone changes such as thinning and increased porosity are seen in individuals with OP. Micro-CT imaging provides high-resolution images of cortical bone thickness and area (Kim et al., 2021). The cortical bone measurements are typically taken in the mid-shaft of the femora, at a defined region of interest, to produce replicability between samples. The cortical thickness, cortical area, and cortical porosity are measured to quantify cortical bone structure (Kim et al., 2021).

Trabecular bone, also known as cancellous bone, is found inside the cortical bone. It is the inner and porous skeletal tissue within bone. A high trabecular value from a CT image indicates healthy bone and a low trabecular score may indicate osteoporotic changes (Sangondimath & Sen, 2023). The standardized method to assess trabecular bone is by analyzing

the trabecular number, thickness, and separation. These values represent the number of connections between trabecular structures per cubic millimeter of volume (see Table 1). These measurements assess the spatial structure of the bone, allowing for the quantification of osteoporotic changes within the skeletal tissue (Kim et al., 2021). Bone microarchitectural assessment aids in diagnosis and the treatment of OP, and is vital for exercise and pharmaceutical prescriptions, to lower the risk of fracture and fragility.

Exercise for Osteoporosis

Exercise is a primary treatment used to attenuate the effects of OP on the skeletal system. Exercise is a valuable preventative measure and treatment for OP. Exercise improves muscular strength, flexibility, coordination, balance, reaction time, and endurance, which may translate into a reduced risk of falls, which ultimately prevents fractures for individuals with OP (Pasqualini et al., 2019).

Strength training is highly recommended for individuals with OP or those at risk because it stimulates osteogenesis, the formation of new skeletal bone tissue. This process increases both trabecular and cortical bone deposition, thereby, enhancing the overall skeletal mechanical integrity (Pasqualini et al., 2019). Strength training produces extraneous forces on the skeletal system through mechanical loading, which serves as the primary stimulus for bone formation. Exercises should target large muscle groups, particularly in the regions with the highest fracture risk, such as the pelvic region (Morin et al., 2023).

Another critical exercise pillar for menopausal females to focus on is weight-bearing activities (Park et al., 2017). Weight-bearing and impact exercise (walking or running) loads the musculoskeletal system, subsequently creating compression, bending, and rotational forces in the bones and joints. A combination of these forces creates osteogenesis during exercise sessions, which ultimately helps balance the bone remodeling cycle through extrinsic stress (Dagklis et al.,

2023). The application of mechanical loads through weight-bearing exercise produces a thickening of trabecular and cortical bone and, consequently, an improvement in BMD and mechanical strength (Pasqualini et al., 2019).

Postural and balance training are also essential components in the management of OP. Postural exercises that target the abdominal musculature, spinal extensors, and shoulder stabilizers can improve excessive thoracic kyphosis and overall spinal alignment. Kyphotic postural changes alter an individual's center of gravity, thereby, impairing postural stability and increasing the risk for falls (Morin et al., 2023). Because falls are a primary cause of osteoporotic fractures, balance training plays a critical role in fracture prevention and functional independence. The Canadian OP clinical guidelines state that individuals with OP should follow a balance and functional fitness program a minimum of twice weekly. Balance exercises should include body weight shifting or reaction to objects that may upset equilibrium, such as throwing or catching a ball. Dynamic and static balance exercises are also recommended, such as one-legged standing or calf raises. Functional exercises that replicate activities of daily living, such as sit-to-stand transfers and stair climbing, are also recommended, as they incorporate body weight or external resistance that imposes mechanical loading on the skeletal system, thereby promoting osteogenic adaptation (Bilek et al., 2016). Exercises that are contraindicated are anything rapid, ballistic, sustained, at the total end of range, and involve twisting or flexion of the spine. Impact exercises should be performed at a moderate intensity level, considering age, fitness level, and fracture risk (Morin et al., 2023). Prior research shows that exercise is osteogenic, which explains why it is an effective intervention for improving OP and osteopenia, while reducing risk of falls and fractures (Morin et al., 2023).

Purpose

ECSWT has been investigated as a potential adjunctive treatment for OP due to its capacity to stimulate osteogenesis by mechanotransduction and the upregulation of osteogenic signaling factors (Makert et al., 2017; Wang et al., 2014). Pre-clinical studies have demonstrated increased osteoblastic activity, improved bone microarchitecture, and significant increases in BMD following ECSWT treatment (Lama et al., 2017; Makert et al., 2017; Wang et al., 2014). Although these findings support the biological plausibility of ECSWT, current evidence remains insufficient to standardize clinical application for OP. Treatment parameters regarding energy flux density, frequency, and application have not yet been established for clinical practice.

ECSWT may have therapeutic value in environments with reduced mechanical loading, such as microgravity, and in individuals with mobility impairments requiring immobilization, where maintenance of BMD is challenging. In these populations, circulating bone turnover biomarkers, including OCN and BAP, may provide a practical method for assessing bone demineralization and monitoring skeletal status, since prior literature indicates an inverse relationship (Singh, 2015). This approach may also be especially beneficial for individuals residing in rural or remote communities, patients with significant mobility limitations, and astronauts during spaceflight, where access to gold-standard imaging modalities such as DXA and CT are limited. The purpose of the study was to examine the effects of ECSWT on osteoporotic changes evident on imaging and blood biomarkers using a pre-clinical model. The following questions guided the research study:

1. Does ECSWT improve bone microarchitecture (cortical and trabecular bone thickness) in the pre-clinical ovariectomy model of OP?
2. Does ECSWT alter blood biomarkers of bone remodeling (OCN and BAP) in the pre-clinical ovariectomy model of OP?

The independent variables in the study were ECSWT treatment and OXV condition. The treatment and condition were randomly assigned to the animals. The dependent variables were blood biomarkers (OCN and BAP concentration) and bone microarchitecture (cortical and trabecular bone thickness). Each treatment and condition group were assigned a placebo and sham counterpart. The ECSWT treatment group (n=8) had a placebo group (n=8) to control for internal validity. The OXV condition group (n=8) also had a sham counterpart (n=8). Random assignment was used to control for biases and equalize each group, treatment, and condition.

Chapter 3: Methodology

Animals

This study was conducted with the approval of the Lakehead University Animal Care Committee). The animals ordered included 3-month-old female Sprague-Dawley rats (Lama et al., 2017). At 3-months of age, the rat's genital glands and endocrine system reach maturity. Their muscles and skeleton are also well formed by this time. 3 months old mimics 20–25 years of age in humans, which is when typical peak bone mass occurs (Luengo-Mateos et al., 2024). Determined using a power analysis, 32 rats were required to achieve statistical significance and have sufficient power. This ensured a medium effect size, 0.80 statistical power, and a *p*-value of .05. This was determined as the study was a 2 x 2 design, consisting of two conditions and two treatments. A medium effect size balanced statistical power and also determined if any clinical significance was present. The Sprague–Dawley rats underwent an OVX or sham surgery by the vendor, Charles River Laboratories, before arriving at the Lakehead University Animal Care Facility (LUACF). The rats were housed and fed according to LUACF standard operating procedures (SOPs), under the care of a veterinarian and a veterinarian technician. The rats were monitored daily and organized using ear notching. The frequency of monitoring was increased to twice daily if decreased health was observed. The rats had access to social housing, firm nesting materials, and tubes, as these measures were implemented to promote natural behavior, reduce stress, and follow animal care guidelines. The rats were housed for 16 weeks before any treatment intervention following LUACF animal care guidelines, to allow for osteoporotic and hormonal changes to develop and occur (Lama et al., 2017).

Procedure

Ovariectomy

As the importance of female reproductive hormones and menopause becomes increasingly recognized, the OVX protocol was important for advancing post-menopausal research. An OVX is the bilateral removal of the ovaries (see Figure 8; Luengo-Mateos et al., 2024). By removing the ovaries, it induces a change of physiology in the rat. Ovaries are the primary producing estrogen gland, therefore, after approximately 1 month, a rapid decline in estrogen occurs (Lelovas et al., 2008). Estrogen is a key modulator to balance bone resorption and formation. This decline in estrogen subsequentially leads to bone demineralization. Once the estrogen levels plummet and stabilize is when stable, chronic, osteoporotic changes may occur (Luengo-Mateos et al., 2024). This was the rationale for implementing a 4-month transition period to allow for hormonal and osteoporotic changes to occur (Lama et al., 2017). This enabled a stable, chronic rate of bone loss at 4 months and further homogenized the osteoporotic changes in the rat sample (Luengo-Mateos et al., 2024). Only 16 of the rats had a bilateral OVX to induce OP, while the remaining 16 rats had a sham surgery in which the ovaries remained intact (Lama et al., 2017). The sham surgery animals underwent an identical procedure as the OVX animals, but without ovary removal, serving as a control for anesthesia and surgical stress. They were also housed for 4 months to acclimate, and recover from surgical procedures, as well as promote natural behavior in the new habitat.

Figure 8

Ovariectomy Diagram

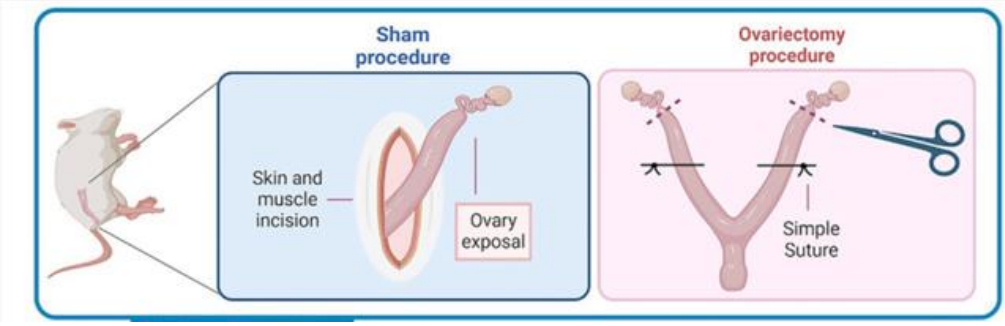

Note. Illustrated diagram of rat ovariectomy (OVX), from the study by Luengo-Mateos et al. (2024). This procedure must be performed bilaterally of the flank in the rat.

Focused Extracorporeal Shockwave Therapy

The 32 rats were randomly assigned to four groups in a two-by-two design, representing condition and treatment (n=8). The treatments included ECSWT and placebo, and the condition was OVX versus sham. The ECSWT and placebo treatment followed the ECSWT treatment parameters used by Lama et al. (2017). All of the treatments were performed at LUACF by a member of the research team who had experience with ECSWT treatment administration, with veterinary technician assistance, and in accordance with LUACF SOPs. Demographic information was also recorded before and after 5 weeks of treatment (body mass, age, and blood volume). The rats were anesthetized during preparation and during ECSWT or placebo treatment. Once anesthesia took effect, the right anterior and lateral hind leg region of the rat was shaved. Ultrasound gel was applied to the treatment area as a coupling agent, and the ECSWT was then administered based on the treatment group randomly assigned to. After each treatment, animals were returned to their cages to recover. The rats were monitored post-treatment, and analgesics (5 mg/mL solution of Children's Tylenol in the rats' drinking water) was administered accordingly after ECSWT, if an adverse reaction occurred. Each animal in the

ECSWT treatment received 5 weeks of focused ECSWT treatments using the Storz Duolith® SD1 Ultra electromagnetically generated unit, to the right anterior and lateral thigh (see Figure 9). A high intensity ECSWT treatment was administered, for a total of 1,000 shockwaves at an intensity of energy flux density 0.33 mJ/mm^2 at 3 Hz (Lama et al., 2017). The entire treatment took a total of 6-7 minutes. The total energy level was calculated in Joules (J) and recorded in Excel. The placebo treatment received a similar treatment protocol; however, the device was deactivated and specialized soft-rubber tip was placed on the device applicator during placebo shockwave therapy, creating an air gap between the rat and the device, and the rat did not receive the ECSWT, but a similar sound was produced simulating the same appearance to ECSWT treatment. The treatment was completed once weekly for 5 weeks.

Figure 9

Femur Treatment Site

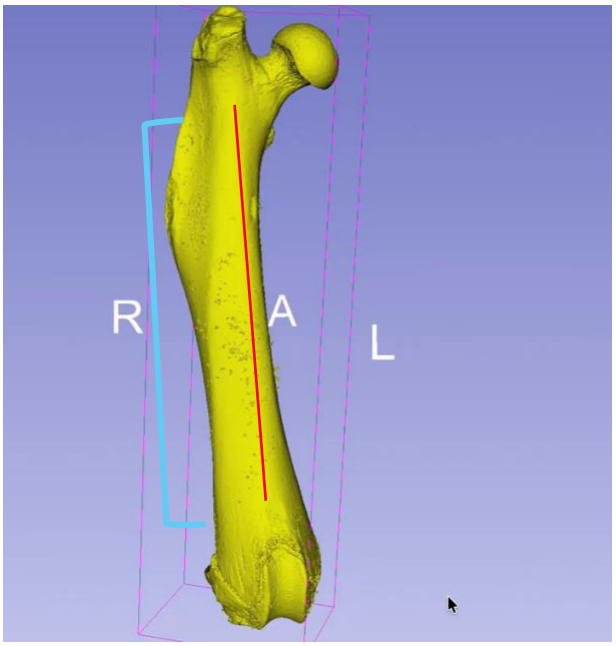

Figure 9 represents a reconstructed rat femur. ECSWT therapy was administered as indicated by the red line anteriorly and by the blue line laterally.

Blood and Femur Extraction

Blood and femoral samples were collected and dissected 1 week following the final treatment to permit the effects of ECSWT. The exsanguination and dissection of the rats occurred at the LUACF facility with supervisor assistance. The first step was to anesthetize the rat using isoflurane and a toe pinch test was performed to ensure the rat was under deep anesthetic plane. A cardiac puncture is terminal because of the structural damage to the heart muscle and the volume of blood drawn is considered to be fatal (Beeton et al., 2007). See Appendix F to review the LUACF SOPs for a cardiac puncture. The rat was then placed in supine and their limbs restrained. After this, the fur and skin on the thorax was removed using a scalpel and scissors to expose the structures below. The thoracic cage was cut open to expose the heart. A 3 mL to 12 mL syringe and an 18 or 21 G x 1" to 1.5" needle was prepared and inserted into the rat at a 5–15° angle immediately caudal to the xyphoid process. It was inserted approximately 1-3 mm deep into the rat's cardiac tissue (Beeton et al., 2007). A drop of blood came into the needle, confirming that the puncture was effective. Once the blood appeared, the needle was stopped and steadied and not inserted any deeper. The plunger was slowly pulled back until the required sample volume of blood was obtained (Beeton et al., 2007). The rat was then euthanized by removal of the heart and head, leading to exsanguination, following LUACF's euthanasia SOPs (see Appendix G) after the cardiac puncture while under deep anesthesia. The heads were sent to the University of Toronto, Department of Anthropology, for further research using the OVX rat model and exploring the effects of ECSWT on shape variation in the bony labyrinth (Ward et al., 2022). 0.5 mL of sodium ethylenediaminetetraacetic acid (EDTA) anticoagulant was added to the blood samples before they were centrifuged, to extract the plasma. The plasma samples were stored in a labelled test tube and placed in a -25°C

freezer located at the Northern Ontario School of Medicine University (NOSMU) wet lab until enzyme-linked immunosorbent assay analysis (ELISA) analysis was completed.

After the blood sample was collected and exsanguination occurred, the right femur was dissected and extracted. The femoral dissection followed the protocols by Kim et al. (2021) on how to prepare and perform a micro-CT image of a rat femur for analysis. The rat femur was dissected after euthanasia was completed. Scissors were used to cut through the fur and skin of the rat, on the area of the acetabulofemoral joint, down to where the tibiofemoral joint was located (distance of the femur). From there, the skin was cut and opened to reveal the soft tissue beneath. When the tissue was cut, and the femur exposed, the acetabular and tibiofemoral joint was dislocated and tendons and ligaments severed and removed. Once the bone was extracted, a paper towel was used to dry excess moisture from the bone and any additional tendon, ligament, or soft tissue was cut off while keeping the femur intact (Kim et al., 2021). After dissection, the femur was stored in 4% paraformaldehyde at 4°C until future analysis was to be completed (Kim et al., 2021). Each femur was in an individual test tube, sealed and labelled by treatment or OVX, and additionally labelled with an Excel code sheet. The blood and femur samples were transported according to Lakehead University biohazard transportation protocol (see Appendix H) and stored in the NOSMU wet laboratory for future analysis.

Micro-Computed Tomography Analysis

Cortical and trabecular bone microarchitectural measurements were assessed using micro-CT imaging. The femoral samples were shipped by Thunder Bay Broom and Chemicals as per Lakehead University SOP biohazard shipping protocols (see Appendix H) and mailed by FedEx to Mahler Small Animal Imaging Lab located on the University of Toronto campus. The imaging protocol was based off the same method as Toyama et al. (2023). All specimens were

imaged using a Skyscan® x-ray microtomography 1173 (camera pixel size 50 µm; voxel resolution 9.6 - 11 µm; source voltage 58 kV; source current 137 µA). A pair of Bruker BMD standards (BMD phantom set SP-4002) were included in each scan for calibration of density measurements (Toyama et al., 2023). The image stacks were reconstructed via "NRecon" V1.7.4.6 (Bruker microCT, Kontich, Belgium). The software used to select a volume that included a representative portion of the midshaft of the femur was CTan (roughly 20-50% of the total femur length; v.1.11.0, SkyScan, Bruker microCT, Belgium). This segmented volume included both the bone tissue and surrounding soft tissues (Toyama et al., 2023). The density of the isolated volume was calculated using the BMD phantoms included in the scans and were binarized (Bruker microCT, 2010), separating bone tissue from the surrounding tissue by applying a mineral density threshold of 0.75 g/cm^3 following visual examination (Toyama et al., 2023). All tissue below this threshold was removed from the analyses.

Figure 10

Computed Tomography Imaging Locations

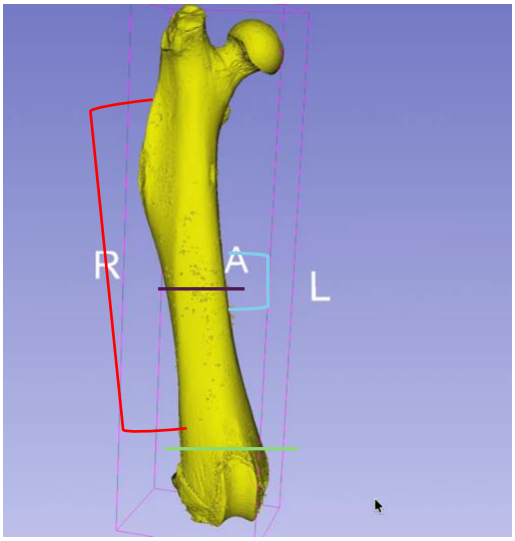

Figure 10 is an image of a reconstructed rat femur. The mean 80% of the diaphysis BMD measurement was completed as indicated by the red line. The central 10% of the diaphysis was completed as indicated by the blue line. The femur was sliced midshaft to measure the cortical thickness, as indicated by the purple line. The femur was sliced at the distal metaphysis to measure the trabecular thickness, as indicated by the green line.

Cortical Thickness Analysis

The cortical thickness analysis was done using 3D Slicer® software. A .ply file of the reconstructed rat femur was inputted, sliced perpendicular using Easy Clip surface model. The arrow tip was placed to align with the shaft of the femur then clipped. The points list was created from points 1 through 8, on the cortical surface from medial to lateral and anterior to posterior, through the midshaft of the right femur (see Figure 9). Then the files with the plotted points were exported, a naming scheme was defined and saved as a script file. The files were analyzed using R studio® coding software, producing landmark distribution values. Each measurement was regressed for body mass by code.

Figure 11

Cortical Bone Thickness Plotted Points

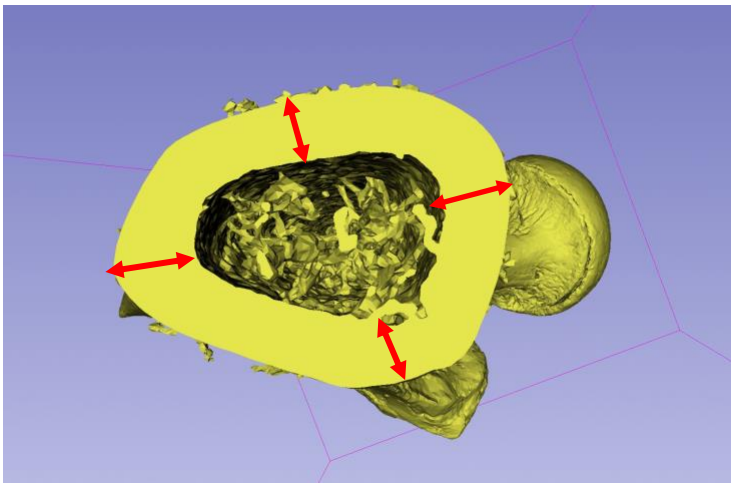

Note. Points were plotted 1 through 8 to measure thickness on each anatomical surface (anterior, posterior, medial, and lateral).

Trabecular Thickness Analysis

Trabecular thickness was measured using a Skyscan® x-ray microtomography 1173. Trabecular thickness, meaning the diameter of the trabecular surface, was extracted using a reconstructed .ply file of the right sided rat femur, using 3D Slicer®. The samples were cut in

half, perpendicular to the long axis of the femur, just above the tibiofemoral joint surfaces. Eight points were plotted along the cortical surfaces and the diameter was measured between the mediolateral and anteroposterior landmarks of the trabecular surface (see Figure 10). the files with the plotted points were exported, a naming scheme was defined and saved as a JSON script file. The script files were analyzed using R studio® coding software, producing a table of landmark distribution values. Each measurement was regressed for body mass by code.

Figure 12

Trabecular Bone Thickness

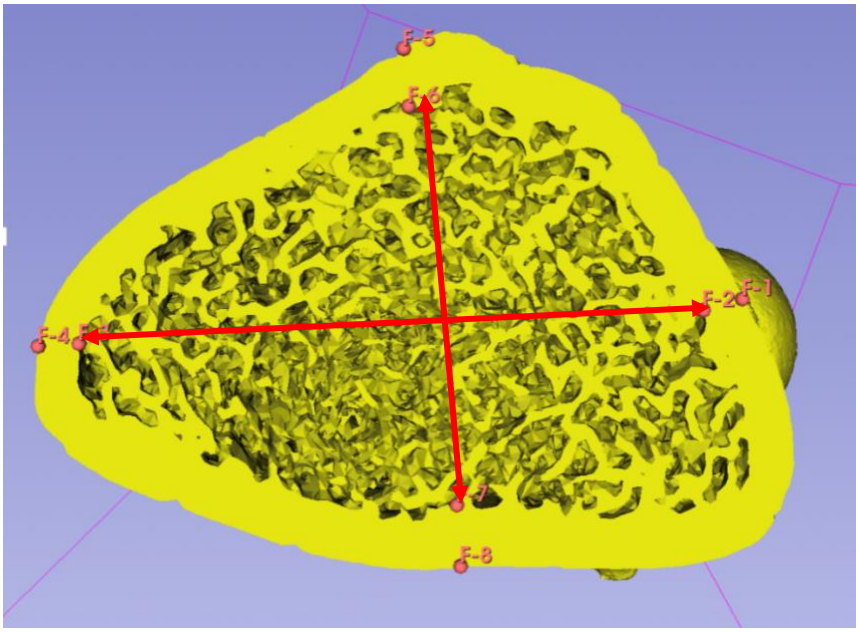

Note. Red lines indicate surfaces measured by landmarks. Mediolateral (F.2-F.3) were measured and anteroposterior (F.6-F.7) thickness were analyzed.

Blood Biomarker Analysis

The blood biomarkers were analyzed in the NOSMU Wet Laboratory using the Biotechne® OCN rat ELISA kit and the Biomatik BAP rat ELISA kit. See Appendix C and D for the supplies required for both kits. The kit used was a sandwich ELISA (see Figure 11). See Appendix I for the manufacturer's instructions, which was followed for the analysis. A plate map was created prior to the analysis. Samples were run in duplicate for consistency, and the mean

measurement of each sample was considered for analysis (Biotechne Manual, 2025). The samples were read at 450 nm wavelength using Cytation 5® plate reader by BioTek (Biotechne Manual, 2025). The standard curve graph was created after the plate was read. The standard curve was plotted as the concentration of each standard solution (Y-axis) versus the absorbance of the standard solution (X-axis; Aydin et al., 2025). OCN and BAP concentration were calculated from the plate reader and analyzed on Excel sheets. Based on the manufacturer's instructions (see Appendix I), a standard curve was created using the ELISA kit standards (see Appendix J). The curve equation was then applied to the mean samples to solve for the concentration. Each concentration value was then plotted along the curve to assess OCN and BAP concentration.

Figure 13

Sandwich ELISA

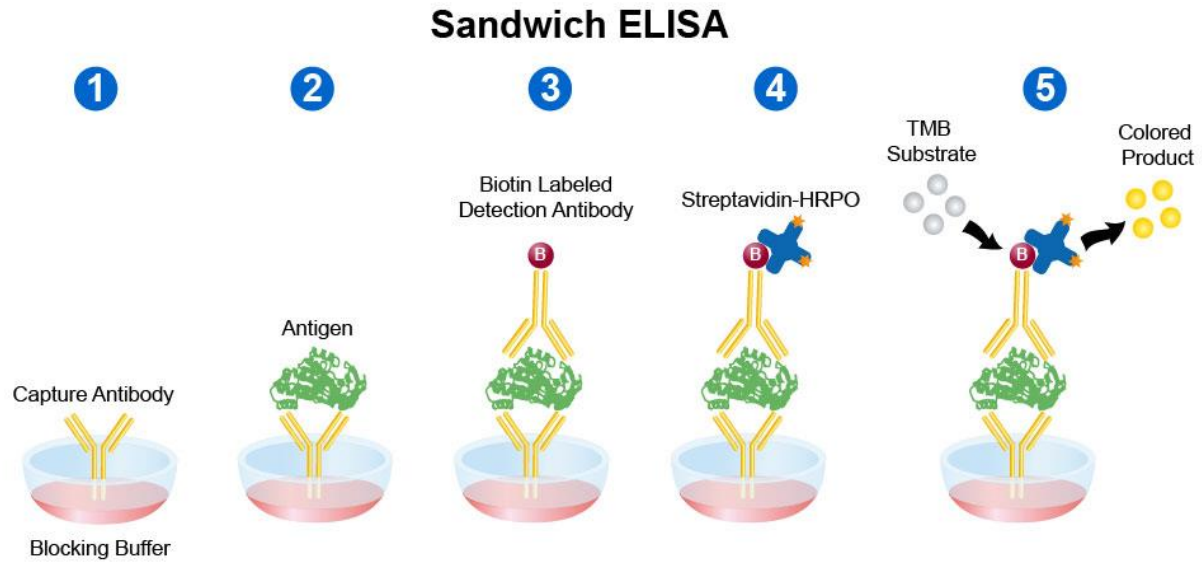

Note. Figure 11 depicts an individual plate well. A capture antibody is placed first into the well, to immobilize and trap the antigen of interest. Second, the antigen is put into each well. The detection antibody immobilizes and sandwiches the antigen of interest. It also binds with streptavidin HRP in stage 4 to amplify the detection signal. A TMB substrate is added and produces a blue-colored compound, then a stop solution to stabilize the reaction before it is read by a plate reader. If the antigen is not present, the wells will look like step 1 through the entirety and have no color reaction (Aydin et al, 2025).

Statistical Analysis

The independent variables of the study were treatment group (ECSWT and placebo treatment) and condition (OVX and sham surgery). The dependent variables of the study were bone microarchitecture (cortical and trabecular bone thickness) and blood biomarker concentration (OCN and BAP). The data was analyzed using IBM© SPSS for Mac© IOS version 31.0.2.0. The analysis was between subjects, using a two-way analysis of variance (ANOVA) for independent measures design, which compared the mean differences, split between independent variables (factors) and was used to simultaneously analyze the effects of multiple factors on the dependent variable, respectively. The alpha level for statistical analyses was set at $.05$. The trabecular bone thickness was measured by the mediolateral thickness and anteroposterior thickness (μm). The cortical bone thickness was measured on the medial, lateral, anterior, and posterior aspect (μm).

Chapter 4: Results

The results of the present study provide insight on whether ECSWT had an effect on osteoporotic differences such as trabecular and cortical bone thickness, and blood biomarkers such as OCN and BAP. An independent measures, between subjects, two-way ANOVA was performed to explore the effects of treatment and condition on blood biomarker concentration and bone microarchitecture. The following section uses inferential statistics to answer the research questions. The descriptive statistics and demographic information from the study is also provided in this section.

Animals

Table 2 contains the demographic information for the rats, including sample size, age, mass, and blood volume. Half of the rats underwent an OXV surgery, and the other half underwent a sham surgery. These measurements were taken to observe homogeneity in the sample, and to monitor the animal's health during the total 22-week period they were housed and treated in LUACF. Table 3 contains the rat age and treatment during the time of exsanguination as well as the energy used for the treatment in J. See Table 4 for the mean differences between rat body mass, pre- and post-intervention

Table 2

Rat Demographic Information

Number of rats	32
Rats receiving ovariectomy	16
Rats receiving sham surgery	16
Rats receiving ECSWT treatment	16
Rats Receiving placebo treatment	16
Age at exsanguination (days)	284.50+/-7.78
Blood volume collected, day of exsanguination (mL)	4.77+/-0.78

Note. The study design entails two conditions (ovariectomy (OVX) and sham surgery) and two treatments (extracorporeal shockwave therapy (ECSWT) and placebo treatment), n=8 per condition and treatment combined, N=32 total. Mean and standard deviation (+/-) for age was recorded in days and blood volume in millilitres.

Table 3

Rat Age and Treatment

Age at exsanguination (placebo with sham)	276
Age at exsanguination (ECSWT with sham)	281
Age at exsanguination (Placebo with OVX)	287
Age at exsanguination (ECSWT with OVX)	294
Energy per treatment (J)	7.358
Total energy administered after five treatments (J)	36.79

Note. Age was recorded in days. Energy administered was reported in Joules (J). The table lists each condition group (ovariectomy (OVX) and sham surgery) and treatment group (extracorporeal shockwave therapy (ECSWT) and placebo).

Table 4

Differences in Rat Body Mass

	Pre-Treatment	Post-Treatment
Sham surgery with placebo treatment	258.62+/-6.92	409.37+/-27.13
Sham surgery with ECSWT treatment	257.12+/-10.56	390.87+/-34.60
OVX with placebo treatment	265.62+/-10.83	452.25+/-40.38
OVX with ECSWT treatment	262.87+/-12.45	493.87+/-43.84

Note. Body mass was measured in grams (g) pre- and post-treatment. Mean and standard deviation (+/-) were reported above, between ovariectomy (OVX) and sham surgery, and extracorporeal shockwave therapy (ECSWT) treatment and placebo treatment.

A repeated measures ANOVA with a Greenhouse-Geisser correction determined that mean body mass (g) differed statistically significantly, between the two time points ($F(1, 28)=30.94$, $p=.001$, $\eta^2=.525$) with a large effect size. The results revealed the OVX rats had a higher body mass overall, indicating that the intended hormonal changes occurred as increased body mass is a side effect from decreased estrogen (Lelovas et al., 2008). Post hoc testing using a Bonferroni adjustment revealed that body mass had a statistically significant increase between OVX and sham surgery conditions (175.53 (95% CI, 163.28 to 187.79) g, $p=.001$, see Figure 12).

Figure 14

Mean Rat Body Mass Pre- and Post Intervention

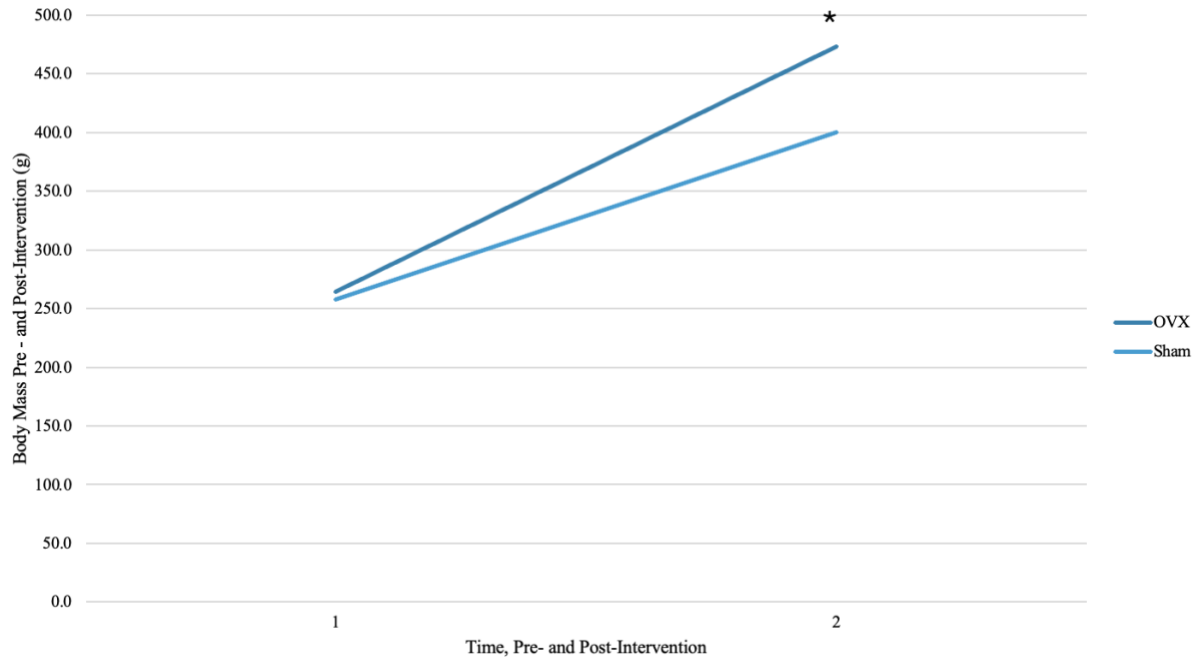

Note. Figure 12 demonstrates the body mass differences between ovariectomized (OVX) rats and sham surgery (sham) treated rats pre- and post-intervention. 1 indicates body mass pre-treatment, 2 indicates body mass post-treatment. * Denotes statistical significance between OVX and sham surgery (p=.001).

Question 1: ***Does ECSWT improve bone microarchitecture in the pre-clinical ovariectomy model of OP?***

Bone Mineral Density

See Table 5 for central 10% BMD of the right femur descriptive statistics, including mean and standard deviation for each treatment (ECSWT and placebo) and condition (OVX and sham surgery). See Table 6 for BMD of 80% of the femoral diaphysis descriptive statistics, including mean and standard deviation for each treatment (ECSWT and placebo) and condition (OVX and sham surgery).

Table 5

Mean and Standard Deviation of Bone Mineral Density for Central 10% of the Right Femur

Sham surgery with placebo treatment	1.53+/-0.059
Sham surgery with ECSWT treatment	1.47+/-0.055
OVX with placebo treatment	1.49+/-0.053
OVX with ECSWT treatment	1.48+/-0.073

Note. The table lists the mean and standard deviation (+/-) for each condition (ovariectomy (OVX) and sham surgery) and treatment (extracorporeal shockwave therapy (ECSWT) and placebo). Findings were reported in g/cm^2.

A two-way independent-measures ANOVA was performed to assess the interaction and main effects of ECSWT treatment and OVX condition on the BMD of the central 10% of the right femur. The analysis revealed no statistically significant interaction effect between treatment and condition ($F(1, 28)=1.37$, $p>.05$, $\eta^2=.05$) with a small effect size. There was no statistically significant main effect of treatment on central 10% BMD (ECSWT and placebo; $F(1, 28)=3.03$, $p>.05$, $\eta^2=.098$) with a small effect size. The findings revealed that ECSWT had no effect on central 10% BMD, meaning the density of the right femur had no changes from the ECSWT treatment. There was also no statistically significant main effect of condition (OVX and sham surgery) on central 10% BMD ($F(1, 28)=0.32$, $p>.05$, $\eta^2=.011$) with a small effect size (see Figure 13).

A Levene's Test was also performed to assess the assumption of homogeneity of variance across the OVX, sham, ECSWT, and placebo groups. The results revealed that the assumption of equal variance was met for the variable BMD, since it was not statistically significant ($F(3,28)=0.65$, $p>.05$)

Figure 15

Mean Bone Mineral Density for Central 10% of the Right Femur

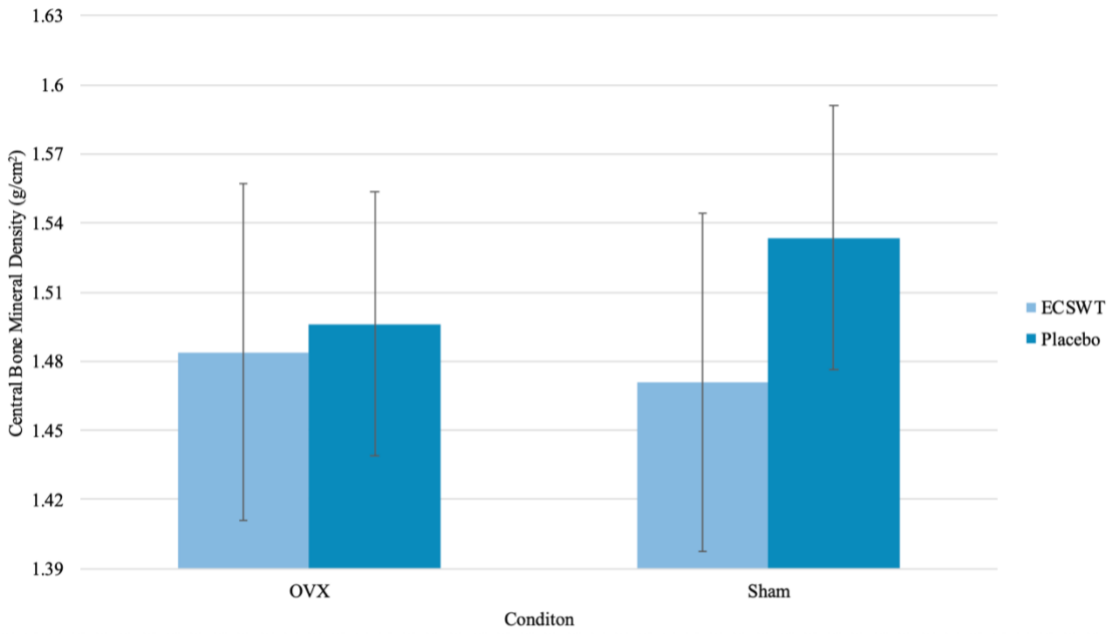

Note. Nonsignificant interaction or main effects were observed for central bone mineral density in ovariectomy (OVX) or sham surgery conditions (p=.525) and extracorporeal shockwave therapy (ECSWT) and placebo treatment (p=.092).

See Table 6 for femoral shaft BMD descriptive statistics, including mean and standard deviation for each treatment (ECSWT and placebo) and condition (OVX and sham surgery).

Table 6

Mean and Standard Deviation of Bone Mineral Density for 80% of the Right Femoral Diaphysis

Sham surgery with placebo treatment	1.59+/-0.057
Sham surgery with ECSWT treatment	1.49+/-0.059
OVX with placebo treatment	1.53+/-0.064
OVX with ECSWT treatment	1.51+/-0.069

Note. The table lists the mean and standard deviation (+/-) for each condition (ovariectomy (OVX) and sham surgery) and treatment (extracorporeal shockwave therapy (ECSWT) and placebo). Findings were reported in g/cm^2.

A two-way independent-measures ANOVA was performed to assess the interaction and main effects of ECSWT treatment and OVX condition on BMD of the right femoral shaft. The analysis revealed no statistically significant interaction effect between treatment and condition ($F(1,28)=2.35$, $p>.05$, $\eta^2=.078$) with a small effect size. There was a statistically significant main effect of treatment on BMD of the right femoral shaft (ECSWT and placebo; $F(1, 28)=7.84$,

p=.009, η^2=.219) with a large effect size. The findings suggest that sham placebo treatment group had the highest BMD, compared to the sham ECSWT group. The OVX and sham surgery condition had no effect on BMD of the right femoral shaft (F(1, 28)=0.759, p>.05, η^2=.026) with a small effect size. Simple main effect analysis demonstrated there was statistically significant changes between ECSWT treatment and placebo groups, between the two sham surgery conditions (p=.005; see Figure 14).

A Levene's Test was also performed to assess the assumption of homogeneity of variance across the OVX, sham, ECSWT, and placebo groups. The results revealed that the assumption of equal variance was met for the variable BMD of the right femoral shaft, since it was not statistically significant (F(3,28)=0.27, p>.05)

Figure 16

Mean of Bone Mineral Density for 80% of the Right Femoral Diaphysis

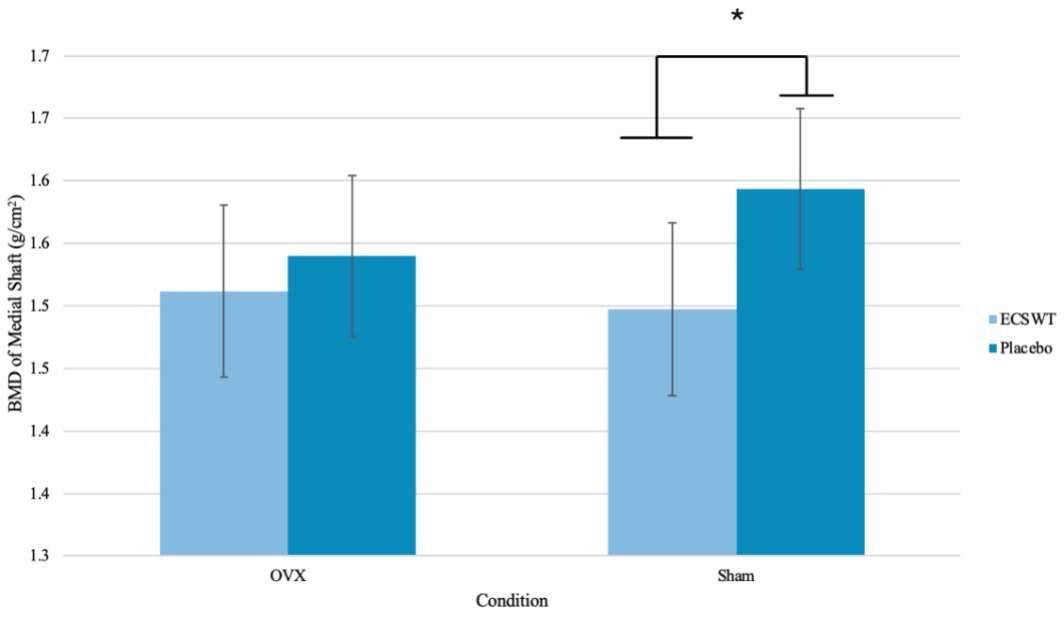

Note. A statistically significant main effect was observed for bone mineral density (BMD) of the femoral shaft in the sham surgery group (sham), between extracorporeal shockwave therapy (ECSWT) and placebo treatment (p=.005). No significance was reported in ovariectomized (OVX) groups (p=.795). A significant simple main effect was observed between the ECSWT and placebo groups within the sham condition (p=0.009) * Denotes statistical significance (p≤.05).

Medial Cortical Bone Thickness

See Table 7 for medial cortical bone thickness descriptive statistics including mean and standard deviation for each treatment (ECSWT and placebo treatment) and condition (OVX and sham surgery).

Table 7

Mean and Standard Deviation of Medial Cortical Bone Thickness

Sham surgery with placebo treatment	0.163+/-0.0097
Sham surgery with ECSWT treatment	0.166+/-0.011
OVX with placebo treatment	0.158+/-0.012
OVX with ECSWT treatment	0.150+/-0.005

Note. The table lists the mean and standard deviation (+/-) for each condition (ovariectomy (OVX) and sham surgery) and treatment (extracorporeal shockwave therapy (ECSWT) and placebo).

A two-way ANOVA for independent measures was performed to compare the interaction effects and main effects of treatment and condition on medial cortical bone thickness. The results revealed that the treatment and condition had no statistically significant interaction effect on medial cortical bone thickness ($F(1,28)=2.83$, $p>.05$, $\eta^2=.092$) with a medium effect size. There was a statistically significant main effect in medial cortical bone thickness between condition (OVX and sham surgery; $F(1,28)=8.395$, $p=.007$, $\eta^2=.231$) with a large effect size, meaning that the OVX created a decrease in medial cortical bone thickness. There was no statistically significant main effect between treatments (ECSWT and placebo treatment; $F(1,28)=0.47$, $p>.05$, $\eta^2=.016$) with a small effect size. Simple main effect analysis revealed there was a statistically significant difference in medial cortical bone thickness in the groups that received an OVX ($p=.003$), compared to the groups that received sham surgery treatment. The medial cortical bone thickness was decreased in the OVX condition groups.

A Levene's Test for homogeneity was also performed to assess the equality of variances in the data between treatment and condition. The results revealed that the assumption of equal

variance was met for the variable medial cortical bone thickness, since it was not statistically significant ($F(3, 28)=.29$, $p>.05$).

Figure 17

Mean Medial Cortical Bone Thickness of the Right Femur

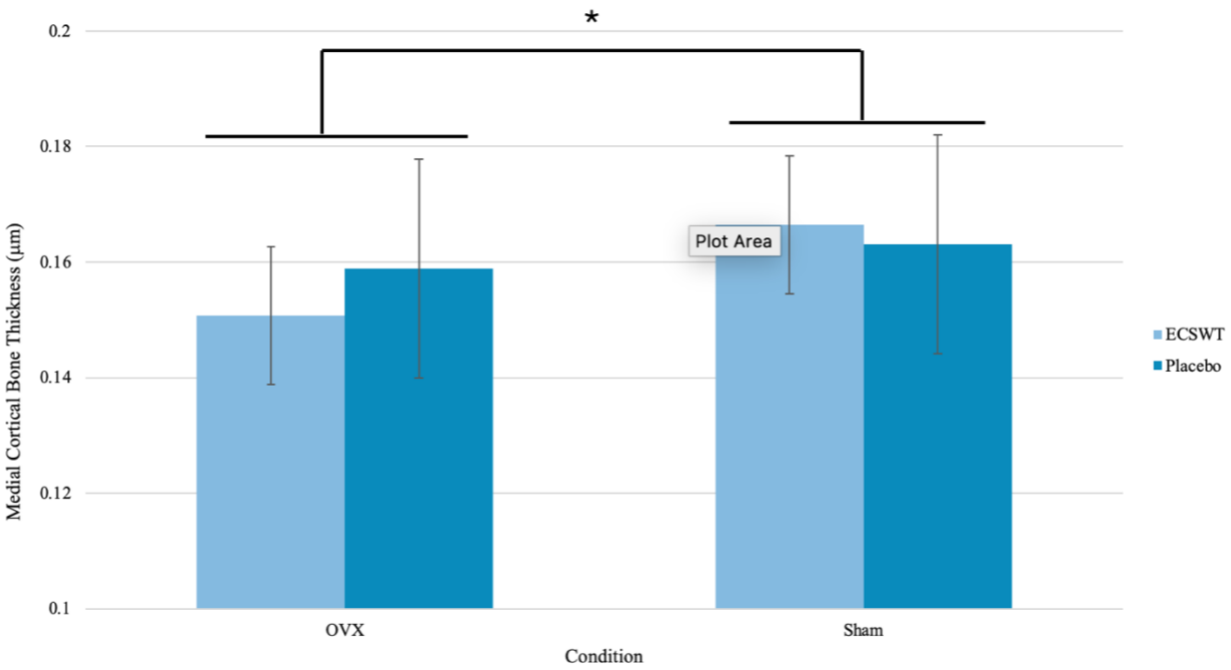

Note. A statistically significant main effect in medial cortical bone thickness was revealed between conditions (ovariectomy (OVX) and sham). * Denotes statistical significance, (p=.007).

Lateral Cortical Bone Thickness

See Table 8 for lateral cortical bone thickness descriptive statistics including mean and standard deviation for each treatment (ECSWT and placebo treatment) and condition (OVX and sham surgery).

Table 8

Mean and Standard Deviation of Lateral Cortical Bone Thickness

Sham surgery with placebo treatment	0.21+/-0.028
Sham surgery with ECSWT treatment	0.19+/-0.026
OVX with placebo treatment	0.22+/-0.032
OVX with ECSWT treatment	0.24+/-0.025

Note. The table lists the mean and standard deviation (+/-) for each condition (ovariectomy (OVX) and sham surgery) and treatment (extracorporeal shockwave therapy (ECSWT) and placebo). Findings were recorded in µm.

A two-way ANOVA for independent measures was performed to compare the interaction effects and main effects of treatment and condition on lateral cortical bone thickness. The results revealed that treatment and condition had no statistically significant interaction effect on lateral cortical bone thickness, ($F(1,28)=6.020$, $p=.058$, $\eta^2=.123$) with a large effect size. There was a statistically significant main effect in lateral cortical bone thickness between condition (OVX and sham surgery, $F(1,28)=6.17$, $p=.019$, $\eta^2=.180$) with a large effect size. There were no statistically significant main effects in treatment groups (ECSWT and placebo treatment, $F(1,28)=.027$, $p>.05$, $\eta^2=.001$) with a small effect size. Simple main effect analysis revealed that there were statistically significant differences in lateral cortical bone thickness in the groups receiving ECSWT treatment, with OVX surgery ($p=.004$), compared to the groups that received placebo treatment and sham surgery ($p=.724$). The group that received ECSWT and OVX surgery which induced OP, had the greatest mean lateral cortical bone thickness, which was the location where the treatment was administered (see Figure 14).

A Levene's Test was performed to assess the equality of variances in the data between treatment and condition. The results revealed that the assumption of equal variance was met for the variable lateral cortical bone thickness, since it was not statistically significant ($F(3,28)=.296$, $p>.05$).

Figure 18

Mean Lateral Cortical Bone Thickness of the Right Femur

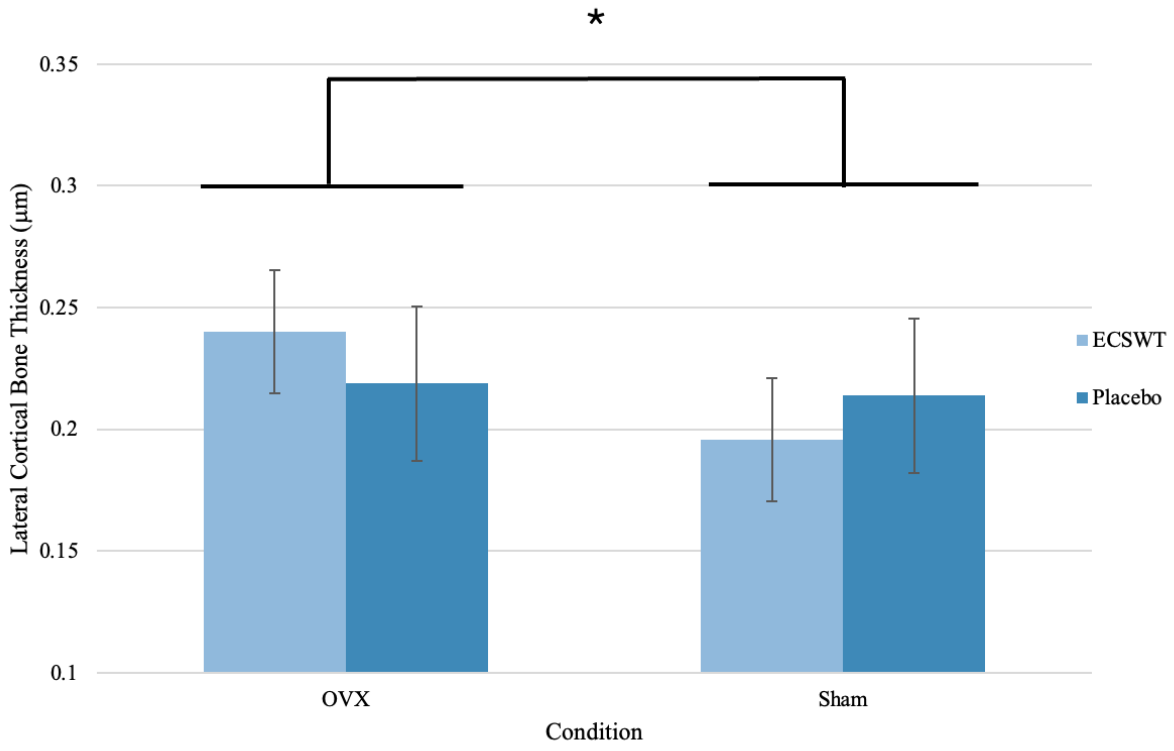

Note. A statistically significant main effect in lateral cortical bone thickness was revealed between conditions (ovariectomy (OVX) and sham surgery). * Denotes statistical significance, (p=.019).

Anterior Cortical Bone Thickness

See Table 9 for anterior cortical bone thickness descriptive statistics including mean and standard deviation for each treatment (ECSWT and placebo treatment) and condition (OVX and sham surgery).

Table 9

Mean and Standard Deviation of Anterior Cortical Bone Thickness

Sham surgery with placebo treatment	0.15+/-0.013
Sham surgery with ECSWT treatment	0.15+/-0.014
OVX with placebo treatment	0.15+/-0.014
OVX with ECSWT treatment	0.14+/-0.005

Note. Table 9 lists the mean and standard deviation (+/-) for each condition (ovariectomy (OVX) and sham surgery) and treatment (extracorporeal shockwave therapy (ECSWT) and placebo). Findings were recorded in µm.

A two-way ANOVA for independent measures was performed to compare the interaction effects and main effects of treatment and condition on anterior cortical bone thickness. The results revealed that treatment and condition had no statistically significant interaction effect on anterior cortical bone thickness, ($F(1, 28)=3.42$, $p>.05$, $\eta^2=.109$) with a medium effect size. There was no statistically significant main effect in anterior cortical bone thickness between condition (OVX and sham surgery, $F(1,28)=1.13$, $p>.05$, $\eta^2=.039$) with a small effect size. There was no statistically significant main effect within treatment groups (ECSWT and placebo treatment, $F(1,28)=.5$, $p=058$, $\eta^2=.018$) with a small effect size. No statistical differences were found in anterior cortical bone thickness between groups (see Figure 15).

A Levene's Test was performed to assess the equality of variances in the data between treatment and condition. The results revealed that the assumption of equal variance was met for the variable anterior cortical bone thickness, since it was nonsignificant ($F(3,28)=.447$, $p>.05$).

Figure 19

Mean Anterior Cortical Bone Thickness of the Right Femur

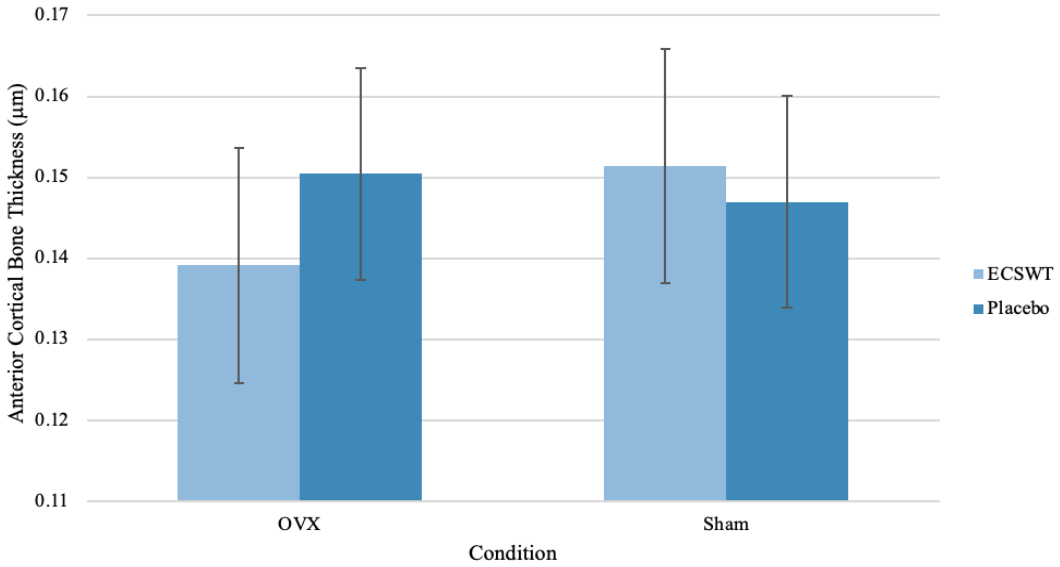

Note. Nonsignificant interaction or main effects were observed for anterior cortical bone thickness of the right femur in ovariectomy (OVX) or sham surgery conditions and extracorporeal shockwave therapy (ECSWT) and placebo treatment.

Posterior Cortical Bone Thickness

See Table 10 for posterior cortical bone thickness descriptive statistics including mean and standard deviation for each treatment (ECSWT and placebo treatment) and condition (OVX and sham surgery).

Table 10

Mean and Standard Deviation of Posterior Cortical Bone Thickness

Sham surgery with placebo treatment	0.17+/-0.016
Sham surgery with ECSWT treatment	0.17+/-0.018
OVX with placebo treatment	0.16+/-0.011
OVX with ECSWT treatment	0.17+/-0.014

Note. The table lists the mean and standard deviation (+/-) for each condition (ovariectomy (OVX) and sham surgery) and treatment (extracorporeal shockwave therapy (ECSWT) and placebo). Findings were recorded in µm.

A two-way ANOVA for independent measures was performed to compare the interaction effects and main effects of treatment and condition on posterior cortical bone thickness. The results revealed that treatment and condition had no statistically significant interaction effect on

posterior cortical bone thickness, (F(1,28)=.049, p>.05, η^2=.002) with a small effect size. There was no statistically significant main effect in posterior cortical bone thickness between condition (OVX and sham surgery), F(1,28)=1.15, p>.05, η^2=.040) with a small effect size. There was no statistically significant main effect in treatment groups (ECSWT and placebo treatment), F(1,28)=.13, p>.05, η^2=.005) with a small effect size (see Figure 16).

A Levene's Test was performed to assess the equality of variances between treatment and condition. The results revealed that the assumption of equal variance was met for the variable posterior cortical bone thickness, since it was not statistically significant (F(3,28)=.581, p>.05).

Figure 20

Mean Posterior Cortical Bone Thickness of the Right Femur

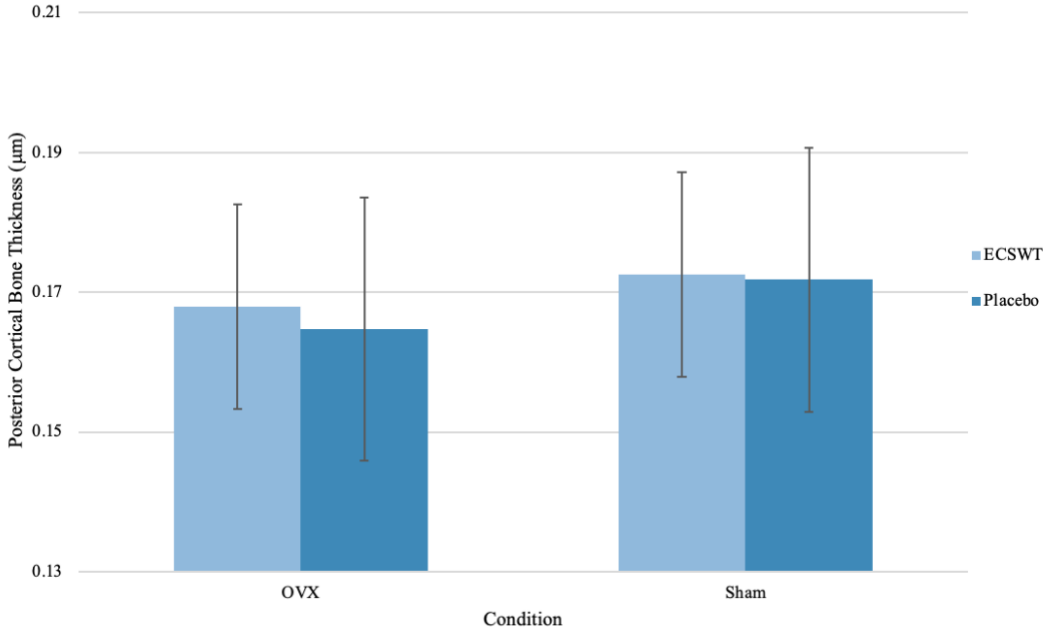

Note. Nonsignificant interaction or main effects were observed for posterior cortical bone thickness in the ovariectomy (OVX) or sham conditions and extracorporeal shockwave therapy (ECSWT) and placebo treatment.

Mediolateral Trabecular Thickness

See Table 11 for mediolateral trabecular bone thickness descriptive statistics including mean and standard deviation for each treatment (ECSWT and placebo treatment) and condition (OVX and sham surgery).

Table 11

Mean and Standard Deviation of Mediolateral Trabecular Bone Thickness

Sham surgery with placebo treatment	0.86+/-0.025
Sham surgery with ECSWT treatment	0.85+/-0.010
OVX with placebo treatment	0.89+/-0.029
OVX with ECSWT treatment	0.88+/-0.018

Note. The table lists the mean and standard deviation (+/-) for each condition (ovariectomy (OVX) and sham surgery) and treatment (extracorporeal shockwave therapy (ECSWT) and placebo). Findings were recorded in μm.

A two-way ANOVA for independent measures was performed to compare the interaction effects and main effects of treatment and condition on mediolateral trabecular bone thickness. The results revealed that treatment and condition had no statistically significant interaction effects on mediolateral trabecular bone thickness ($F(1,28)=.058$, $p>.05$, $\eta^2=.002$) with a small effect size. There was a statistically significant main effect present for mediolateral trabecular bone thickness in the condition (OVX and sham surgery), $F(1,28)=12.978$, $p=.001$, $\eta^2=.317$) with a large effect size. These results suggest that the OVX increased mediolateral trabecular thickness when compared to the sham surgery groups. No statistically significant main effects were observed between treatments (ECSWT and placebo), $F(1,28)=1.27$, $p>.05$, $\eta^2=.044$) with a small effect size. Simple main effect analysis revealed there were statistically significant differences in mediolateral trabecular thickness between rats that received OVX ($p=.011$) and between the rats that received the sham surgery ($p=.025$; see Figure 17).

A Levene's Test was performed to assess the equality of variances in the data between OVX, sham surgery, ECSWT, and placebo groups. The results revealed that the assumption of

equal variance was met for the variable mediolateral trabecular thickness, since it was not statistically significant ($F(3, 28)=.322$, $p>.05$).

Figure 21

Mean Mediolateral Trabecular Bone Thickness of the Right Femur

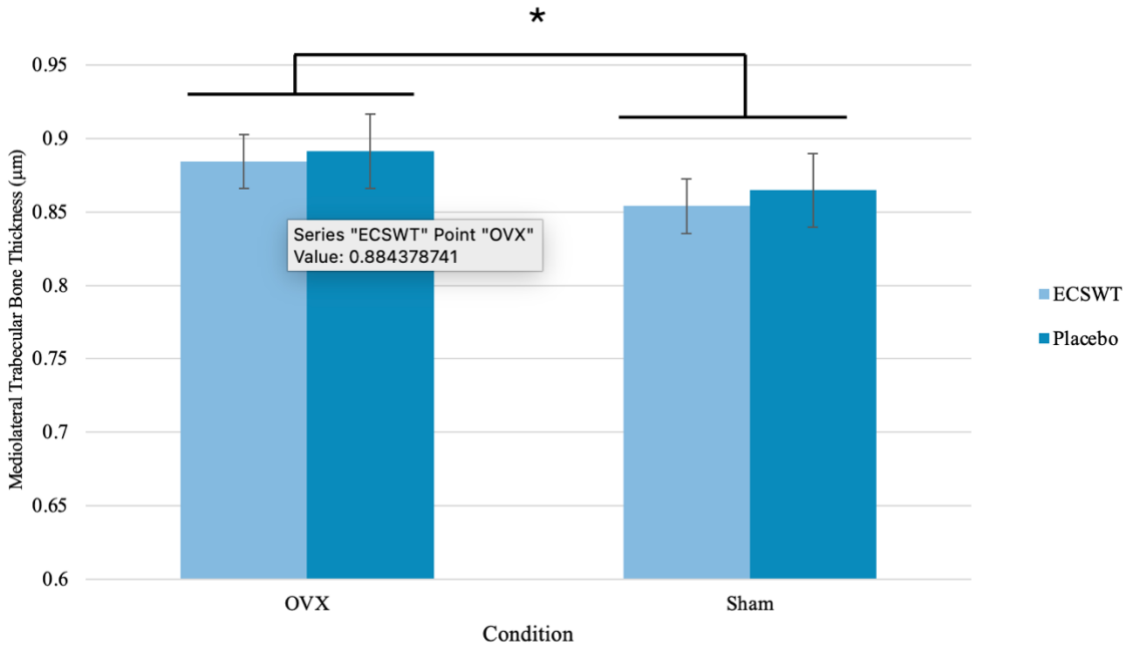

Note. A statistically significant main effect in mediolateral trabecular bone thickness was revealed between conditions (ovariectomy (OVX) and sham surgery). * Denotes statistical significance (p=.001).

Anteroposterior Trabecular Bone Thickness

See Table 12 for all descriptive statistical information for anteroposterior trabecular bone thickness including mean and standard deviation for each treatment (ECSWT and placebo) and condition (OVX and sham surgery).

Table 12

Mean and Standard Deviation of Anteroposterior Trabecular Bone Thickness

Sham surgery with placebo treatment	0.67+/-0.032
Sham surgery with ECSWT treatment	0.67+/-0.011
OVX with placebo treatment	0.65+/-0.013
OVX with ECSWT treatment	0.66+/-0.018

Note. The table lists the mean and standard deviation (+/-) for each condition (ovariectomy (OVX) and sham surgery) and treatment (extracorporeal shockwave therapy (ECSWT) and placebo). Findings were recorded in µm.

A two-way ANOVA for independent measures was performed to compare the interaction effects and main effects of treatment and condition on anteroposterior trabecular bone thickness. The results revealed that treatment and condition had no statistically significant interaction effects on anteroposterior trabecular bone thickness, (F(1,28,)=.058, p>.05, η^2=.002) with a small effect size. There was no statistically significant main effect present for anteroposterior trabecular bone thickness in the condition (OVX and sham surgery), F(1,28)=4.02 p=.055, η^2=.13) with a large effect size. No statistically significant main effect was found within treatment groups (ECSWT and placebo) for anteroposterior trabecular bone thickness, (F(1,28)=.395, p>.05, η^2=.014) with a small effect size. ECSWT or placebo treatment had no effect on the anteroposterior trabecular bone thickness (see Figure 18).

Levene's Test of equality of variances was significant (F(3,28)=3.93, p=.018), indicating unequal variances across groups. Therefore, the results of the two-way independent-measures ANOVA was interpreted with caution, as the assumption of homogeneity of variances was not met.

Figure 22

Mean Anteroposterior Trabecular Bone Thickness of the Right Femur

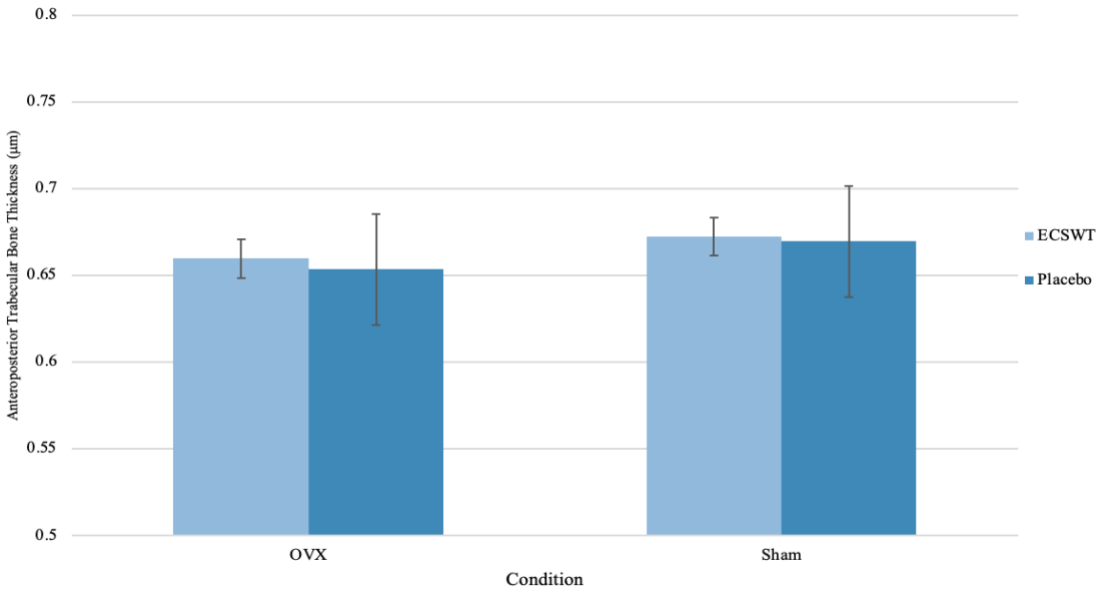

Note. Nonsignificant interaction or main effects were observed for anteroposterior trabecular bone thickness of the right femur in ovariectomy (OVX) or sham conditions and extracorporeal shockwave therapy (ECSWT) and placebo treatment.

Question 2: ***Does ECSWT alter blood biomarkers of bone remodeling (OCN and BAP) in the pre-clinical ovariectomy model of OP?***

Bone-Specific Alkaline Phosphatase

See Table 13 for all descriptive statistical information including mean and standard deviation of BAP for each treatment (ECSWT and placebo treatment) and condition groups. (OVX and sham surgery). See Appendix J for the BAP standard curve.

Table 13

Mean and Standard Deviation of Bone-Specific Alkaline Phosphatase Concentrations

Sham surgery with placebo treatment	0.24+/-0.067
Sham surgery with ECSWT treatment	0.25+/-0.063
OVX with placebo treatment	0.25+/-0.025
OVX with ECSWT treatment	0.22+/-0.036

Note. The table lists the mean and standard deviation (+/-) for each condition (ovariectomy (OVX) and sham surgery) and treatment (extracorporeal shockwave therapy (ECSWT) and placebo). Values were recorded in ng/ml.

A two-way ANOVA for independent measures was performed to compare the interaction effects and main effects of treatment and condition on BAP concentration. The results revealed that treatment and condition had no statistically significant interaction effects on BAP, ($F(1,28)=0.96$, $p>.05$, $\eta^2=.033$) with a small effect size. There were no statistically significant main effects of the condition (OVX and sham surgery) on BAP, ($F(1,28)=0.20$, $p>.05$, $\eta^2=.007$) with a small effect size or in the treatment group (ECSWT and placebo), $F(1,28)=0.64$, $p>.05$, $\eta^2=.022$) with a small effect size (see Figure 19). No statistically significant differences were reported in BAP concentration between treatment or condition groups.

A Levene's Test was performed to assess the equality of variances in the data between OVX, sham surgery, ECSWT, and placebo groups. The results revealed that the assumption of equal variance was met for the variable BAP, since it was not statistically significant ($F(3,28)=0.145$, $p>.05$).

Figure 23

Mean Bone-Specific Alkaline Phosphatase Concentration

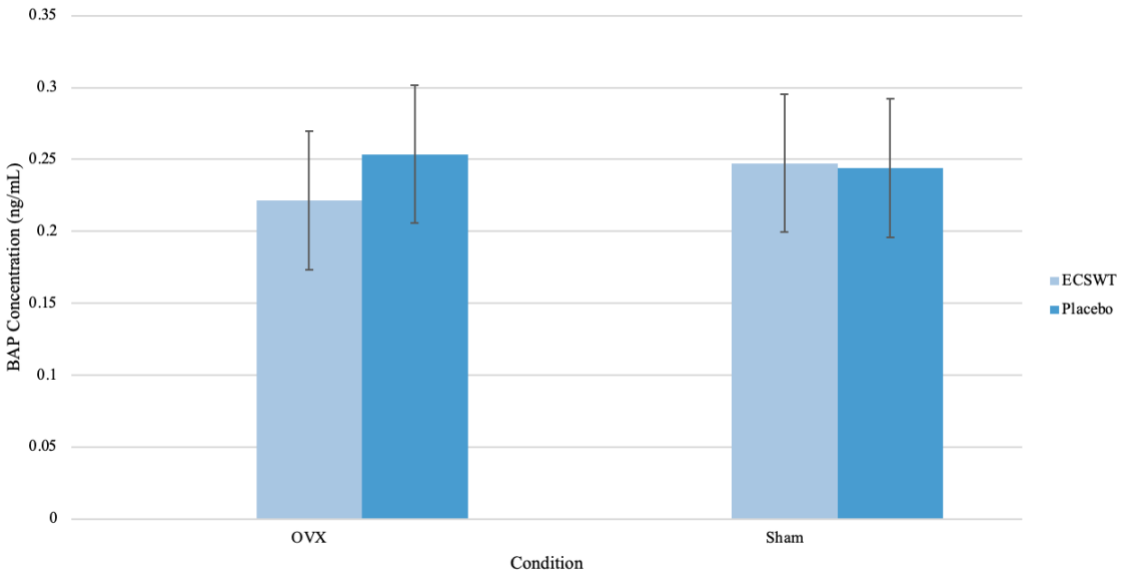

Note. Nonsignificant interaction or main effects were observed for bone-specific alkaline phosphatase (BAP) concentration in ovariectomy (OVX) or sham surgery conditions and extracorporeal shockwave therapy (ECSWT) and placebo treatment.

Osteocalcin

See Table 14 for all descriptive statistical information for OCN concentration including mean and standard deviation for each treatment (ECSWT and placebo treatment) and condition (OVX and sham surgery)**.** See Appendix K for the OCN standard curve.

Table 14

Mean and Standard Deviation of Osteocalcin Concentration

Sham surgery with placebo treatment	0.042+/-0.0076
Sham surgery with ECSWT treatment	0.044+/-0.0085
OVX with placebo treatment	0.050+/-0.0028
OVX with ECSWT treatment	0.053+/-0.0068

Note. The table lists the mean and standard deviation for each condition (ovariectomy (OVX) and sham surgery) and treatment (extracorporeal shockwave therapy (ECSWT) and placebo). Values were recorded in ng/ml.

A two-way ANOVA for independent measures was performed to compare the interaction effects and main effects of treatment and condition on OCN concentration. Treatment and condition had no statistically significant interaction effect on OCN concentration, ($F(1,28)=0.017$, $p>.05$, $\eta^2=.001$) with a small effect size. There was no statistically significant main effect of ECSWT or placebo treatment on OCN concentration ($F(1,28)=1.055$, $p>.05$, $\eta^2=0.036$) with a small effect size. There was a statistically significant main effect of OVX on OCN concentration, ($F(1,28)=11.278$, $p=.002$, $\eta^2=.287$) with a large effect size. This suggests that the OVX increased OCN blood biomarker concentration. Simple main effect analysis revealed there were statistically significant differences in OCN concentration between rats that underwent an OVX ($p=.02$) and between the rats that had the sham surgery ($p=.03$). The results suggest that the OVX created an increase in OCN concentration when comparing the sham surgery and OVX groups (see Figure 20).

A Levene's Test was performed to assess the equality of variances in the data between OVX, sham, ECSWT, and placebo groups. There was no violation in the equality of variance in

the data between the treatment and condition groups and the assumption of homogeneity was met since it was not statistically significant, ($F(3,28)=0.40$, $p>.05$).

Figure 24

Mean Osteocalcin Concentration

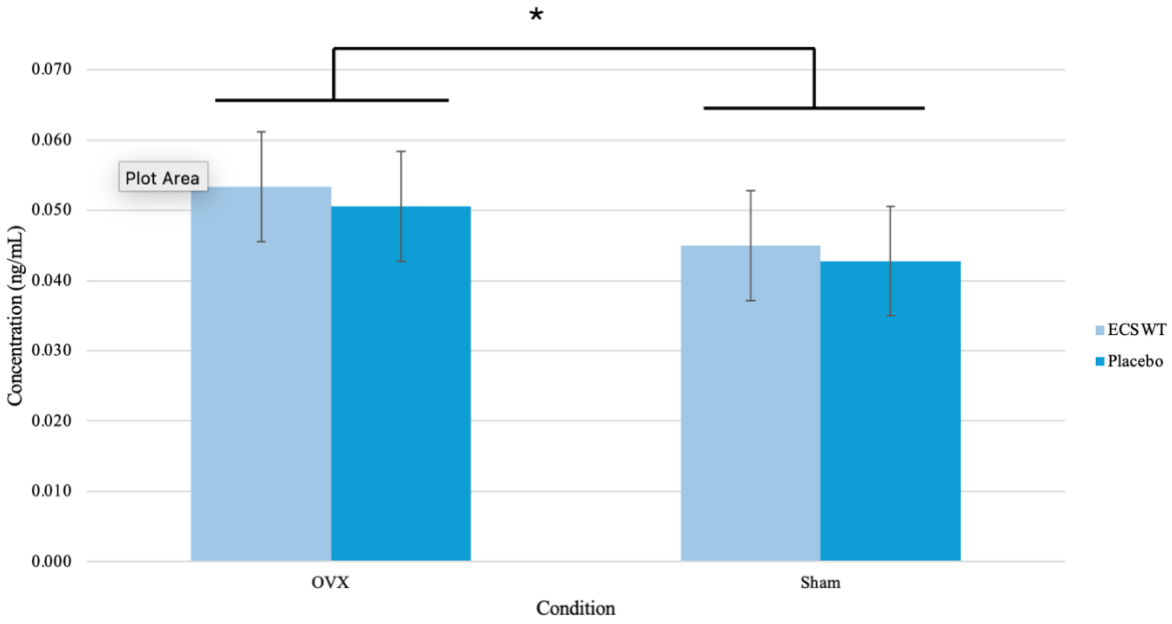

Note. Statistical significance in osteocalcin (OCN) concentration was revealed between condition (ovariectomy (OVX) and sham surgery). * Denotes statistical significance ($p=.002$).

Chapter 5: Discussion

This study examined the effects of ECSWT on osteoporotic changes in a pre-clinical, OVX rat model. The hypothesis was that ECSWT alters blood biomarkers (OCN, BAP) and bone microarchitecture (cortical and trabecular bone thickness) in an OVX-induced model of OP. Previous research has highlighted promise in treating osteoporotic changes using ECSWT, however, there is variability across studies for ECSWT application, energy flux density, and dosage (Wen et al., 2026).

The aim of the study was to inform clinical application for ECSWT, to reduce bone demineralization from OVX induced OP, and further assess bone formation markers as a potential screening or monitoring tool for OP. These findings contribute to the growing body of research, investigating ECSWT as a potential adjunctive intervention for OP. The following section will discuss the results within the context of existing literature for each research question and explore implications of the present study for future research.

Question 1: ***Does ECSWT improve bone microarchitecture in the pre-clinical ovariectomy model of OP?***

ECSWT did not alter BMD, cortical bone thickness, or trabecular bone thickness compared with placebo. This result was inconsistent with preceding research reporting bone microarchitecture differences after ECSWT (Lama et al., 2017; Li et al., 2021a; Wen et al., 2026). Results from the present study demonstrated that the ECSWT treatment parameters were insufficient to produce measurable structural adaptations in bone within 1 week after the final treatment.

BMD did not reveal significant differences between rats that received OVX and those that received sham surgery, and OVX did not decrease BMD as predicted. BMD is a quantitative

measure of the mineral content of bone relative to the measured bone area or volume. It is commonly used as an indicator of bone mass and mineralization (Liu et al., 2021).

Akhter et al. (2007) measured trabecular bone architecture in peri- and post-menopausal women. The researchers reported significant deterioration in trabecular bone architecture and noted that this can occur without a significant change in trabecular thickness or BMD. The researchers measured bone volume fraction (BV/TV), trabecular number, trabecular spacing, and structural model index (SMI). BV/TV represents the proportion of the analyzed bone volume occupied by mineralized trabecular bone and indicates the overall amount of trabecular bone present. Trabecular number describes the number of trabeculae per unit length, with lower values generally indicating trabecular loss. Trabecular spacing represents the average distance between trabeculae, with increased spacing suggesting greater separation and deterioration of the trabecular network. SMI describes trabecular architecture through analyzing the proportion of plate-like and rod-like structures. An increased SMI indicates a rod-like microarchitecture and is associated with compromised bone structure. A decreased SMI indicates a plate-like microarchitecture, suggesting healthy bone. Together, these measures provide detailed information about iliac crest trabecular bone quality, quantity, and organization (Akhter et al., 2007).

Akhter et al. (2007) aimed to capture true longitudinal transmenopausal changes using 3D trabecular bone architecture measures. The researchers took a bone biopsy of the transilial iliac crest, for micro-CT analysis. They reported a significant decrease in BV/TV, trabecular number, and trabecular spacing. SMI increased, indicating trabecular bone demineralization. In contrast, trabecular thickness was unaltered despite significant deterioration in other trabecular measurements. These findings proved that changes in bone microarchitecture may occur through changes in BV/TV, trabecular number, trabecular spacing, and SMI rather than trabecular

thickness alone. Akhter et al. (2007) highlighted the value of assessing multiple microarchitectural parameters when evaluating changes in bone health, as trabecular thickness alone might not sufficiently capture structural deterioration. Akhter et al. (2007) findings supported the present study by showing no changes in trabecular thickness or BMD, while other microarchitectural measures decreased (BV/TV, trabecular number, trabecular spacing).

BMD does not provide insight into structural morphology or organization within cortices or trabeculae (Liu et al., 2021). Akhter et al. (2007), Bouxsein et al. (2010), and Liu et al. (2021) similarly reported that BMD alone cannot measure bone fragility, as both bone microarchitecture and composition play key roles in assessing bone strength. Parameters such as trabecular number, separation, connectivity density, SMI, cortical thickness, and cortical porosity may detect subtle changes not apparent from BMD or cortical and trabecular thickness alone (Akhter et al., 2007; Bouxsein et al., 2010; Liu et al., 2021). BMD, cortical thickness, and trabecular thickness are useful measurements; however, they do not fully represent all aspects of bone microarchitecture that matter in OP (Akhter et al., 2007; Bouxsein et al., 2010; Liu et al., 2021) and we may see some variability where one measure increases and the other decreases for a variety of complex and multifaceted reasons.

Bouxsein et al. (2010) created guidelines for assessing bone microstructure in CT imaging of small rodents. The researchers stated that the most valuable measurements for trabecular microarchitecture are BV/TV, trabecular number, trabecular bone thickness, and trabecular separation, which aligns with Akhter et al. (2007). Together, these measurements provide a comprehensive analysis of trabecular microarchitecture and structural changes. However, in the present study, only BMD and trabecular bone thickness were analyzed; therefore, the trabecular bone analysis may not be as comprehensive as suggested by previous literature guidelines (Bouxsein et al., 2010). Trabecular thickness was chosen in the present

study to assess the structural integrity of the trabecular network, which is disrupted by OP causing thinner and weaker trabeculae. Cortical thickness measurements were also chosen in the present study because cortical bone contributes substantially to bone strength and resistance to fracture. Thinning of the cortices occur in post-menopausal OP, and lead to increased fracture risk. BMD was also measured in the study to assess the amount of mineralized bone present, to identifying reductions that would indicate the presence of OP (Liu et al., 2021).

The present study found that ECSWT had no effect on cortical bone thickness, and OVX caused minimal decreases in lateral cortical thickness, and increases in medial cortical thickness. Bouxsein et al. (2010) also stated that the minimal set of variables to report for cortical bone analysis should include total cross-sectional area, cortical bone area, cortical thickness, and cortical bone fraction. The present study reported only cortical thickness, which showed some significant changes after OVX, but this measure alone was not sufficient to demonstrate additional cortical microarchitectural changes. Additionally, the anatomical region where BMD, trabecular thickness, and cortical thickness measurements were taken may differ from prior literature, which may explain differences in outcomes for these measurements. In the present study, cortical thickness was measured at the mid-shaft of the right femur. This standardized site was markedly easier to target consistently than any other part of the bone and avoided interference from thickening near the epiphyses, which vary with individual morphology. Liu et al. (2021) and Rosales Rocabado et al. (2018) also both used the femoral midshaft to analyze cortical bone thickness again to create a standardized method of measurement for an OVX rat model. Alternative and multiple sites of measurement can be explored in future research.

Rosales Rocabado et al. (2018) also analyzed trabecular microarchitecture from the distal femoral metaphysis, the same location as in the present study. This landmark contains a substantial amount of trabecular bone and responds strongly to changes in bone remodelling.

It provides a visible anatomical landmark for repeatable measurements, making it well suited for this study. The distal joint was used rather than the proximal joint because the greater trochanter generates remarkable individual variability (Rosales Rocabado et al., 2018).

In the present study, BMD was taken from the central 10% of the shaft and also taken from 80% of the diaphysis, then averaged. This approach differs from previous studies. For example, Liu et al. (2021) divided the total tissue mineral density in each bone voxel by the total volume, including bone, pores, and marrow cavity. Liu et al. (2021) show that BMD results may also differ across prior research, depending on the analysis location and which parts of the femora are included in the voxel count.

In contrast, Rosales Rocabado et al. (2018) also measured BMD and tissue mineral density at the midshaft, similar to the present study. The researchers reported no changes in tissue mineral density, and a high-resolution analysis revealed that the decline in BMD after OVX was due to increased trabecular bone volume, not changes in BMD. Rosales Rocabado et al. (2018) stated that BMD alone does not capture the full microarchitectural analysis.

It is also important to assess the timeline of OVX, ECSWT treatment, and analysis for pre-clinical models and ECSWT findings. In the present study, rats underwent OVX at 3 months of age and were housed for approximately 4 months after OVX before treatment began at 7 months of age; femora were then extracted at 9 months of age. Thus, the rats were estrogen deficient for 16 weeks before receiving ECSWT, allowing time for the development of hormonal osteoporotic changes. Treatment consisted of five weekly sessions, with 1,000 shockwaves delivered at an energy flux density of 0.33 mJ/mm^2 and a frequency of 3 Hz. The rats were exsanguinated 1 week after the final treatment. The chosen time points, methods, and treatment parameters were a summary of the available research at the time that had great variability. These treatment parameters were used and sufficient in the study by Lama et al. (2017) to initiate and

visualize changes in BMD and bone microarchitecture; however, 1 week post-treatment may have been too brief for these responses to translate into measurable changes in BMD or bone microarchitecture. Therefore, the absence of changes in BMD or bone microarchitecture at 1 week does not necessarily exclude a biological response to ECSWT. One remodeling cycle in the average human adult is approximately 6 to 9 months. A bone remodeling cycle in a Sprague Dawley rat lasts approximately 6 to 10 days (Lelovas et al., 2008). Systemic, structural remodelling may require additional time to become detectable on CT imaging.

Liu et al. (2021) reported micro-CT findings following OVX in 6-month-old rats, with trabecular microarchitecture assessed 2 months after OVX. The researchers found significant decreases in femoral BV/TV, trabecular number, trabecular thickness, and BMD, along with a significant increase in trabecular separation. A cross-sectional cortical region at 55% of the femoral length from the head was where the measurements were taken. However, they observed no significant changes in cortical bone thickness or other measures of cortical microarchitecture. These findings highlight the potential importance of age when interpreting the effects of OVX in rat models of bone loss. The rats used by Liu et al. (2021) were considerably older when the study was performed than those in this study. Overall, differences in the age at OVX and the buffer period after OVX may contribute to variation in bone microarchitecture outcomes across rat studies (Lelovas et al., 2008) which may further help in trying in interpreting the current findings.

The present study yielded different findings from Lama et al. (2017), despite using identical ECSWT treatment parameters and the same 16-week interval between OVX and treatment. Both studies administered 5 weekly treatment sessions to the right femur using an energy flux density of 0.33 mJ/mm², 1,000 shockwaves, and a frequency of 3 Hz. Despite these similarities, the present study found no significant effects of ECSWT on BMD or trabecular

thickness in the right femur. Lama et al. (2017) findings reported that ECSWT increased the speed of sound values which were reduced by OVX, indicating an improvement of BMD. Based on histology measurements, all ECSWT treatments were shown to be more effective than raloxifene in reversing histological features of OP, in the OVX rats.

One possible explanation for the differences between studies is the use of different imaging methods. Lama et al. (2017) reported improvements in bone quality following ECSWT in OVX rats based on ultrasound-derived measures, whereas the present study assessed BMD and trabecular thickness using CT. Ultrasound and CT provide different types of information about bone structure. Ultrasound-derived measures are influenced by the propagation of sound through bone tissue. It provides information related to bone material and structural properties, whereas CT directly assesses bone mineralization and three-dimensional bone morphology (Schultz & Wolf, 2019). Therefore, improvements detected using ultrasound may not necessarily correspond to measurable changes in BMD or trabecular thickness (Schultz & Wolf, 2019).

Differences in imaging modalities may also matter when interpreting bone microarchitecture in response to ECSWT. Lama et al. (2017) evaluated bone changes using ultrasound-derived indices. BMD was assessed using quantitative ultrasound. Ultrasound was transmitted through the longitudinal axis of the femur and detected by a receiver positioned on the opposite side of the bone. The speed of sound was calculated from the ultrasound transit through the femur. Speed of sound was used as an indirect indicator of BMD. In contrast, the present study focused on BMD, cortical thickness, and trabecular thickness using CT imaging. The BMD was measured in the diaphysis (central 10% of diaphysis, mean 80% of diaphysis). Lama et al. (2017) may have seen positive results from ECSWT treatment due to methodology of measurements. The different imaging modalities may explain why the present study did not reproduce the findings of Lama et al. (2017), despite using the identical treatment protocol.

Ultrasound propagation through the femur is influenced by several structural and material properties of bone, including elasticity, porosity, density, and microarchitecture, which can affect the speed of sound through femoral tissue (Schultz & Wolf, 2019). In contrast, CT measures X-ray attenuation, which can be used to estimate BMD. As calcium and phosphate are deposited within the collagen matrix during bone mineralization, the resulting mineralized tissue increases the attenuation of x-ray passing through the femur (Schultz & Wolf, 2019).

While there are limitations to DXA imaging, it remains the gold standard imaging modality for BMD analysis. Newer modalities to measure bone quality may allow for better characterization of bone fragility or microarchitecture but are not standard of care procedures (Link & Kazakia, 2020). Oo et al. (2018) also published a systematic review and concluded that quantitative ultrasound has some benefits for fracture risk prediction, however, current literature does not support the substitution of QUS for DXA in the diagnosis and monitoring of OP in the rheumatic disease population.

Wen et al. (2026) published a systematic review examining the effects of ECSWT on BMD and bone microarchitecture in animal models of OP. The review found pre-clinical evidence that ECSWT may improve BMD and several measures of trabecular microarchitecture. However, evidence strength varied by outcome. Trabecular thickness had low-quality evidence, with only three studies reporting this measure, whereas BMD had moderate-quality evidence based on four studies. All four studies included in the analysis reported increased BMD after ECSWT. Sensitivity analyses also showed that ECSWT was mainly associated with increased BV/TV, decreased trabecular separation, and increased trabecular number. These findings remained after excluding studies identified as contributing to heterogeneity. Together, BV/TV, trabecular separation, and trabecular number had the strongest support among the microarchitectural measures examined in the review.

The findings of Wen et al. (2026) differ from the present study, which found no significant effects of ECSWT on BMD or trabecular thickness. However, comparisons between studies should be made cautiously because the review included considerable heterogeneity in treatment protocols and study designs. The studies varied in ECSWT treatment parameters, as well as the timing of OVX, treatment, and outcome assessment. These differences make it difficult to determine whether differences in treatment response were related to the intervention itself or to differences in experimental design.

Previous research has associated the present study treatment protocols with significant changes in bone microarchitecture (Lama et al., 2017). Other previous studies have reported significant changes in microarchitecture with increased frequent weekly treatments at both lower and higher energy flux densities (Li et al., 2021a). The lack of significant changes in the present study may, therefore, reflect differences in treatment frequency or other treatment parameters. In particular, the once weekly treatment protocol used in the present study differed from the higher treatment frequency used by Li et al. (2021a).

Li et al. (2021a) examined ECSWT for osteogenic differentiation in a rabbit model of OP. The researchers performed the ECSWT treatment three times weekly, for 4 weeks, using two different energy flux densities of 0.12 mJ/mm^2 and 0.5 mJ/mm^2 (low and high), 2,000 pulses at 4 Hz. The Li et al. (2021a) treatment protocol was more frequent than the present study, used a higher frequency, and administered double the shockwaves per treatment. The present study administered 1,000 shockwaves at 3 Hz (energy flux density 0.33 mJ/mm^2) and due to the amount of energy delivered to the target treatment area and treatment parameters used may have resulted in different findings. Li et al. (2021a) reported statistically significant changes in trabecular microarchitecture at both energy flux densities and localized trabecular bone formation at the treatment sites. In contrast, Li et al. (2021a) may have found statistically

significant trabecular bone microarchitecture differences from OVX because they used a higher treatment frequency (three times per week) than the present study, which was once weekly. These protocol differences highlight the importance of treatment energy level, dose, and frequency when assessing the clinical significance of ECSWT in improving bone microarchitecture.

Makert et al. (2017) investigated the effects of low-energy ECSWT on metaphyseal fracture healing in an osteoporotic rat model. The researchers waited 8 weeks after OVX before beginning treatment and used trabecular nodes to assess osteoporotic changes in the sham and ovariectomized groups. The researchers tested three energy levels (0.15, 0.35, and 0.55 mJ/mm^2) with 2,000 impulses delivered at 1 Hz. Although there were no significant differences between treatment groups in trabecular nodes or structure, the low-energy treatment (0.15 mJ/mm^2) promoted callus formation in the endosteal and dorsal regions of the femur and enhanced fracture union. In comparison, the present study used a higher energy flux density (0.33 mJ/mm^2), fewer impulses (1,000), and a higher frequency (3 Hz). These differences in treatment parameters should be considered when comparing the findings between studies and in the design of future studies possibly comparing different parameters directly. More importantly, the studies had different objectives. Makert et al. (2017) examined the effects of ECSWT on localized fracture healing in osteoporotic bone, whereas the present study examined its effects on systemic bone. Localized treatment aims to mediate fracture site healing while also increasing stability and function (Haffner et al., 2016). Systemic ECSWT aims to improve bone microarchitecture and attenuate osteoporotic changes, thereby reducing future fracture risk (Lama et al., 2017; Wang et al., 2014). Therefore, the significant effects observed by Makert et al. (2017) may reflect the localized response associated with fracture healing and should not be directly compared with the absence of significant changes in the systemic bone measures assessed in the present study.

Compared with previous studies, the present study's findings indicate the potential importance of imaging modalities, treatment dosage, timing, and energy distribution. The present study did not observe statistically significant changes; however, methodological inconsistencies across prior research impaired direct comparisons (Wen et al., 2026). Although ECSWT did not significantly improve cortical or trabecular bone thickness or BMD, future studies incorporating different treatment parameters, a repeated-measures study design, ultrasound or DXA imaging modalities for BMD, and a wider range of bone microarchitectural measurements may clarify whether ECSWT produced changes in the femora from ECSWT.

Question 2: ***Does ECSWT alter blood biomarkers of bone remodeling (OCN and BAP) in the pre-clinical ovariectomy model of OP?***

ECSWT did not significantly alter BAP or OCN concentrations in the pre-clinical OVX model of OP. Both biomarkers were expected to increase after OVX because of decreased estrogen and increased bone remodeling. OCN concentration was significantly different in the OVX and sham surgery groups, consistent with previous research (Singh, 2015). In contrast, BAP concentration did not differ significantly within groups. These biomarker findings provided additional information on systemic bone remodelling but did not align with the CT results, as no significant changes in BMD or trabecular thickness were observed following OVX.

OCN increased significantly in OVX groups in the present study, whereas BAP did not change within groups. OCN increased without significant changes in BMD or trabecular thickness; the results suggest that the biochemical response to estrogen deficiency was inconsistent with the measured CT parameters at the time of femur and blood collection (rats were 9 months of age). Thus, the elevated OCN concentration without a corresponding increase in BAP concentration may indicate that ECSWT influenced a specific aspect of bone formation, rather than causing a general increase in overall bone formation. OCN is an osteoblast-associated

marker that reflects bone formation and remodeling. It is also released from the bone matrix into blood during bone resorption, suggesting that OCN is also a marker of bone turnover. BAP is an enzyme associated with early mineralization and formation. OCN concentration may have been more prominent when sample collection occurred, based on the stage of bone remodeling or higher resorption (Atalay et al., 2012; Liu et al., 2021).

The OCN findings in the current study were partially consistent with those reported by Guo et al. (2022). The researchers reported increased OCN following OVX and interpreted this increase, alongside other biochemical markers such as procollagen type I N-terminal propeptide, as additional evidence of increased bone turnover. In the present study, no significant changes in BMD were observed, whereas significant changes were observed in OCN. Differences in the duration of estrogen deficiency may help explain these findings in the present study.

Guo et al. (2022) measured OCN at 4, 8, 12, and 16 weeks post-OVX. The researchers reported that OCN changes following OVX were time-dependent, with OCN concentrations changing significantly over the 16-week study period. However, concentrations did not differ significantly between the OVX and sham groups at individual time points. This suggests that changes in bone formation from estrogen deficiency may occur independently of changes in measurements of bone microarchitecture. Guo et al. (2022) also found that, despite differences in OCN concentration over time, trabecular thickness CT measurements remained nonsignificant throughout the study, which aligns with the present study's results. This finding suggests that OCN may be sensitive to changes in bone metabolism from estrogen deficiency, even when trabecular thickness changes were not detected in the present study but further study is warranted.

Changes in OCN despite no change in BMD may reflect the different processes represented by these measures. OCN reflects osteoblast activity and bone remodeling, whereas

BMD reflects the amount of mineralized bone present at the time of assessment (Liu et al., 2021). Therefore, differences in OCN do not necessarily result in measurable differences in BMD. The timing of blood collection following OVX may also have influenced the results, as bone loss occurs after estrogen deficiency before reaching a plateau (Guo et al., 2022). Consequently, the significant change in OCN concentration may demonstrate increased bone remodeling. This may have occurred before mineralization processed accumulated to produce marked differences in BMD on CT imaging. This may suggest that changes in bone formation were detectable at the biochemical level before corresponding changes in BMD were measurable by CT imaging. The present study aligns with findings from Atalay et al. (2012) and Gao et al. (2022), who reported significant increases in OCN concentration before detectable OP changes in BMD on DXA imaging. However, OCN and BAP concentration alone were not sufficient to conclude that overall bone formation increased, since CT imaging in the measured sensitivities did not reveal any significant changes. Changes in other structural parameters, such as trabecular number, trabecular separation, connectivity, or BV/TV, may have been more sensitive to changes in trabecular bone microarchitecture. Therefore, the elevated OCN observed in the present study may reflect alterations in the biological markers and sensitivity measures not captured by the CT measures.

The present study found no changes in BAP concentration with ECSWT or OVX. BAP concentration was hypothesized to elevate in OVX group, reflective of estrogen changes as demonstrated in previous research. It was expected to remain unchanged within the sham surgery groups. ECSWT treatment was expected to decrease the BAP concentration from OVX. BAP reflects osteoblastic activity and early mineralization. This enzyme can provide status on alterations in bone turnover. Because bone formation and resorption are closely coupled, BAP

can be used alongside other bone turnover markers and measures of bone microarchitecture when assessing changes associated with OP (Atalay et al., 2012; Xu et al., 2022).

Miyazaki et al. (2004) explored the changes in receptor activator of nuclear factor-kappa-B, and its ligand, osteoprotegerin, BAP, and tartrate-resistant acid phosphatase in OVX rats. Using 8-week-old female Wistar rats, an OVX or sham procedure was performed. Miyazaki et al. (2004) reported that BAP showed a transient increase after OVX, rising to 158.6% of pre-operative levels 1 week after OVX before declining to 38.7% by 8 weeks. These findings suggested that osteoblast activity increased quickly during the early stages of estrogen deficiency but plateaued and declined dramatically over time, as stated by Gao et al. (2022). This finding highlights the importance of timing the BAP assessment when interpreting changes in bone metabolism following OVX or in measuring at multiple and longer time points to have a true idea of the changes occurring. In the present study, blood samples were collected at 9 months of age and 6 months after OVX. Therefore, the timing of sample collection may have captured a low concentration of BAP due to the stage of bone remodelling. Since it is expected to sharply increase after OVX, plateau, and decrease, lower concentrations of BAP may be expected in an OVX group (Guo et al., 2022)

Atalay et al. (2012) explored the diagnostic utility of undercarboxylated OCN, OCN, and alkaline phosphatase in peri- and post-menopausal females. The study grouped participants by age and analyzed BMD using DXA imaging. The researchers reported that OCN had the highest predictive value for assessing OP when compared with participant demographics. The average OCN, undercarboxylated OCN, and BAP concentrations were also significantly higher in post-menopausal than in peri-menopausal women in the study, but OCN had the highest predictive value. The highest serum OCN, undercarboxylated OCN, and BAP concentrations were observed in individuals within 1-5 years after the onset of menopause. This finding was similar to

Miyazaki et al. (2004) and Gao et al. (2022), where biomarker concentrations were highest early on in menopause. The outcome of Atalay et al. (2012) was similar to the present study, in that OCN was highly responsive to OVX or menopausal estrogen changes. Since OCN is produced by osteoblasts and can also be released during bone resorption, it may provide a broader indication of bone remodelling, whereas BAP is more specifically associated with osteoblast activity and bone mineralization. Atalay et al. (2012) used an electrochemiluminescence immunoassay, which detected OCN, undercarboxylated OCN, and alkaline phosphatase. It detected biomarkers by measuring light emitted from the chemical reaction and is triggered by electricity on an electrode surface. In contrast, the present study used an antibody based sandwich ELISA for plasma OCN, with a colorimetric detection method (see Appendix I for manufactures information). The OCN ELISA used in the present study did not differentiate between carboxylated and undercarboxylated forms of OCN. The measurement represents OCN concentration, carboxylated or undercarboxylated is unspecified in the present study.

ECSWT did not significantly alter blood biomarker concentration, indicating there was no systemic bone remodeling inflicted by ECSWT treatment. The elevated OCN concentration in the OVX group was similar findings to Atalay et al. (2012), except the researchers explored menopausal females. They stated that the highest blood biomarker concentrations were shortly after initial menopause.

Prior literature comparing OCN and BAP suggests that OCN may be a more responsive biomarker for detecting changes in bone metabolism following estrogen deficiency. Across pre-clinical and clinical studies, OCN has shown sensitivity to alterations in bone turnover even when corresponding changes in BAP were lower, or bone microarchitecture was nonsignificant (Atalay et al., 2012; Miyazaki et al., 2004; Singh, 2015). Similarly, the present study found a significant difference in OCN concentration following OVX, without significant difference in

BAP, BMD, or trabecular thickness. These findings reveal that OCN may reflect changes in bone remodelling that were not yet reflected in changes in bone mineralization or the specific structural parameters assessed by CT imaging and can be further examined in future studies implementing some of the suggested changes.

The timing of assessment may partly explain the lack of change in BAP in the present study. Miyazaki et al. (2004) showed that BAP increased substantially during the early period after OVX, reaching 158.6% of pre-operative levels at one week before declining to 38.7% by 8 weeks. In the present study, blood and femoral samples were collected six months after OVX, when rats were 9 months of age. Therefore, the variable and transient increase in BAP described by Miyazaki et al. (2004) may have occurred well before sample collection in the present study. In contrast, the significant difference in OCN observed at six months suggests that OCN may remain responsive to altered bone remodeling during later stages of estrogen deficiency.

This interpretation was further supported by Guo et al. (2022), who demonstrated that OCN concentrations changed over time following OVX, indicating that OCN was sensitive to the dynamic changes in bone metabolism associated with estrogen deficiency. In addition, trabecular thickness remained nonsignificant throughout their study, which was consistent with the present findings. Together, these results suggest that biochemical changes in bone turnover may occur independently of detectable changes in selected measures of bone microarchitecture and the timing of the measures greatly affect the interpretation of the variable findings (i.e., some increase and some decrease at different time points). Atalay et al. (2012) also reported that OCN had the highest predictive value for OP when comparing OCN and BAP in peri- and post-menopausal women, further supporting OCN potential sensitivity to estrogen-related changes in bone metabolism.

Overall, the findings of the present study, when compared to previous literature, suggest that OCN may be a more responsive biomarker than BAP for detecting changes in bone metabolism following estrogen deficiency, particularly at later time points following OVX (Atalay et al., 2012; Guo et al., 2022; Miyazaki et al., 2004; Singh, 2015; Yoon et al., 2012). Prior studies suggest BAP shows a transient response in the early stages after OVX, whereas OCN may provide a more sustained indication of altered bone remodelling (Guo et al., 2022; Miyazaki et al., 2004; Yoon et al., 2012). In summary, OCN or BAP alone may not reflect OP changes but instead serve as an adjunct assessment of altered osteoblast activity in response to estrogen deficiency.

Limitations

A limitation of this study was the relatively small number of observations within each treatment and condition group (n=8), which may limit the generalizability and precision of the findings despite the study having adequate statistical power to test the hypotheses.

Additionally, there was no comparison pre- and post-treatment in the present study. A limitation was that the bone microarchitecture and blood biomarkers were unable to be assessed before OVX, before ECSWT, and after ECSWT. A repeated measures design would be more precise and establish a baseline between blood biomarkers and bone microarchitecture, to compare the changes from OVX and ECSWT. The frequency of measurements was limited by the amount of research funding available and the associated high costs to design and complete such a study.

Another limitation was that the present study only measured BMD, cortical, and trabecular bone thickness. Previous studies report positive findings from ECSWT within BV/TV measurements, trabecular thickness, SMI, and trabecular separation (Wen et al., 2026). The present study could not directly compare the effectiveness of ECSWT treatment on osteoporotic

changes because treatment parameters and CT analysis methods differed from prior studies (Wen et al., 2026).

Future Studies

Future studies should measure BV/TV, trabecular separation, and trabecular number for a comprehensive analysis of trabecular microarchitecture in combination with cortical and trabecular thickness and be completed in multiple locations on the bone and multiple time points. Additional research should compare different energy flux densities and increased weekly treatment frequencies in pre-clinical models to determine optimal ECSWT treatment parameters.

Future studies should also examine ECSWT in alternative OP models, such as immobilization-induced OP, to determine whether its effects on bone microarchitecture are consistent across different mechanisms of bone loss (e.g., post-fracture, OP, versus immobilization-induced).

In addition, incorporating biomechanical testing such as bending and compression testing would further determine the functionality of ECSWT. Biomechanical testing evaluates the mechanical strength and structural integrity of bone by measuring its response to applied forces, which is completed after excising the femur (Wang et al., 2014). A bending test is when a femur is supported at two points while a force is applied at a third point to evaluate its mechanical strength and resistance to bending (Wang et al., 2014). Compression testing measures a bone's ability to withstand compressive forces without deforming. Force is applied to the bone along a defined axis while the resulting deformation and failure are measured (Wang et al., 2014). Biomechanical testing would determine if ECSWT improves the mechanical strength and functionality of bone after treatment, not just the microarchitectural measures.

Chapter 6: Conclusion

The purpose of this study was to examine the effects of ECSWT on bone microarchitecture and blood biomarkers of bone remodeling in a pre-clinical OVX rat model of OP. The findings demonstrated that ECSWT treatment resulted in nonsignificant in cortical bone thickness, trabecular bone thickness, BMD, and biomarker concentrations of OCN and BAP under these experimental conditions.

BMD did not differ as expected after OVX surgery and ECSWT did not alter bone microarchitecture. However, the measurements used in the present study may not provide a comprehensive analysis of trabecular and cortical microarchitecture as the study assessed only trabecular and cortical bone thickness in the midshaft and distal metaphysis. Future studies should explore other bone microarchitecture variables simultaneously.

ECSWT treatment did not result in systemic changes in the blood biomarkers analyzed. The OVX produced differences in bone remodeling markers and the OCN concentration increased in the OVX group when compared to the sham surgery group, suggesting altered bone remodeling following estrogen deficiency. In contrast, OVX did not significantly affect BAP concentrations. Only measuring OCN or BAP alone may not reflect biological marker changes associated with OP. Measuring bone resorption markers such as C-terminal telopeptide of type I collagen alongside formation markers such as OCN and BAP. Assessment of resorption and formation markers would provide more details on bone remodelling status.

Further research should explore different ECSWT treatment parameters to establish optimal dosage incorporating additional microarchitecture measures such as BV/TV, trabecular thickness, trabecular separation, and SMI, using a repeated measures study design over multiple time points and locations on bone for a comprehensive analysis and comparison of bone

microarchitecture. This could be combined with multiple biological marker analysis of blood over a longer pre- and post-treatment period.

References

Akhter, M. P., Lappe, J. M., Davies, K. M., & Recker, R. R. (2007). Transmenopausal changes in the trabecular bone structure. *Bone (New York, N.Y.)*, *41*(1), 111–116. https://doi.org/10.1016/j.bone.2007.03.019

Alawi, M., Begum, A., Harraz, M., Alawi, H., Bamagos, S., Yaghmour, A., & Hafiz, L. (2021). Dual-energy x-ray absorptiometry (DXA) scan versus computed tomography for bone density assessment. *Curēus (Palo Alto, CA), 13*(2), https://doi.org/10.7759/cureus.13261

Atalay, S., Elci, A., Kayadibi, H., Onder, C. B., & Aka, N. (2012). Diagnostic utility of osteocalcin, undercarboxylated osteocalcin, and alkaline phosphatase for osteoporosis in premenopausal and postmenopausal women. *Annals of Laboratory Medicine*, *32*(1), 23–30. https://doi.org/10.3343/alm.2012.32.1.23

Aydin, S., Emre, E., Ugur, K., Aydin, M. A., Sahin, İ., Cinar, V., & Akbulut, T. (2025). An overview of ELISA: a review and update on best laboratory practices for quantifying peptides and proteins in biological fluids. *The journal of international medical research*, *53*(2), 3000605251315913. https://doi.org/10.1177/03000605251315913

Baran, R., Wehland, M., Schulz, H., Heer, M., Infanger, M., & Grimm, D. (2022). Microgravity-related changes in bone density and treatment options: A systematic review. *International Journal of Molecular Sciences*, *23*(15), 8650. https://doi.org/10.3390/ijms23158650

Beeton, C., Garcia, A., & Chandy, K. G. (2007). Drawing blood from rats through the saphenous vein and by cardiac puncture. *Journal of Visualized Experiments, 7, 266*. https://doi.org/10.3791/266

Beling, A., & Tenforde, A. (2023). Outcomes using focused shockwave for the treatment of stress fractures in runners: 2602. *Medicine and Science in Sports and Exercise*, *55*(9S), 863–863. https://doi.org/10.1249/01.mss.0000987964.07429.6e

Biomatik Rat BALP (Bone Alkaline Phosphatase) ELISA kit manual. (2025).

Boonchum, H., Vachalathiti, R., Smith, R., Muraki, S., & Bovonsunthonchai, S. (2026). The relationship between clinical outcomes and gait biomechanics in individuals with plantar fasciitis. *Archives of Physiotherapy*, *16*, 23–33. https://doi.org/10.33393/aop.2026.3626

Bouxsein, M. L., Boyd, S. K., Christiansen, B. A., Guldberg, R. E., Jepsen, K. J., & Müller, R. (2010). Guidelines for assessment of bone microstructure in rodents using micro–computed tomography. *Journal of Bone and Mineral Research*, *25*(7), 1468–1486. https://doi.org/10.1002/jbmr.141

Burkhart, K., Allaire, B., Anderson, D. E., Lee, D., Keaveny, T. M., & Bouxsein, M. L. (2020). Effects of long-duration spaceflight on vertebral strength and risk of spine fracture. *Journal of Bone and Mineral Research: The Official Journal of the American Society for Bone and Mineral Research*, 35(2), 269–276. https://doi.org/10.1002/jbmr.3881

Chen, H., Li, J., & Wang, Q. (2018). Associations between bone-alkaline phosphatase and bone mineral density in adults with and without diabetes. *Medicine (Baltimore)*, *97*(17), e0432–e0432. https://doi.org/10.1097/MD.0000000000010432

Crevenna, R., Mickel, M., Schuhfried, O., Gesslbauer, C., Zdravkovic A., & Keilani M. (2021) Focused extracorporeal shockwave therapy in physical medicine and rehabilitation. *Current Physical Medicine and Rehabilitation Reports* (9)1–10. https://doi.org/10.1007/s40141-020-00306-z

Gabel, L., Liphardt, A. M., Hulme, P. A., Heer, M., Zwart, S. R., Sibonga, J. D., Smith, S. M., & Boyd, S. K. (2022). Pre-flight exercise and bone metabolism predict unloading-induced bone loss due to spaceflight. *British Journal of Sports Medicine*, *56*(4), 196–203. https://doi.org/10.1136/bjsports-2020-103602

Gatenby, C., & Simpson, P. (2024). Menopause: Physiology, definitions, and symptoms. *Bailliere's Best Practice & Research. Clinical Endocrinology & Metabolism*, *38*(1), 101855. https://doi.org/10.1016/j.beem.2023.101855

Guo, X., Yu, X., Yao, Q., & Qin, J. (2022). Early effects of ovariectomy on bone microstructure, bone turnover markers and mechanical properties in rats. *BMC Musculoskeletal Disorders*, *23*(1), Article 316. https://doi.org/10.1186/s12891-022-05265-1

Haffner, N., Antonic, V., Smolen, D., Slezak, P., Schaden, W., Mittermayr, R., & Stojadinovic, A. (2016). Extracorporeal shockwave therapy ameliorates healing of tibial fracture non-union, unresponsive to conventional therapy. *Injury: Volume 7, issue 7, 47(7),* 1506–151*3.* https://doi.org/10.1016/j.injury.2016.04.010

Karimiahmadabadi, A., Sohani, S. M., Tabatabaei, A., & Limouei, G. (2025). The effects of focused extracorporeal shockwave therapy versus deep friction massage in supraspinatus tendinopathy: a randomized controlled trial. *Journal of Bodywork and Movement Therapies., 42, 823–830*. https://doi.org/10.1016/j.jbmt.2025.01.035

Kim, Y., Brodt, M. D., Tang, S. Y., & Silva, M. J. (2021). Micro-CT for scanning and analysis of mouse bones. *Methods in Molecular Biology (Clifton, N.J.)*, *2230*, 169–198. https://doi.org/10.1007/978-1-0716-1028-2_11

Lama, A., Santoro, A., Corrado, B., Pirozzi, C., Paciello, O., Pagano, T. B., Russo, S., Calignano, A., Mattace Raso, G., & Meli, R. (2017). Extracorporeal shockwaves alone or combined with raloxifene promote bone formation and suppress resorption in ovariectomized rats. *PloS One, 12(2),* e0171276–e0171276. https://doi.org/10.1371/journal.pone.0171276

Lelovas, P. P., Xanthos, T. T., Thoma, S. E., Lyritis, G. P., & Dontas, I. A. (2008). Laboratory Rat as an Animal Model for Osteoporosis Research. *Comparative Medicine*, *58*(5), 424–430.

Li, B., Wang, R., Huang, X., Ou, Y., Jia, Z., Lin, S., Zhang, Y., Xia, H., & Chen, B. (2021a). Extracorporeal shockwave therapy promotes osteogenic differentiation in a rabbit osteoporosis model. *Frontiers in Endocrinology (Lausanne). 12*, 627718. https://doi.org/10.3389/fendo.2021.627718

Li, C., Li, Z., Shi, L., Wang, P., Gao, F., & Sun, W. (2021b). Effectiveness of focused shockwave therapy versus radial shockwave therapy for non-calcific rotator cuff tendinopathies: A randomized clinical trial. *BioMed Research International*. (1), 6687094. https://doi.org/10.1155/2021/6687094

Link, T. M., & Kazakia, G. (2020). Update on imaging-based measurement of bone mineral density and quality. *Current Rheumatology Reports*, *22*(5), Article 13. https://doi.org/10.1007/s11926-020-00892-w

Liu, J., Kim, E. K., Ni, A., Kim, Y.-R., Zheng, F., Lee, B. S., & Kim, D.-G. (2021). Multiscale characterization of ovariectomized rat femur. *Journal of Biomechanics, 122*, Article 110462. https://doi.org/10.1016/j.jbiomech.2021.110462

Luengo-Mateos, M., González-Vila, A., Torres Caldas, A. M., Alasaoufi, A. M., González-Domínguez, M., López, M., González-García, I., & Barca-Mayo, O. (2024). Protocol for ovariectomy and estradiol replacement in mice. *STAR Protocols*, *5*(1), Article 102910. https://doi.org/10.1016/j.xpro.2024.102910

Lumachi, F., Ermani, M., Camozzi, V., Tombolan, V., & Luisetto, G. (2009). Changes of bone formation markers osteocalcin and bone-specific alkaline phosphatase in postmenopausal women with osteoporosis. *Annals of the New York Academy of Sciences*, *1173*(s1), E60–E63. https://doi.org/10.1111/j.1749-6632.2009.04953.x

Mackert, G., Schulte, M., Hirche, C., Kotsougiani, D., Vogelpohl, J., Hoener, B., Fiebig, T., Kirschner, S., Brockmann, M. A., Lehnhardt, M., Kneser, U., Harhaus, L., & Tang, C.H. (2017). Low-energy extracorporeal shockwave therapy improves metaphyseal fracture healing in an osteoporotic rat model. https://doi.org/10.1371/journal.pone.0189356

Man, J., Graham, T., Squires-Donelly, G. Lasett, A.L. (2022). The effects of microgravity on bone structure and function. *NPJ Microgravity* 8, (9) https://doi.org/10.1038/s41526-022-00194-8

Morin, S. N., Feldman, S., Funnell, L., Giangregorio, L., Kim, S., McDonald-Blumer, H., Santesso, N., Ridout, R., Ward, W., Ashe, M. C., Bardai, Z., Bartley, J., Binkley, N., Burrell, S., Butt, D., Cadarette, S. M., Cheung, A. M., Chilibeck, P., Dunn, S., Wark, J. D. (2023). Clinical practice guidelines for management of osteoporosis and fracture prevention in Canada: 2023 update. *Canadian Medical Association Journal (CMAJ)*, *195*(39), E1333–E1348. https://doi.org/10.1503/cmaj.221647

Moser, S. C., & van der Eerden, B. C. J. (2019). Osteocalcin—A versatile bone-derived hormone. *Frontiers in Endocrinology (Lausanne)*, *9*, 794. https://doi.org/10.3389/fendo.2018.00794

Oo, W. M., Naganathan, V., Bo, M. T., & Hunter, D. J. (2018). Clinical utilities of quantitative ultrasound in osteoporosis associated with inflammatory rheumatic diseases. *Quantitative imaging in medicine and surgery*, *8*(1), 100–113. https://doi.org/10.21037/qims.2018.02.02

Palanisamy, P., Alam, M., Li, S., Chow, S. K. H., & Zheng, Y. (2022). Low-Intensity pulsed ultrasound stimulation for bone fracture healing: A review. *Journal of Ultrasound in Medicine*, *41*(3), 547–563. https://doi.org/10.1002/jum.15738

Park, K.-S., Yoo, J.-I., Kim, H.-Y., Jang, S., Park, Y., & Ha, Y.-C. (2017). Education and exercise program improves osteoporosis knowledge and changes calcium and vitamin D dietary intake in community dwelling elderly. *BMC Public Health*, *17*(1), 966–966. https://doi.org/10.1186/s12889-017-4966-4

Pasqualini, L., Ministrini, S., Lombardini, R., Bagaglia, F., Paltriccia, R., Pippi, R., Collebrusco, L., Reginato, E., Sbroma Tomaro, E., Marini, E., D'Abbondanza, M., Scarponi, A. M., De Feo, P., & Pirro, M. (2019). Effects of a 3-month weight-bearing and resistance exercise training on circulating osteogenic cells and bone formation markers in postmenopausal women with low bone mass. *Osteoporosis International*, *30*(4), 797–806. https://doi.org/10.1007/s00198-019-04908-9.

Rat Osteocalcin ELISA Kit (Colorimetric). (2024). *NBP2-69957 Manual Biotechne*. https://resources.bio-techne.com/products/documents/manual/NBP2-69957-Manual.pdf

Rosales Rocabado, J. M., Kaku, M., Nozaki, K., Ida, T., Kitami, M., Aoyagi, Y., & Uoshima, K. (2018). A multi-factorial analysis of bone morphology and fracture strength of rat femur in response to ovariectomy. *Journal of orthopaedic surgery and research*, *13*(1), 318. https://doi.org/10.1186/s13018-018-1018-4

Rowe, P., Koller, A., & Sharma, S. (2023). Physiology, bone remodeling. *StatPearls Publishing*. https://www.ncbi.nlm.nih.gov/books/NBK499863/

Sangondimath, G. & Sen, R. K. (2023). DXA and imaging in osteoporosis. *Indian Journal of Orthopedics.*, *57*(Suppl 1),82–93. https://doi.org/10.1007/s43465-023-01059-2

Sanzo, P., & Oakley, E. (2014). A randomized control trial on the effects of extracorporeal shockwave therapy, joint mobilizations and exercise on plantar heel pain in patients with plantar fasciitis. *International Journal of Sports Science, 4*(1), 27-37

Schindeler, A., McDonald, M. M., Bokko, P., & Little, D. G. (2008). Bone remodeling during fracture repair: The cellular picture. *Seminars in Cell & Developmental Biology, 19*(5), 459–466. https://doi.org/10.1016/j.semcdb.2008.07.004

Schultz, K., & Wolf, J. M. (2019). Emerging technologies in osteoporosis diagnosis. *Journal of Hand Surgery (American Ed.)*, *44*(3), 240–243. https://doi.org/10.1016/j.jhsa.2018.07.006

Singh, S. (2015). Serum Osteocalcin as a Diagnostic Biomarker for Primary Osteoporosis in Women. *Journal of Clinical and Diagnostic Research*, *9*(8), RC04–RC07. https://doi.org/10.7860/JCDR/2015/14857.6318

Dagklis, T., Rentzeperi, E., Kalogiannidis, I., Athanasiadis, A., Kourtis, A., Tsakiridis, I., Mamopoulos, A., & Pegiou, S. (2023). Diagnosis and management of osteoporosis: A comprehensive review of guidelines. Obstetrical & gynecological survey, 78(11), 657–681. https://doi.org/10.1097/OGX.0000000000001181

Su, Y., Zhou, X., Foster, B. K., Grills, B. L., Xu, J., & Xian, C. J. (2018). Roles of neurotrophins in skeletal tissue formation and healing. *Journal of Cellular Physiology*, *233*(3), 2133–2145. https://doi.org/10.1002/jcp.25936

Swaffield, T. P., Neviaser, A. S., & Lehnhardt, K. (2018). Fracture risk in spaceflight and potential treatment options. *Aerospace Medicine and Human Performance*, 89(12), 1060–1067. https://doi.org/10.3357/AMHP.5007.2018

Talaulikar, V. (2022). Menopause transition: Physiology and symptoms. *Bailliere's Best Practice and Research in Clinical Obstetrics and Gynecology.*, *81*, 3–7. https://doi.org/10.1016/j.bpobgyn.2022.03.003

Tam, K. F., Cheung, W. H., Lee, K. M., Qin, L., & Leung, K. S. (2009). Shockwave exerts osteogenic effect on osteoporotic bone in an ovariectomized goat model. *Ultrasound in Medicine & Biology*, *35*(7), 1109–1118. https://doi.org/10.1016/j.ultrasmedbio.2009.01.001

Tenforde, A. S., Borgstrom, H. E., DeLuca, S., McCormack, M., Singh, M., Hoo, J. S., & Yun, P. H. (2022). Best practices for extracorporeal shockwave therapy in musculoskeletal medicine: clinical application and training consideration. *PM & R: The Journal of Injury, Function, and Rehabilitation*, *14*(5), 611–619. https://doi.org/10.1002/pmrj.12790

Toyama, K. S., Tinius, A., & Mahler, D. L. (2023). Evidence supporting an evolutionary trade-off between material properties and architectural design in *anolis* lizard long bones. *Evolution*, *78*(2), 315–328. https://doi.org/10.1093/evolut/qpad208

Wang, C.-J., Huang, C.-Y., Hsu, S.-L., Chen, J.-H., & Cheng, J.-H. (2014). Extracorporeal shockwave therapy in osteoporotic osteoarthritis of the knee in rats: an experiment in animals. *Arthritis Research & Therapy*, *16*(4), R139–R139. https://doi.org/10.1186/ar4601

Ward, D. L., Schroeder, L., Tinius, A., Niccoli, S., Voth, R., Lees, S. J., Silcox, M., Viola, B., & Sanzo, P. (2022). Ovariectomized rat model and shape variation in the bony labyrinth. *Anatomical Record*, *305*(11), 3283–3296. https://doi.org/10.1002/ar.24878

Wen, X., Xiangli, J., He, Q., & Yin, Z. (2026). The effects of extracorporeal shockwave therapy on bone mineral density and microarchitecture in animal models of osteoporosis: a

systematic review and meta-analysis. *Frontiers in Rehabilitation Sciences*, *6*, Article 1731044. https://doi.org/10.3389/fresc.2025.1731044

Wu, S., Wang, L., Zhang, X., Cai, L., Ke, Q., & Xu, J. (2026). Bone turnover markers (β-CTX, PINP, ALP) in osteoporosis: Correlation with bone loss and fracture risk stratification. *Frontiers in Endocrinology*, *16*, 1628434. https://doi.org/10.3389/fendo.2025.1628434

Xu, Y., Shen, L., Liu, L., Zhang, Z., & Hu, W. (2022). Undercarboxylated osteocalcin and its associations with bone mineral density, bone turnover markers, and prevalence of osteopenia and osteoporosis in a Chinese population: A cross-sectional study. *Frontiers in Endocrinology (Lausanne)*, *13*, 843912–843912. https://doi.org/10.3389/fendo.2022.843912

Appendix A: Materials for Dissection and Storage of Femurs

1. Dissection equipment (scissors, forceps, etc.).
2. 4% paraformaldehyde.
3. 70% ethanol.
4. Phosphate buffered saline.
5. Parafilm®.
6. 2 ml snap lock Eppendorf tube.

Appendix B: Supplies for Rat Osteocalcin Enzyme Linked Immunosorbent Assay

- Micro ELISA plate
- Reference Standard
- Concentrated Biotinylated Detection Ab (100x)
- Concentrated HRP Conjugate (100x)
- Reference Standard & Sample Diluent
- Biotinylated Detection Ab Diluent
- HRP Conjugate Diluent
- Concentrated Wash Buffer
- Substrate Reagent
- Stop Solution
- Plate Sealer
- Product Manual

Appendix C: Contents for Rat Bone Alkaline Phosphatase Enzyme-Linked Immunosorbent Assay

- ELISA Microplate
- Lyophilized Standard
- Sample Dilution Buffer
- Biotin-labelled Antibody (concentrated)
- Antibody Dilution Buffer
- HRP-streptavidin conjugate (SABC)
- SABC Dilution Buffer
- TMB Substrate
- Stop Solution
- Wash Buffer (25X)
- Plate Sealer
- User Manual

Appendix D: Additional Supplies Needed for Enzyme-Linked Immunosorbent Assay

- Supplies needed:
  - Micro Plate Reader
  - High-precision pipettes, multichannel pipette, Eppendorf tubes
  - Incubator that will maintain 37°C
  - Distilled water
  - Absorbent paper
  - Ethanol 70% to sterilize equipment, workspace and manage spills
  - Personal Protective Equipment (lab coat, gown, gloves, goggles)

Appendix E: Biosafety Level 2 Certificate

CERTIFICATE
OF COMPLETION

THIS IS TO CERTIFY THAT

BIOSAFETY PROGRAM

Ashley Wright

has successfully completed **Biosafety Level 2 Training** including Biosecurity and Dual-Use Hazards on: Friday, August 15, 2025

This training is valid until: Tuesday, August 15, 2028

Important Numbers:

8911 TBay Emergency
3911 OR Emergency

8671 Health & Safety
8806 Lab Safety

Brenda Huska
Biosafety Officer

Appendix F: Lakehead University Animal Care Facility Standard Operating Procedure for Cardiac Puncture

5.8 Cardiac Blood Collection:

Figure 7. Insertion of needle for cardiac blood collection.

5.8.1 Deeply anaesthetize or euthanize the mouse as per study protocol.
- 5.8.1.1 If euthanizing the animal prior to sampling, sampling must occur immediately after euthanasia.
- 5.8.1.2 If anaesthetized, perform a toe pinch test to ensure the animal is in a deep plane and unable to feel pain (surgical plane of anesthesia).

5.8.2 Place animal in dorsal recumbency and secure with masking tape (optional).
- 5.8.2.1 The forelimbs are taped separately and should be at a 90 degree angle to the body of the animal.
- 5.8.2.2 If experienced with the procedure, taping may not be necessary.

5.8.3 Before inserting needle into animal, pull back on the syringes plunger to ensure smooth movement.
- 5.8.3.1 For mice: Use a 1 mL to 3 mL syringe and a 21G or 22 G x 1" needle.
- 5.8.3.2 For rats: Use a 3 mL to 12 mL syringe and an 18 or 21 G x 1" to 1.5" needle.

5.8.4 Insert the needle at an approximate 5 to 15 degree angle immediately caudal to the xyphoid process (Figure 7). A larger animal will require a larger degree angle.

5.8.5 Place a slight negative pressure on the syringe, by pulling back on plunger, upon immediate entry into the skin.

5.8.6 Advance the needle forward until blood appears in the hub of the needle.

5.8.7 Once blood appears, stop advancing and steady the needle. Slowly "milk" back on the plunger until the required sample volume is obtained.

5.8.8 If blood flow stops, slowly and gently move your needle forward, back, up or down until blood flows again. This will take very small movements; otherwise you will exit the heart. Do not move the needle in a circular motion when inserted into the chest cavity.

5.8.9 Once adequate blood volume has been obtained, release pressure on the syringe before exiting the chest cavity.

5.8.10 If anesthetized, euthanize the animal via an ACC approved method once the sample has been obtained.

5.8.11 No more than 1 sample can occur with this technique and death of the animal must be assured once sample has been obtained.

Appendix G: Euthanasia of Rat Model by Exsanguination

8. Physical Methods of Euthanasia

Use of Physical methods as primary form of euthanasia: Physical methods of euthanasia (cervical dislocation and decapitation) in rodents are conditionally acceptable by the CCAC and must have prior approval of the ACC. These techniques should not be undertaken in the presence of casual observers or the uninformed for they are aesthetically unpleasant. When properly applied by trained and experienced persons, the animal is immediately rendered unconscious and insensitive to pain. Pre-medication followed by deep general anaesthesia is always recommended prior to cervical dislocation or decapitation. Use of these techniques without anesthesia must be justified and pre-approved by the ACC.

8.1. **Cervical Dislocation:**

8.1.1. This procedure is for use in mice and small rats (under 200 gm).
8.1.2. Place the animal on a flat surface (ventral surface of the animal down).
8.1.3. Place the dislocation instrument (bar or scalpel handle) just caudal (posterior) to the base of the skull and hold the instrument firmly in place. Similarly, use of the index and middle fingers placed behind the ears at the base of the skull without use of an instrument can be performed by experienced technicians.
8.1.4. Grasp the base of the tail with the thumb and forefingers and with a quick motion pull away and slightly upward from the skull.
8.1.5. This should cause a separation of the spinal cord from the brain that the technician can "feel" as the procedure is conducted.

8.2. **Decapitation:**

8.2.1. Guillotines that are designed to accomplish decapitation in adult rodents in a uniformly instantaneous manner are commercially available.
8.2.2. Ensure guillotine is in good working order with sharp blades.
8.2.3. Use the appropriately sized apparatus for the size of the animal.
8.2.4. Place animal in guillotine and separate head from body at the cervical level.
8.2.5. Personnel using the guillotine must recognize the inherent danger of the apparatus and take adequate precautions to prevent personal injury.

8.3. **Exsanguination:**

8.3.1. Exsanguination must be done under deep anaesthesia (not just sedation).
8.3.2. Verify that withdrawal reflex is absent by pinching the toes to ensure adequate anaesthesia depth.
8.3.3. Withdraw the maximum volume of blood.
8.3.3.1. Animal's total blood volume is 10% of body weight.
8.3.3.2. Cardiac blood collection is the most rapid and efficient technique for a terminal blood draw. Follow *SOP R-09-LUACF-Blood Collection Techniques in Rodents, section 5.8 Cardiac Blood Collection.*
8.3.4. Ensure death with another form of euthanasia such as cervical dislocation.
8.3.5. Removal of the heart will also ensure death.

Appendix H: Lakehead University Standard Operating Procedure for Transportation of Biohazardous Goods

(h) the report requirements in Part 8, Accidental Release and Imminent Accidental Release Report Requirements;
(i) safe handling and transportation practices for dangerous goods, including the characteristics of the dangerous goods;
(j) the proper use of any equipment used to handle or transport the dangerous goods;
(k) the reasonable emergency measures the person must take to reduce or eliminate any danger to public safety that results or may reasonably be expected to result from an accidental release of the dangerous goods;
(l) for air transport, the aspects of training set out in Chapter 4, Training, of Part 1, General, of the ICAO Technical Instructions for the persons named in that Chapter and the requirements in Part 12, Air, of these Regulations; and
SOR/2002-306

The ICAO Technical Instructions require the approval of training programmes for air carriers. Information may be obtained from the Chief, Dangerous Goods Standards, Civil Aviation, Transport Canada.

(m) for marine transport, the requirements set out in the IMDG Code and the "Dangerous Goods Shipping Regulations", as applicable, and the requirements in Part 11, Marine, of these Regulations.

The certificate issued to an employee must contain the following information:

6.3(a) the name and address of the place of business of the employer;
The place of business could be a local office, a regional office or a head office.
(b) the employee's name;
(c) the date the training certificate expires, preceded by the words "Expires on" or "Date d'expiration"; and
(d) the aspects of handling, offering for transport or transporting dangerous goods for which the employee is trained, including the specific topics set out in section 6.2.

The training certificate must be signed by the employer and the employee and must be carried on the employee at all times. A training certificate expires 24 months after the date of issuance for Air and 36 months after the date of issuance for road vehicle, railway vehicle or ship.

Training and Certification Requirements

The ability to handle emergencies and assess risk is learned through employee education and training, well written procedures, useful information charts and posters, approachable managers, emergency drills and a sense of being a part of a radiation safety team.

The following excerpts from the legislation pertain to the training requirements:

6.1(1) A person who handles, offers for transport or transports dangerous goods must

(a) be adequately trained and hold a training certificate in accordance with this Part; or

(b) perform those activities in the presence and under the direct supervision of a person who is adequately trained and who holds a training certificate in accordance with this Part.

(2) An employer must not direct or allow an employee to handle, offer for transport or transport dangerous goods unless the employee

(a) is adequately trained and holds a training certificate in accordance with this Part; or

(b) performs those activities in the presence and under the direct supervision of a person who is adequately trained and who holds a training certificate in accordance with this Part.

6.2 A person is adequately trained if the person has a sound knowledge of all the topics listed in paragraphs (a) to (m) that relate directly to the person's duties and to the dangerous goods the person is expected to handle, offer for transport or transport:

(a) the classification criteria and test methods in Part 2, Classification;
(b) shipping names;
(c) the use of Schedules 1, 2 and 3;
(d) the shipping document and train consist requirements in Part 3, Documentation;
(e) the dangerous goods safety marks requirements in Part 4, Dangerous Goods Safety Marks;
(f) the certification safety marks requirements, safety requirements and safety standards in Part 5, Means of Containment;

Appendix I: Biotechne Osteocalcin Enzyme Linked Immunosorbent Assay Manufacture's Manual and Biomatik Bone-Specific Alkaline Phosphatase Enzyme Linked Immunosorbent Assay Manufacture's Manual

Rat BALP

Assay Procedure

When diluting samples and reagents, they must be mixed completely and evenly. Before adding TMB into wells, equilibrate TMB Substrate for 30 minutes at 37°C. It is recommended to plot a standard curve for each test.

1. Set standard, **test samples (diluted at least 1/2 with Sample Dilution Buffer)**, control (blank) wells on the pre-coated plate respectively, and then, records their positions. It is recommended to measure each standard and sample in duplicate.
2. **Prepare Standards:** Aliquot 100ul of zero tube, 1st tube, 2nd tube, 3rd tube, 4th tube, 5th tube, 6th tube and Sample Dilution Buffer (blank) into the standard wells.
3. **Add Samples:** Add 100ul of properly diluted sample into test sample wells.
4. **Incubate:** Seal the plate with a cover and incubate at 37°C for 90 minutes.
5. **Wash:** Remove the cover and discard the plate content, and wash plate 2 times with Wash Buffer. Do NOT let the wells dry

This Kit is for Research Use Only. Not for Diagnostic Procedures.

This is a sample ELISA kit manual only.Always refer to the hard copy manual included in the kit for your experiment.

completely at any time.

6. **Biotin-labeled Antibody:** Add 100ul Biotin-labeled Antibody working solution into above wells (standard, test sample and blank wells). Add the solution at the bottom of each well without touching the sidewall, cover the plate and incubate at 37°C for 60 minutes.
7. **Wash:** Remove the cover, and wash plate 3 times with Wash Buffer, and let the Wash Buffer stay in the wells for 1-2 minutes each time.
8. **HRP-Streptavidin Conjugate (SABC):** Add 100ul of SABC Working Solution into each well, cover the plate and incubate at 37°C for 30 minutes.
9. **Wash:** Remove the cover and wash plate 5 times with Wash Buffer, and let the wash buffer stay in the wells for 1-2 minutes each time.
10. **TMB Substrate:** Add 90ul TMB Substrate into each well, cover the plate and incubate at 37°C in dark within 10-20 minutes. (**Note:** The reaction time can be shortened or extended according to the actual color change, but not more than 30 minutes. You can terminate the reaction when apparent gradient appeared in standard wells.)
11. **Stop:** Add 50ul Stop Solution into each well. The color will turn yellow immediately. The adding order of Stop Solution should be as the same as the TMB Substrate Solution.
12. **OD Measurement:** Read the O.D. absorbance at 450nm in Microplate Reader immediately after adding the stop solution.

Regarding calculation, (the relative O.D.450) = (the O.D.450 of each well) – (the O.D.450 of blank well). The standard curve can be plotted as the relative O.D.450 of each standard solution (Y) vs. the respective concentration of the standard solution (X). The target concentration of the samples can be interpolated from the standard curve. It is recommended to use some professional software to do this calculation, such as **Curve Expert 1.3 or 1.4.**

Note: If the samples measured were diluted, multiply the dilution factor to the concentrations from interpolation to obtain the concentration before dilution.

Summary

Step1: Set standard, test samples, control (blank) wells on the pre-coated plate respectively, and then, records their positions.

Step2: Add 100ul standard or sample to each well and incubate for 90 minutes at 37°C.

Wash step: Aspirate and wash plates 2 times.

Step3: Add 100ul Biotin-labeled Antibody working solution to each well and incubate for 60 minutes at 37°C.

Wash step: Aspirate and wash plates 3 times.

Step4: Add 100ul SABC Working Solution into each well and incubate for 30 minutes at 37°C.

Wash step: Aspirate and wash plates 5 times.

Step5: Add 90ul TMB Substrate Solution. Incubate 10-20 minutes at 37°C.

Step6: Add 50ul Stop Solution. Read at 450nm immediately and calculation.

Rat Osteocalcin

Assay Procedure Summary

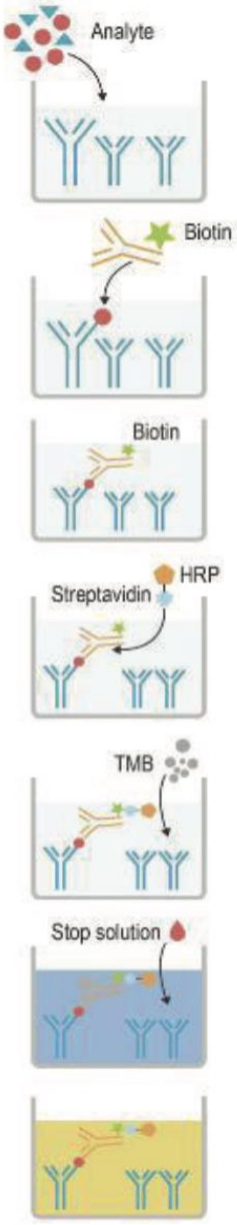

1. Add 100μL standard or sample to the wells. Incubate for 90 min at 37°C

2. Discard the liquid, immediately add 100μL Biotinylated Detection Ab working solution to each well. Incubate for 60 min at 37°C

3. Aspirate and wash the plate for 3 times

4. Add 100μL HRP conjugate working solution. Incubate for 30 min at 37°C. Aspirate and wash the plate for 5 times

5. Add 90μL Substrate Reagent. Incubate for 15 min at 37°C

6. Add 50μL Stop Solution

7. Read the plate at 450nm immediately. Calculation of the results

Reagent preparation

1. Bring all reagents to room temperature (18-25℃) before use. If the kit will not be used up in one assay, please only take out the necessary strips and reagents for present experiment, and store the remaining strips and reagents at required condition.
2. **Wash Buffer:** Dilute 30 mL of Concentrated Wash Buffer with 720 mL of deionized or distilled water to prepare 750 mL of Wash Buffer. Note: if crystals have formed in the concentrate, warm it in a 40℃ water bath and mix it gently until the crystals have completely dissolved.
3. **Standard working solution:** Centrifuge the standard at 10,000×g for 1 min. Add 1mL of Reference Standard &Sample Diluent, let it stand for 10 min and invert it gently several times. After it dissolves fully, mix it thoroughly with a pipette. This reconstitution produces a working solution of 50 ng/mL (or add 1 mL of Reference Standard &Sample Diluent, let it stand for 1-2 min and then mix it thoroughly with a vortex meter of low speed. Bubbles generated during vortex could be removed by centrifuging at a relatively low speed). Then make serial dilutions as needed. The recommended dilution gradient is as follows: 50、25、12.5、6.25、3.13、1.57、0.78、0 ng/mL.

   Dilution method: Take 7 EP tubes, add 500 μL of Reference Standard & Sample Diluent to each tube. Pipette 500 μL of the 50 ng/mL working solution to the first tube and mix up to produce a 25 ng/mL working solution. Pipette 500 μL of the solution from the former tube into the latter one according to this step. The illustration on the next page is for reference. Note: the last tube is regarded as a blank. Don't pipette solution into it from the former tube. Gradient diluted standard working solution should be prepared just before use.

4. **Biotinylated Detection Ab working solution:** Calculate the required amount before the experiment (100 μL/well). In preparation, slightly more than calculated should be prepared. Centrifuge the Concentrated Biotinylated Detection Ab at 800×g for 1 min, then dilute the 100×Concentrated Biotinylated Detection Ab to 1× working solution with Biotinylated Detection Ab Diluent (Concentrated Biotinylated Detection Ab: Biotinylated Detection Ab Diluent= 1: 99). The working solution should be prepared just before use.
5. **HRP Conjugate working solution:** HRP Conjugate is HRP conjugated avidin. Calculate the required amount before the experiment (100 μL/well). In preparation, slightly more than calculated should be prepared. Centrifuge the Concentrated HRP Conjugate at 800×g for 1 min, then dilute the 100×Concentrated HRP Conjugate to 1× working solution with HRP Conjugate Diluent (Concentrated HRP Conjugate: HRP Conjugate Diluent= 1: 99). The working solution should be prepared just before use.

Appendix J: Standard Curves

Osteocalcin Standard Curve

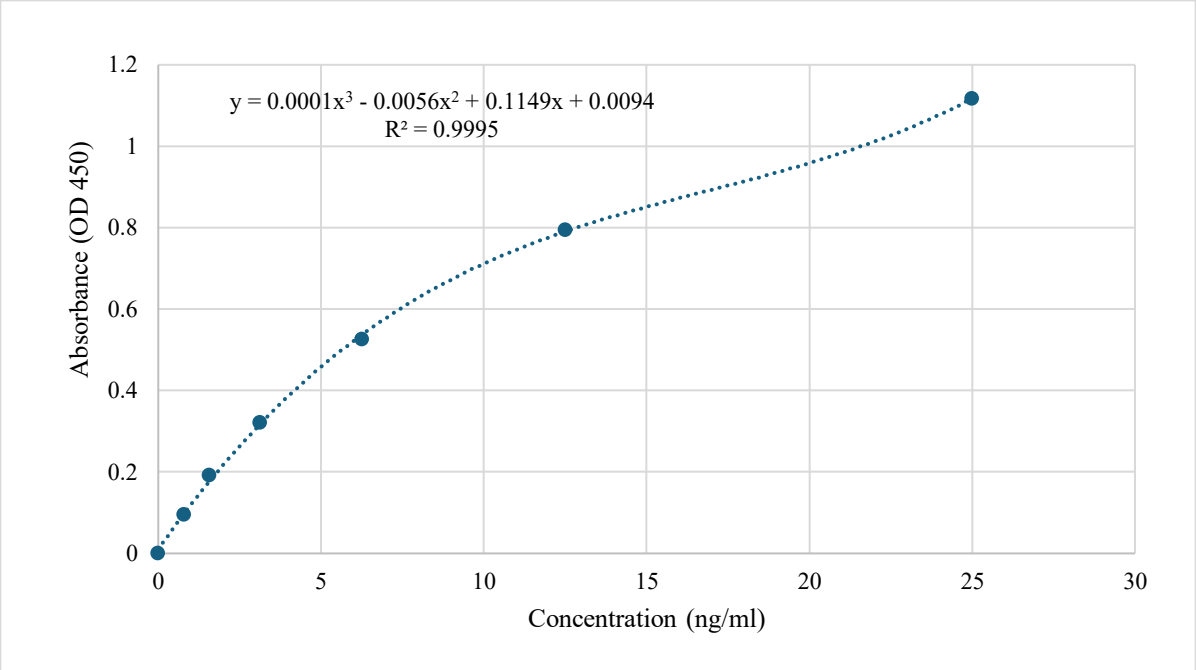

Bone Alkaline Phosphatase Standard Curve